

## Response to Referee #1

We really appreciate the constructive comments/suggestions from Referee #1, which will greatly help us to improve this manuscript. We have provided our responses in blue-colored font following each of the Referee's suggestions (below).

Anonymous Referee #1

Received and published: 16 August 2019

The authors have run the same atmospheric model with 6 different biomass burning (BB) inventories and analysed the differences using AOD and aeronet. These differences are often substantial and to some degree the authors have pointed to reasons why those differences exist. I feel the paper helps other modellers in understanding where some of the uncertainties in biomass burning emissions originate from but at the same time I feel the reader is left a bit wondering what **the main messages are in the end**. Ideally one would come up with recommendations about when and where to use a certain dataset, or when and where to avoid those. But given that the dataset to evaluate the results is also used to construct some this may be too much asked. Please find below a number of suggestions to further improve the paper.

**Response:** The six BB datasets analyzed in this study differ in various ways and scales across different biomass burning regions and seasons. Hence, it is challenging to come up with comprehensive recommendations about when and where to use or avoid a particular dataset. Nevertheless, we agree that some recommendations, even in general terms, would be beneficial to the community. Thus, we have added the following statement towards the end of the abstract:

“Although model simulations based on QFED2.4 show overall closest agreement with satellite AOD retrievals, we recommend FEER1.0 for aerosol-focused hindcast experiments in the two biomass-burning dominated regions in the southern hemisphere, SHAF and SHSA (as well as in other regions but with lower confidence), mainly because QFED2.4 is tuned with the GEOS model, whereas FEER1.0 is derived in a more model-independent fashion and is more physical-based since its emission coefficients are independently derived at each grid box.”

First sentence in introduction is spelled a bit awkward, please break up in two. Likewise for the second paragraph (L79).

**Response:** The first sentence in introduction has been modified to:

Biomass burning (BB) is estimated to contribute about 62% of the global particulate organic carbon (OC) and 27% of black carbon (BC) emissions annually (Wiedinmyer et al., 2011). Therefore, biomass burning emissions significantly affect air quality by acting as a major source of particulate matter (PM), and the climate system by modulating solar radiation and cloud properties.

the second paragraph in introduction has been broken up into:

With the advent of satellite remote sensing of active fire and burned area products in the last couple of decades, a number of global BB emission datasets based on these observations have become available (e.g., Ichoku et al., 2012). Six of such major BB datasets will be compared in this study, including three datasets based on burned area approaches,

namely, the Fire INventory from NCAR (FINN, Wiedinmyer et al., 2011) and two versions of the Global Fire Emissions Database (GFED, van der Werf et al., 2006, 2010, 2017), and three datasets based on fire radiative power (FRP) approaches, namely, the Global Fire Assimilation System (GFAS, Kaiser et al., 2012) developed in the European Centre for Medium-Range Weather Forecasts (ECMWF), and two National Aeronautics and Space Administration (NASA) products, i.e., the Fire Energetics and Emissions Research algorithm (FEER, Ichoku and Ellison, 2014) and the Quick Fire Emissions Dataset (QFED, Darmenov and da Silva, 2015).

159: Not sure why that small fire paper is cited in the GFED3 description

**Response:** We have removed “Randerson et al., 2012”.

208: Kaiser et al: : , -> Kaiser et al.,

**Response:** This has been corrected.

The link on L213 does not work, at least not on my two computers

**Response:** They changed the website address recently. Sorry about that. This link in the revised version has been updated as:

<https://confluence.ecmwf.int/display/CKB/CAMS++Global+Fire+Assimilation+System+%28GFAS%29+data+documentation>

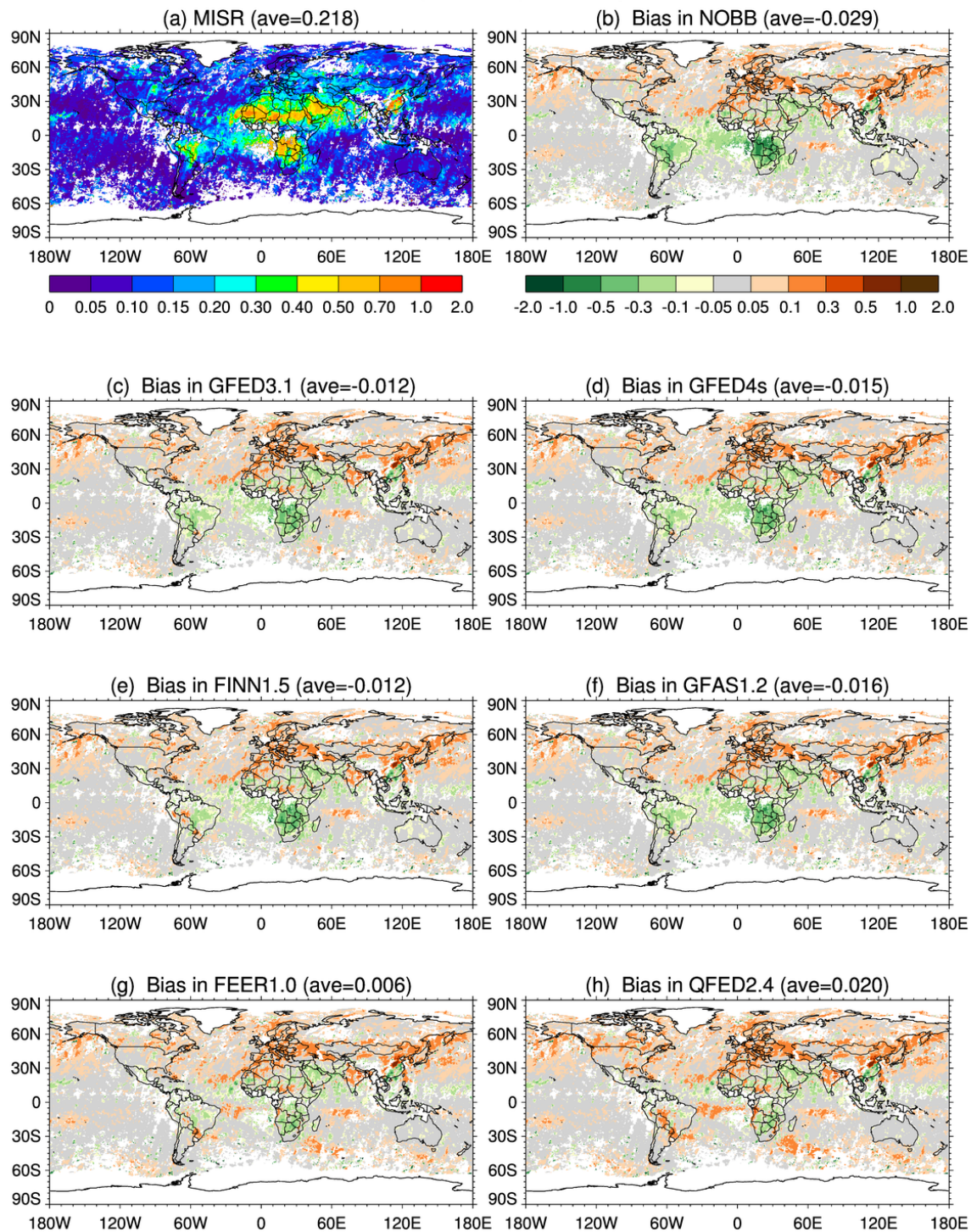
L282: I am a bit surprised that BB aerosols are injected near the surface. There is quite a bit of literature showing the importance of injection heights in for example the Boreal region

**Response:** We agree that this is a concern. Incidentally, this is one of the current limitations of this model and many other models, such as GEOS-chem (Zhu et al., 2018), due to the lack of observational constraint on plume vertical profiles. We have recently promoted an AeroCom multiple-model initiative to constrain the vertical profile of plume height in a model with the MISR plume height (see more details at the Wiki website: <https://wiki.met.no/aerocom/phase3-experiments>).

L297: So basically, you use the same AOD data that was used to construct one of the BB inventories to evaluate a suite of models. That just doesn’t feel right and requires careful explanation why this is done and what the consequences are

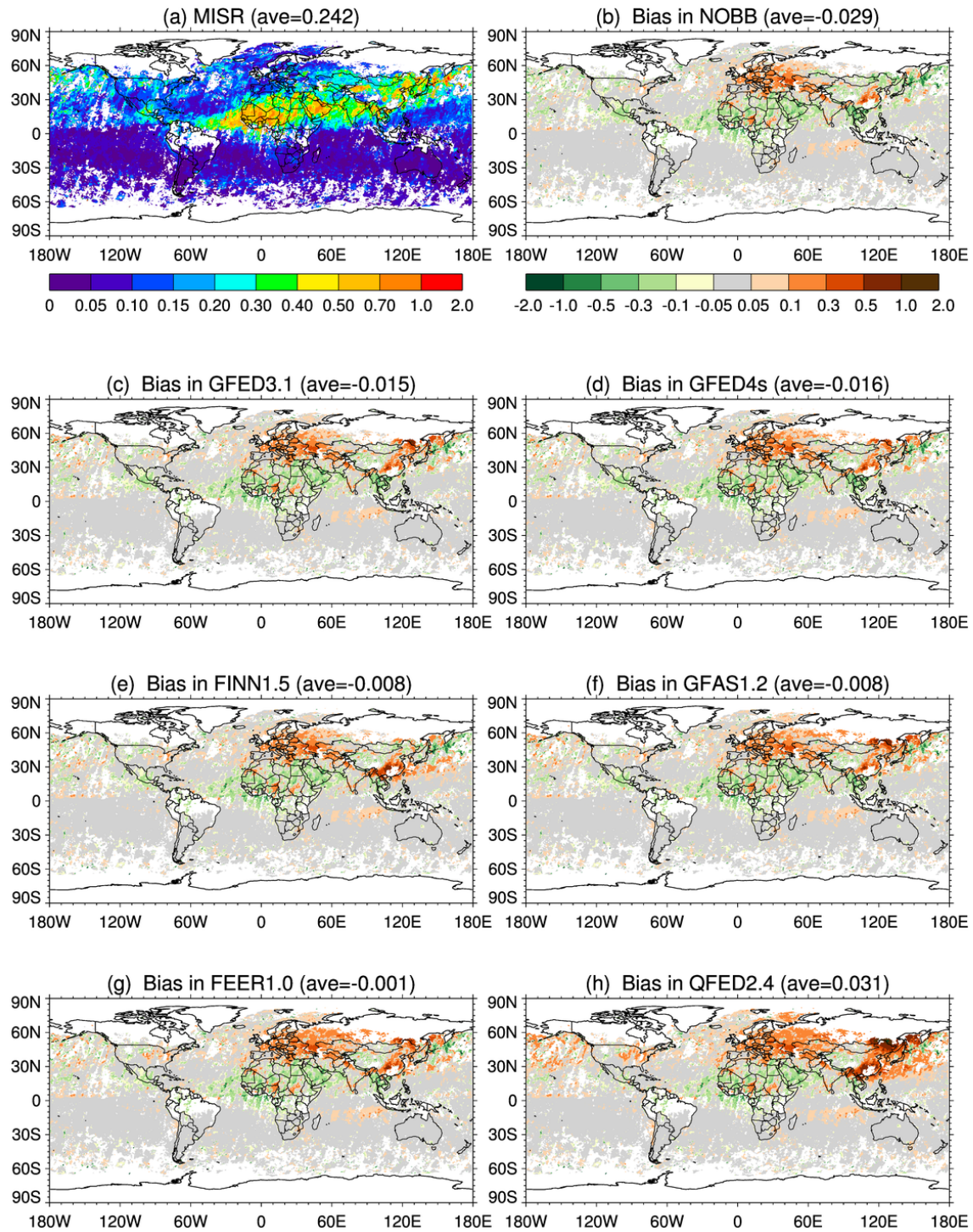
**Response:** We have replaced MODIS AOD with MISRv23 AOD in the Figure 5-7 as below. In general, the results with MISR AOD are consistent with those with MODIS AOD. We also have changed the text part accordingly in the revised version (but not shown here because too numerous).

## AOD (550nm) for Sep 2008



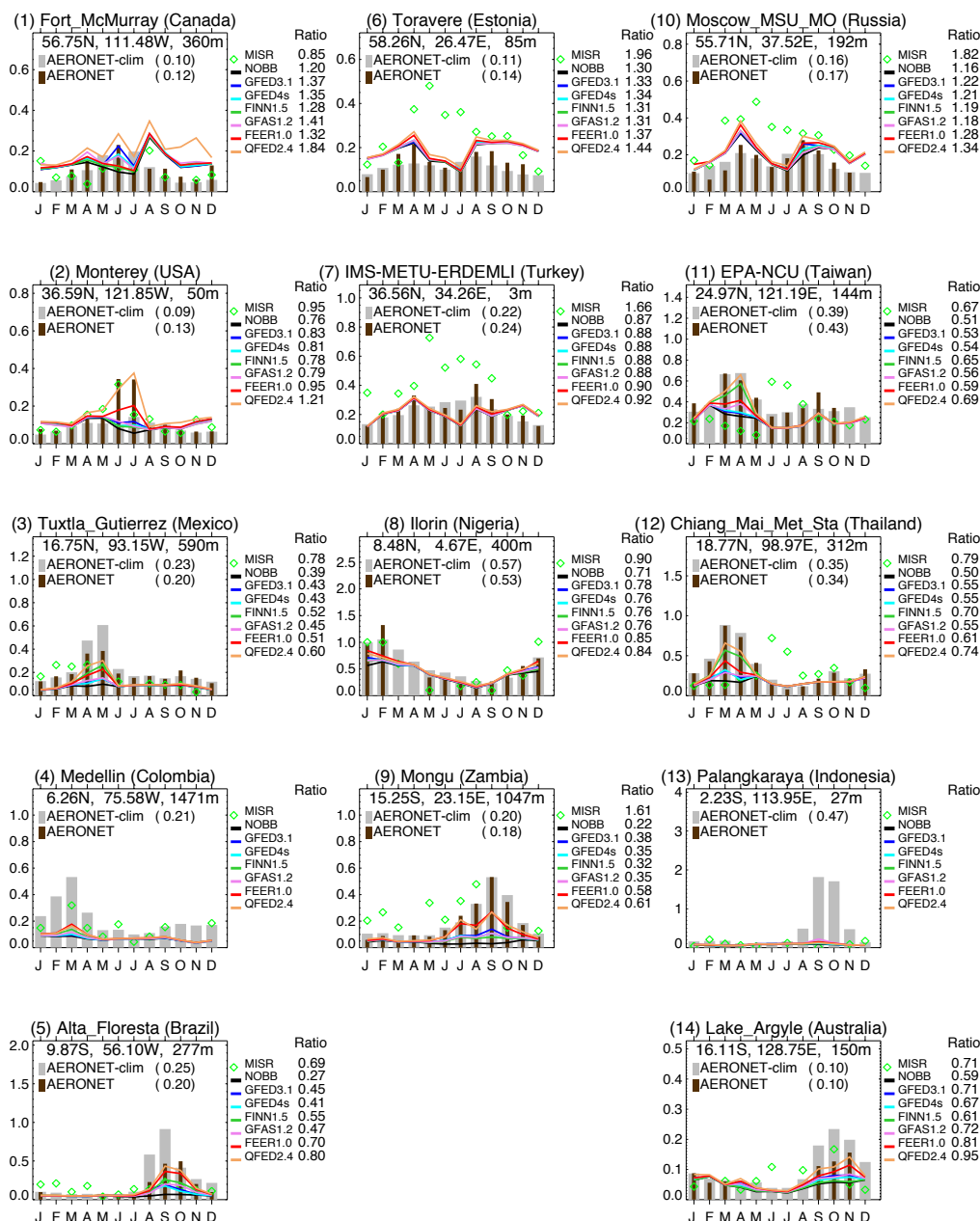


## AOD (550nm) for Apr 2008





## Monthly AOD (550nm) at AERONET sites for 2008



L305: I feel this is more useful and scientific sound; evaluate the various inventories with independent data

**Response:** Please see our response above.

L393: But isn't April outside the main fire season in EQAS? In other words, if emissions are very low then a factor two difference (for example due to the detection of small fires in GFED4) is not that noteworthy I guess

**Response:** It is actually in August (not April), the peak of the fire season in EQAS, that GFED4s is a factor of two higher than GFED3.1. Sorry about the confusion. We have corrected it in the revised version. Now it reads like this:

“In particular, it is noteworthy that in EQAS, the annual OC emissions from GFED4s was lower than that of GFED3.1 by 18%, but higher by a factor of two in the month of **August** when peatland burning is predominant.”

L402: This is indeed a key question and I doubt we will make much progress as long as we keep using one single dataset to constrain emissions. Broadly speaking, the “gas community” (CO, NO<sub>2</sub>) has shown that the traditional inventories do reasonably well while the “aerosol community” has shown for over 10 years now that the emissions of those inventories are too low to reconstruct measured AOD. It would be very nice if someone would address why those two communities come to different conclusions.

**Response:** It is a good point. We have added the statement below in the introduction part:

Andreae (2019) commented that “In contrast to gaseous compounds, which are chemically well defined, aerosols are complex and variable mixtures of organic and inorganic species and comprise particles across a wide range of sizes. This affects in particular the measurements of organic aerosol, black/elemental carbon, and size fractionated aerosol mass”.

In the Section 4.3, we mentioned in the manuscript that many models like GEOS version used in this study did not consider the secondary organic carbon produced from biomass burning emissions”.

L416 lights -> light

**Response:** Changed. Thanks.

L419: GOES -> GEOS

**Response:** Changed. Thanks.

L452: This is a bit confusing, I don’t think emissions peaked in April but you found elevated AOD levels due to burning

**Response:** This was due to an oversight on our part. Thank you for pointing it out. We rewrote that paragraph as:

“Being mixed with, and often surpassed by, other aerosol types in certain regions, however, the contribution of biomass burning aerosols to the total AOD is hardly distinguishable from those of other sources in the peak months, such as April (Fig. 6) in the regions of Southeast Asia (SEAS), Central Asia (CEAS), and Boreal Asia (BOAS).”

L467: Given the very large interannual variability, especially in EQAS, this should be avoided. Please scale with active fire detections or so

**Response:** We agree that the biomass burning has large interannual variability in certain regions, especially in EQAS, as we have shown in one of our recent publications on Indonesian fires (Pan et al., 2018). Thus, we overlaid the AERONET climatology and MODIS-Aqua and MODIS-Terra to complement AERONET whenever it has missing data in 2008.

L529: Now shown -> Not shown (I guess)

**Response:** This has been corrected. Thanks.

L624: This could be a place where this paper could make a difference. Given that the emission factors used in the various datasets are not wildly different, the variability stems from variability in dry matter fuel consumption. GFED has been tuned to match measured fuel consumption, how about FEER and QFAS? Are their levels of fuel consumption (per unit burned area that is) similar to literature-based values? I understand that the FRP approach aims to avoid burned area but these datasets are becoming better constrained and by dividing fuel consumption from FEER and QFED with burned area there could be a useful constraint. Right now we compare AOD with AOD-derived datasets and that just does not help us further I am afraid

**Response:** We agree that it would be much more useful to the community to go beyond mere comparisons between the different emissions datasets to develop a constraint that can eventually lead to a realistic understanding of the reasons for the disagreements and how to account for them, and hopefully improve the emissions. The current paper is the initial step toward that goal, as it helps to understand the high-level relationships/disagreements between the different emissions datasets, at the global, regional, and local scales, based on simulations using the exact same global model. Detailed diagnosis of the issues with the individual dataset and finding appropriate synergistic connections between them can follow from this in a systematic manner. Using laboratory measurements of small fires, Ichoku et al. (2008) showed a relationship between the traditional emission factors (EF) based on the burned-biomass approach and the emission coefficients (Ce) based on the FRP approach. These two factors are related via the combustion factor (Fc) that relates time-integrated FRP and total burned biomass. Such relationships can potentially be applied as a useful constraint for improving emissions, but will need to be pursued in a future study that is more focused on addressing such a question.

L731: Actually most of the emission factors are from actual fires, not from lab-based measurements.

**Response:** We have added the contribution from field campaigns. The paragraph now reads as follows:

“**Emission factor (EF).** ... However, the EFs can have significant uncertainties (Andreae, 2019), because each EF results from a particular experiment or field campaign. Some *EFs* are derived from lab-based studies whereby samples of fuels are burned in combustion chambers (e.g., Christian et al., 2003; Freeborn et al., 2008), where the combustion characteristics can be very different from those of large-scale open biomass burning and wildfires; and some *EFs* are derived from field campaigns, where the measurement locations are often not close enough to the biomass burning source due to personnel safety and other logistic factors (Aurell et al., 2019).”

#### **References:**

Andreae, M. O.: Emission of trace gases and aerosols from biomass burning – an updated assessment, Atmos. Chem. Phys., 19, 8523–8546, <https://doi.org/10.5194/acp-19-8523-2019>, 2019.



Aurell, J., Mitchell B., Greenwell D., Holder A., Tabor D., Kiros F., and Gullett B.: Measuring Emission Factors from Open Fires and Detonations. AWMA Air Quality Measurement Methods and Technology, Durham, North Carolina, April 02 - 04, 2019.

Ichoku, C., J. V. Martins, Y. J. Kaufman, M. J. Wooster, P. H. Freeborn, W. M. Hao, S. Baker, C. A. Ryan, and B. L. Nordgren (2008), Laboratory investigation of fire radiative energy and smoke aerosol emissions, *J. Geophys. Res.*, 113, D14S09, doi:10.1029/2007JD009659.

Pan, X., Chin, M., Ichoku, C. M., & Field, R. D. (2018). Connecting Indonesian fires and drought with the type of El Niño and phase of the Indian Ocean dipole during 1979–2016. *Journal of Geophysical Research: Atmospheres*, 123, 7974–7988. <https://doi.org/10.1029/2018JD028402>

Zhu, L., M. Val Martin, A. Hecobian, M.N. Deeter, L.V. Gatti, R.A. Kahn, and E.V. Fischer, 2018. Development and implementation of a new biomass burning emissions injection height scheme for the GEOS-Chem model. *Geosci. Model Develop.* 11, 4103–4116, doi:10.5194/gmd-11-4103-2018.

## Response to Referee #2

We really appreciate the constructive comments from Dr. Parrington. We have provided our responses below in blue font following each comment/suggestion.

The manuscript presents a comparison of biomass burning emissions estimated using satellite observations of active fires including burnt area and fire radiative power. Evaluation of the different emissions datasets is performed by application in a global aerosol model and comparing the relative changes in the organic matter aerosol fields over MODIS satellite and AERONET ground-based observations of aerosol optical depth (AOD). The authors acknowledge the limitations of the nature of a model-specific study like this but the inter-comparison is very thorough and provides valuable, and timely, insights into variability of estimating biomass burning emissions for application in models. The manuscript is well written and in the scope of Atmospheric Chemistry and Physics, and I recommend it for publication subject to the authors addressing the comments below.

**Response:** Thank for your encouraging comment on the merit of this manuscript. We hope that this study will contribute toward advanced understanding of the differences between BB emission datasets, and will eventually facilitate the improvement of the estimation of BB aerosol emissions in models.

### General comments:

Discussion of uncertainties in emission factors – would the known underestimate of PM emission factors, especially for peat fires in South East Asia, impact on the model AOD? <https://www.mdpi.com/2072-4292/10/4/495/htm> or <https://agupubs.onlinelibrary.wiley.com/doi/pdf/10.1029/2017JD027827>

**Response:** Yes, it is true that the emission factors estimated from those two studies are far larger than those by Andreae and Merlet (2001) and Akagi (2011). With the higher PM emission factor and thus PM emission, AOD will be enhanced accordingly in the model. In equatorial Asia (EQAS), the experiments based on all six BB emission datasets underestimated AOD during September (the peak of the burn season) to the same degree (~50%) as the run without any biomass burning emission input, compared to MODIS-Aqua (See Figure 5 and Table S1 in the ACPD version), regardless of whether these BB aerosol emissions are based on the burned-area or FRP approach. This may be largely attributed to missing fire detection from satellite, for example, due to low signal from peat fires, which are predominantly smoldering. In addition, the *EF* values for aerosols emitted from peat fires may be underestimated as well (Table 2 in Kiely et al., 2019). Several studies based on in-situ measurements of *EF* reported that the *EFs* of PM<sub>2.5</sub> for peat fires provided by Andreae and Merlet (2001) and Akagi et al. (2011) as 9.05 and 9.10 g PM<sub>2.5</sub> per kg dry matter (see Table 2), respectively, are much lower than their measurements. For example, the studies by Wooster et al. (2018), Stockwell et al. (2016), and Roulston et al. (2018) reported *EF* values of  $21 \pm 4.6$ , 17.8 to 22.3, and 24 g PM<sub>2.5</sub> per kg dry matter, respectively, for peat fires in EQAS. Unfortunately, the underestimation of AOD is not shown in the revised version against the MISR AOD, because MISR observation is missing in this region during September 2008. We are asked by the referee #1 to use MISR AOD to evaluate model simulation in the revised version (Figure 5-7), considering QFED and FEER derived their BB emission datasets with historical MODIS AOD.

**Specific comments/questions:**

Page 4, line 107: specify the multi-model study (is it “The AeroCom multi-model study”?).

**Response:** Yes, we have clarified it in the revised version as “The AeroCom multi-model study”.

Page 9, lines 365-367: could it be the case that the two day persistence in FINN1.5 is more representative of peat fires which may be more prevalent in EQAS?

**Response:** The two-day persistence approach used by FINN1.5 in the tropical regions may have been more representative of peat fires that are quite prevalent in EQAS. This may be because peat fires typically burn less vigorously and potentially last longer than other fire regimes. We pointed out this in the Section 4.1.2.

Page 9, section 3.1.2: it may be useful to describe briefly why 2008 was chosen to investigate the seasonal variation. Does each emissions dataset capture inter-annual variability in the same way?

**Response:** The reason we chose 2008 is because it is the year assigned as a benchmark year by AeroCom community with which this study is associated; it is also because the AeroCom Multi-model study of biomass burning lead by Petrenko (mentioned in the introduction part of our manuscript) also chose 2008 as a focus year. As such, the results from these two studies can be intercompared if needed and some synthesized conclusions drawn. In addition, 2008 was chosen because it is a neutral ENSO year, which represents normal burning conditions.

**Figure a** shows the comparison of the interannual variation of OC biomass burning emissions in three biomass burning (BB) datasets during the period of 1997-2018 over the Amazon. The three BB emission datasets are FEER, GFED4s, and QFED, which are analyzed in our study. The interannual variability are pronounced across the three BB datasets although with different magnitudes. Apparently, 2007 is the highest burn year, 2009 is the least burn year, while 2008 is a normal burn year. Overall, QFED has the highest OC BB emission, FEER has the second highest, and GFED4s has the least (~1/3 of QFED) from year to year, which are consistent with our result for 2008. A similar result can be drawn from the region of Africa (**Figure b**), where the interannual variability is less pronounced though. In summary, these BB datasets capture similar interannual variability although they have different magnitudes, with QFED having the highest OC BB emission, FEER the second highest, and GFED4s the least.



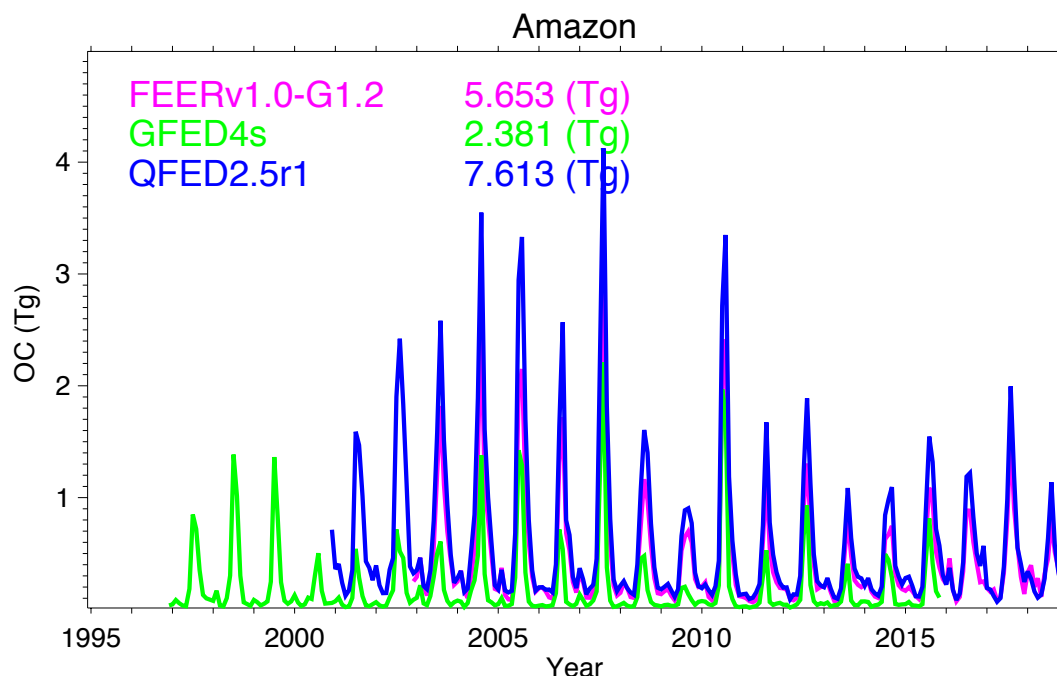


**Figure a.** The comparison of the interannual variation of OC biomass burning emissions in three biomass burning datasets during the period of 1997-2018 over Amazon (80°W-30°W, 60°S-15°N; the combination of two regions used in our study, i.e., northern hemisphere South America (NHSA) and southern hemisphere South America (SHSA)). The annual mean OC emissions over this region are displayed in the figure as well.

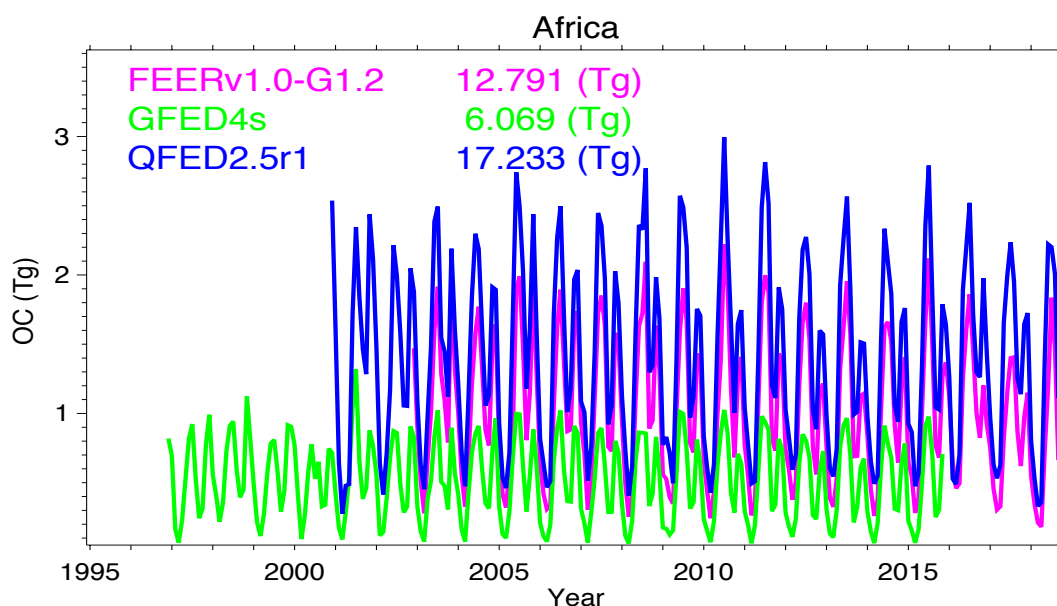


**Figure b.** The comparison of the interannual variation of OC biomass burning emissions in three biomass burning datasets during the period of 1997-2018 over Africa (24°W-50°E, 40°S-20°N; representing a combination of two regions used in our study, i.e., northern hemisphere Africa (NHAF) and southern hemisphere Africa (SHAF)). The annual mean biomass burning OC emissions over this region are displayed in the figure as well.

Page 10, line 409: “with each BB emission dataset instead” is repeating the earlier part of the sentence.

**Response:** We have changed this sentence to “Therefore, in this study we have implemented all six global BB emission datasets separately in the GEOS model, and evaluated their respective simulated aerosol loadings.”

Page 11, line 433: change “peaking” to “peak”.

**Response:** Changed.

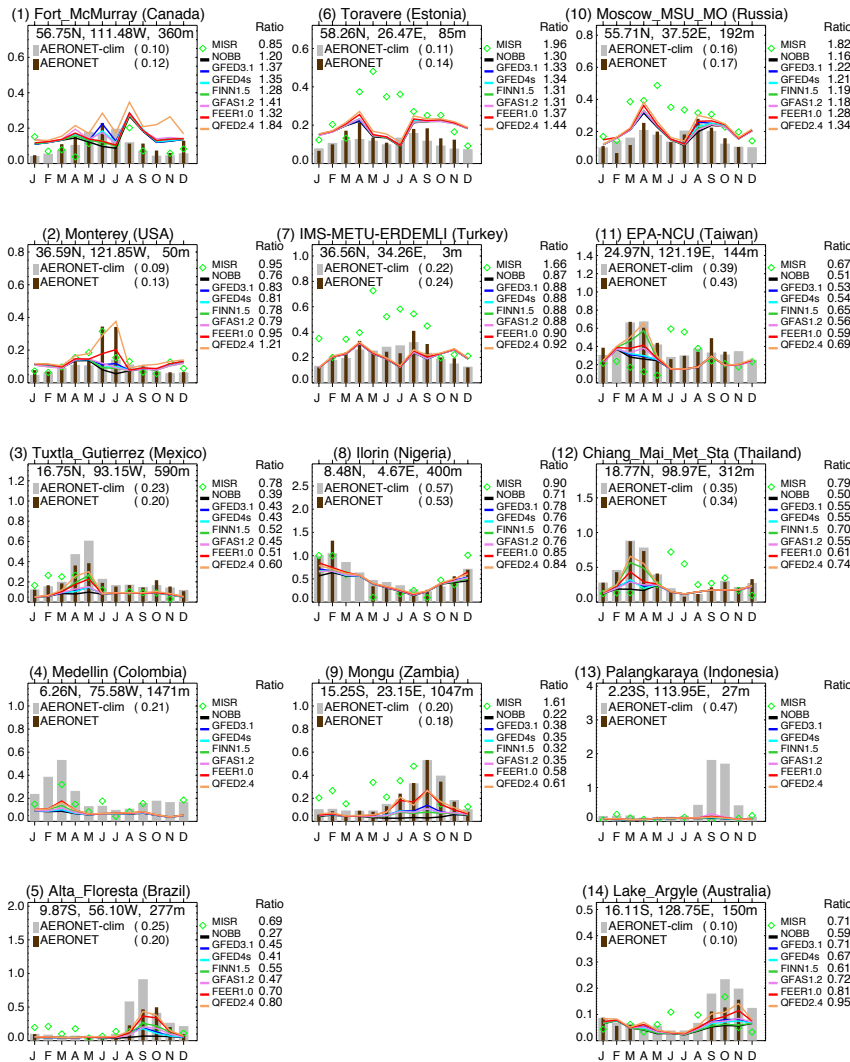
Page 11, section 3.2.1: it may be useful to a reader to give the names of each region as well as the acronym.

**Response:** The full names of the regions have been added in the revised version, such as southern hemisphere South America (SHSA), and southern hemisphere Africa (SHAF).

Page 12, section 3.2.2: it may be useful to give the country of the named AERONET sites, which is more intuitive to understanding the geography than giving just the regions.

**Response:** The country names of the AERONET sites have been added in Figure 7 as below.

Monthly AOD (550nm) at AERONET sites for 2008



Page 12, lines 487-488: “in each respective region”.

**Response:** We changed to “in each region”.

Page 12, line 488: change “At most other AERONET” to “At most of the other AERONET”.

**Response:** Thank you. We have changed “most” to “most of the”.

Page 13, line 534: “resembled with” should be “resembled”.

**Response:** We have deleted “with”.

Page 13, lines 537-538: “All of these evidences” should be “All of this evidence”.

**Response:** We have changed to “All of this evidence”.

Page 13, line 539: should “respond” be “correspond”.

**Response:** The meanings of “respond” and “correspond” are very similar in some sense. Here we prefer to use “respond” to mean doing something in reply.

Page 13, line 543 (and other locations): would using “active fire detections” rather than “fire hotspots” be a more scientific way of describing this?

**Response:** Changed.

Page 13, line 553: “over entire” should be “over the entire”.

**Response:** Changed.

Page 14, line 566: should “emitted from smoke aerosols” be “emitted as smoke aerosols”?

**Response:** Changed to “the dominance of the fine-mode aerosol particles in smoke aerosols”.

Page 14, line 567: change “These evidences” to “This”.

**Response:** We changed to “This evidence”.

Page 14, line 574: change “On broader: : :” to “Over broader: : :”?

**Response:** Changed to “in regional emission”, which is relative to the local scale.

Page 14, line 577: “largest month” should be “largest monthly”.

**Response:** Changed.

Page 15, line 624: should GFAS1.2 also be included as an FRP-based estimation?

**Response:** Right, we have added GFAS1.2.

Page 16, line 662: change “on inclusion” to “in including”.

**Response:** Changed “on inclusion of” to “in including”.

Page 16, line 675: change “exceeds” to “is greater”.

**Response:** Changed.

Page 16, line 677: change “emissions is 10%” to “emissions are 10%”.

**Response:** Changed.

Page 17, lines 713-715: please clarify this last sentence as it isn’t clear what is meant “by active fire product”. I thought that FINN1.5 and GFED4s are based on the burnt area product available from MODIS.

**Response:** FINN1.5 actually uses active fire product to estimate the burned area by assuming each active fire pixel represents a burned area of 1 km<sup>2</sup> for most biome types (see details in *Sect. 2.1.3*). GFED4s uses the official burned area product for large fires, but estimates burned area for small fires using active fire detections. We have rewritten the sentences in the revised version as:

“This issue also affects FINN1.5 (Wiedinmyer et al., 2011), which derives the burned area by assuming each active fire pixel to correspond to a burned area of 1 km<sup>2</sup> for most biome types (see details in *Sect. 2.1.3*), and GFED4s, which uses burned area product for large fires but derives burned areas for small fires using the MODIS active fire product.”



Page 17, line 721: “scares” should be “scars”.

**Response:** Changed.

Page 18, line 758: a citation for other model assumptions may be helpful to the reader.

**Response:** We have removed this vague expression, i.e., other model assumptions, from the revised version.

Page 19, final paragraph: while the focus of the evaluation has been based on AOD observations from MODIS and AERONET, it would be useful if some comments could be made on the potential use of in situ, especially aircraft, observations could be used in this context – for example, measurements made during the WE-CAN or FIREX AQ campaigns in recent years. Also some comment on potential improvements to fire emissions estimates based on FRP products from geostationary satellite observations, especially in combination with low Earth orbit observations such as MODIS (and VIIRS).

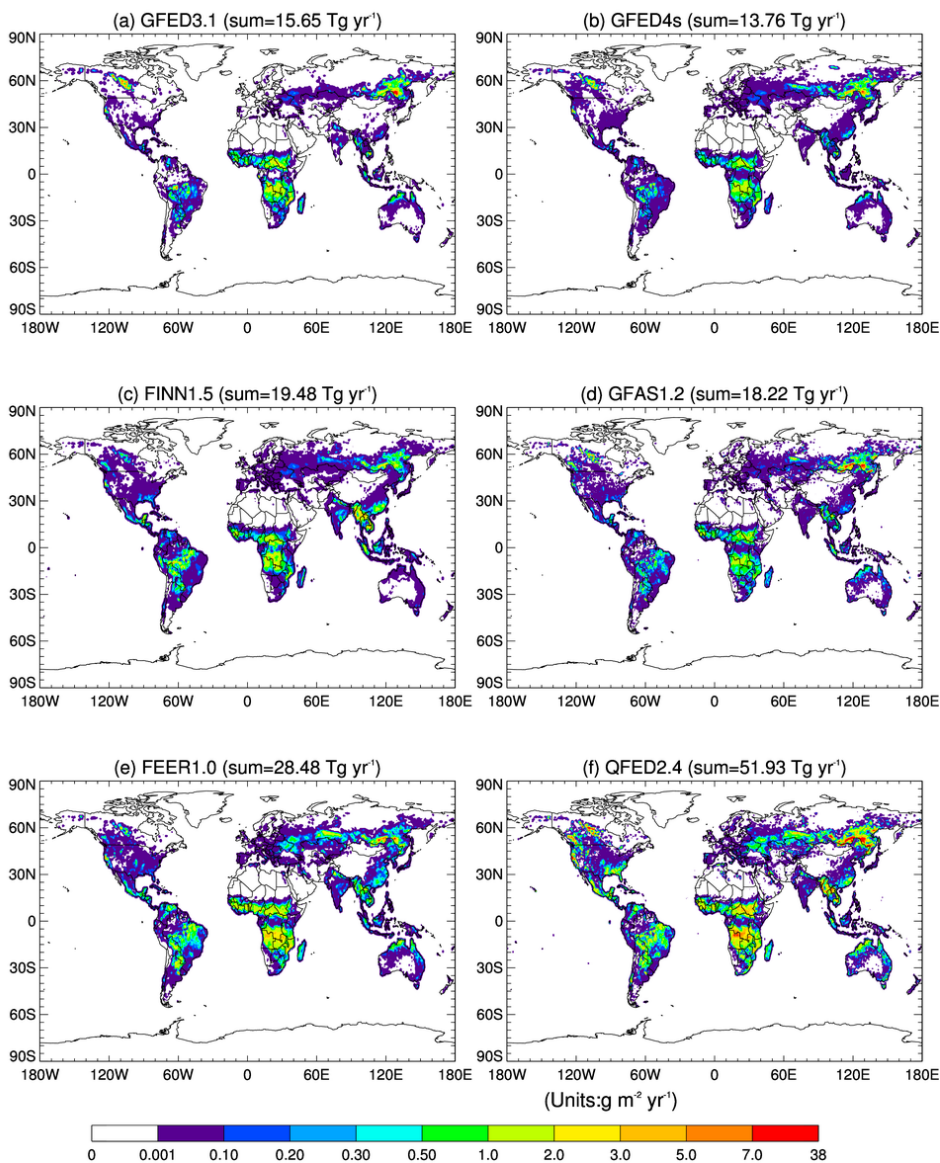
**Response:** Thank you for your suggestions. We have added your suggestions in the last paragraph as

“The investigated global BB emission datasets driven by fire remote sensing and retrievals of FRP and burned-area products, which have hitherto depended heavily on MODIS, can be augmented with products from higher resolution sensors such as Visible Infrared Imaging Radiometer Suite (VIIRS), and the global suite of geostationary meteorological satellites such as Meteosat (covering Europe, Africa and the Indian Ocean), Geostationary Operational Environmental Satellite (GOES, covering North, Central, and South America) and Himawari (covering east Asia, southeast Asia, and Australia). Also, measurements from the recent field campaigns such as WE-CAN ([https://www.eol.ucar.edu/field\\_projects/we-can](https://www.eol.ucar.edu/field_projects/we-can)) and FIREX-AQ (<https://www.esrl.noaa.gov/csd/projects/firex-aq/science/motivation.html>) are expected to contribute toward advancing our knowledge of biomass burning emissions in North America. The evaluation in this study has been solely based on remote sensing AOD data, including retrievals from both satellite and ground-based (AERONET) sensors. Continuous mass concentration measurements are needed to validate the fire-generated aerosol loading in specific contexts, such as in analyzing collocated surface and vertical aerosol concentrations and composition, at least in the major BB regions.”

Page 30: specify “annual total organic carbon biomass burning emissions”? I also think that removing the sites from the maps could be useful as they aren’t that clear to discriminate from the colours on the map, and is a bit distracting from the values in the data.

**Response:** We have specified “The spatial distribution of annual total organic carbon biomass burning emissions” in the caption of Figure 2. The AERONET sites have been removed from Figure 2 as below.

## OC biomass burning emission for 2008



Page 35, line 1290-1291: clarify that the climatology of AERONET AOD is AERONETclim in the legend.

**Response:** We have added it in the caption of Figure 7, “The climatology of AERONET AOD (i.e., AERONET-clim)”.

### References:

Kiely, L., Spracklen, D. V., Wiedinmyer, C., Conibear, L., Reddington, C. L., Archer-Nicholls, S., Lowe, D., Arnold, S. R., Knote, C., Khan, M. F., Latif, M. T., Kuwata, M., Budisulistiorini, S. H., and Syaufina, L.: New estimate of particulate emissions from Indonesian peat fires in 2015, *Atmos. Chem. Phys.*, 19, 11105–11121, <https://doi.org/10.5194/acp-19-11105-2019>, 2019.

Roulston, C., Paton-Walsh, C., Smith, T. E. L., Guérette, É.-A., Evers, S., Yule, C. M., et al.: Fine particle emissions from tropical peat fires decrease rapidly with time since ignition. *Journal of Geophysical Research: Atmospheres*, 123, 5607–5617. <https://doi.org/10.1029/2017JD027827>, 2018.

Stockwell, C.E., Jayarathne, T., Cochrane, M.A., Ryan, K.C., Putra, E.I., Saharjo, B.H., Nurhayati, A.D., Albar, I., Blake, D.R., Simpson, I.J., et al.: Field measurements of trace gases and aerosols emitted by peat fires in Central Kalimantan, Indonesia during the 2015 El Niño. *Atmos. Chem. Phys.*, 16, 11711–11732, 2016.

Wooster, M., Gaveau, D., Salim, M., Zhang, T., Xu, W., Green, D., Huijnen, V., Murdiyarso, D., Gunawan, D., Borchard, N., Schirrmann, M., Main, B. and Sepriando, A.: New Tropical Peatland Gas and Particulate Emissions Factors Indicate 2015 Indonesian Fires Released Far More Particulate Matter (but Less Methane) than Current Inventories Imply. *Remote Sensing*. 10 (4), p.495, <https://doi.org/10.3390/rs10040495>, 2018.

## Six Global Biomass Burning Emission Datasets: Inter-comparison and Application in one Global Aerosol Model

Xiaohua Pan<sup>1,2,\*</sup>, Charles Ichoku<sup>3</sup>, Mian Chin<sup>2</sup>, Huisheng Bian<sup>4,2</sup>, Anton Darmenov<sup>2</sup>, Peter Colarco<sup>2</sup>, Luke Ellison<sup>5,2</sup>, Tom Kucsera<sup>6,2</sup>, Arlindo da Silva<sup>2</sup>, Jun Wang<sup>7</sup>, Tomohiro Oda<sup>6,2</sup>, Ge Cui<sup>7</sup>

1. Earth System Science Interdisciplinary Center, University of Maryland, College Park, MD, USA
2. NASA Goddard Space Flight Center, Greenbelt, MD, USA
3. Howard University, Washington DC, USA
4. Joint Center for Earth Systems Technology, University of Maryland Baltimore City, Baltimore, MD, USA
5. Science Systems and Applications, Inc., Lanham, MD, USA
6. Universities Space Research Association, Columbia, MD, USA
7. University of Iowa, College of Engineering, Iowa City, IA, USA

\* xpan333@umd.edu

### Abstract

Aerosols from biomass burning (BB) emissions are poorly constrained in global and regional models, resulting in a high level of uncertainty in understanding their impacts. In this study, we compared six BB aerosol emission datasets for 2008 globally as well as in 14 sub-regions. The six BB emission datasets are: (1) GFED3.1 (Global Fire Emissions Database version 3.1); (2) GFED4s (GFED version 4 with small fires); (3) FINN1.5 (Fire INventory from NCAR version 1.5); (4) GFAS1.2 (Global Fire Assimilation System version 1.2); (5) FEER1.0 (Fire Energetics and Emissions Research version 1.0), and (6) QFED2.4 (Quick Fire Emissions Dataset version 2.4). The global total emission amounts from these six BB emission datasets differed by a factor of 3.8, ranging from 13.76 to 51.93 Tg for organic carbon and from 1.65 to 5.54 Tg for black carbon. In most of the regions, QFED2.4 and FEER1.0, which are based on the satellite observations of fire radiative power (FRP) and constrained by aerosol optical depth (AOD) data from the Moderate Resolution Imaging Spectroradiometer (MODIS), yielded higher BB emissions than the rest by a factor of 2-4. By comparison, the BB emission estimated from GFED4s and GFED3.1, which are based on satellite burned-area data, but with no AOD constraints, were at the low end of the range. In order to examine the sensitivity of model simulated AOD to the different BB emission datasets, we ingested these six BB emission datasets separately into the same global model, the NASA Goddard Earth Observing System (GEOS) model, and compared the simulated AOD with observed AOD from the AEROSOL RObotic NETwork (AERONET) and the Multiangle Imaging SpectroRadiometer (MISR) in 14 sub-regions during 2008. In Southern hemisphere Africa (SHAF) and South America (SHSA), where aerosols tend to be clearly dominated by smoke in September, the simulated AOD were underestimated almost in all experiments compared to MISR, except for the QFED2.4 run in SHSA. The model-simulated AOD based on FEER1.0 and QFED2.4 were the closest to the corresponding AERONET data, being, respectively, about 73% and 100% of the AERONET observed AOD at Alta-Floresta in SHSA, and about 49% and 46% at Mongu in SHAF. The simulated AOD based on the other four BB emission datasets accounted for only ~ 50% of the AERONET AOD at Alta Floresta and ~ 20% at Mongu. Overall, during the biomass burning peak seasons, at most of the selected

Formatted: Font color: Text 1

Deleted: Global Fire Emissions Database

Deleted: i

Deleted: Although biomass burning emissions of aerosols from these six BB emission datasets showed similar spatial distributions, t

Deleted: ir

Deleted: 3-

Deleted: 4

Formatted: Font color: Text 1

Deleted: and

Formatted: Font color: Text 1

Deleted: utilize

Deleted: the

Deleted: In

Deleted: retrieval of

Deleted:

Deleted: and

Deleted: the simulated AOD were underestimated in all experiments. More specifically, t

Deleted: , respectively

Deleted: of

AERONET sites in each region, the AOD simulated with QFED2.4 were the highest and closest to AERONET and MISR observations, followed closely by FEER1.0. However, the QFED2.4 run tends to overestimate AOD in the region of SHSA, and the QFED2.4 BB emission dataset is tuned with the GEOS model. In contrast, the FEER1.0 BB emission dataset is derived in a more model-independent fashion and is more physical-based since its emission coefficients are independently derived at each grid box. Therefore, we recommend to choose the FEER1.0 BB emission dataset for aerosol-focused hindcast experiments in the two biomass-burning dominated regions in the southern hemisphere, SHAF and SHSA (as well as in other regions but with lower confidence). The differences between these six BB emission datasets are attributable to the approaches and input data used to derive BB emissions, such as whether AOD from satellite observations is used as a constraint, whether the approaches to parameterize the fire activities are based on burned area, FRP, or active fire count, and which set of emission factors is chosen.

Deleted: MODIS



## 1. Introduction

Biomass burning (BB) is estimated to contribute about 62% of the global particulate organic carbon (OC) and 27% of black carbon (BC) emissions annually (Wiedinmyer et al., 2011). Therefore, biomass burning emissions significantly affect air quality by acting as a major source of particulate matter (PM), and the climate system by modulating solar radiation and cloud properties. For instance, a number of studies have revealed that wildfire smoke exposure is harmful to human health by causing general respiratory morbidity and exacerbating asthma, because approximately 80–90% of the smoke particles produced by biomass burning fall within the PM<sub>2.5</sub> size range (PM with aerodynamic diameter less than 2.5 µm) (Reid et al., 2005, 2016). Moreover, biomass burning emissions have been shown to impact the atmospheric composition in different regions, such as South America (Reddington et al., 2016), Central America (Wang et al., 2006), sub-Saharan African region (Yang et al., 2013), Southeast Asia (Wang et al., 2013; Pan et al., 2018), Indo-China (Zhu et al., 2017), and Western Arctic (Bian et al., 2013). Additionally, BB-produced aerosols can also directly impact the upper troposphere and lower stratosphere via extreme pyro-convection events associated with intense wildfires that generate the storms injecting smoke particles and trace gases into high altitudes (e.g., Peterson et al., 2018). Therefore, emissions from biomass burning constitute a significant component of the climate system, and are crucial inputs required by chemical transport and atmospheric circulation models used to simulate the atmospheric compositions, radiation, and circulation processes needed for air-quality and climate-impact studies (e.g., van Marle et al., 2017).

With the advent of satellite remote sensing of active fire and burned area products in the last couple of decades, a number of global BB emission datasets based on these observations have become available (e.g., Ichoku et al., 2012). Six of such major BB datasets will be compared in this study, including three datasets based on burned area approaches, namely, the Fire INventory from NCAR (FINN, Wiedinmyer et al., 2011) and two versions of the Global Fire Emissions Database (GFED, van der Werf et al., 2006, 2010, 2017), and three datasets based on fire radiative power (FRP) approaches, namely, the Global Fire Assimilation System (GFAS, Kaiser et al., 2012) developed in the European Centre for Medium-Range Weather Forecasts (ECMWF), and two National Aeronautics and Space Administration (NASA) products, i.e., the Fire Energetics and Emissions Research algorithm (FEER, Ichoku and Ellison, 2014) and the Quick Fire Emissions Dataset (QFED, Darmenov and da Silva, 2015).

Although much progress has been made over the last couple of decades in improving the quality of BB emission datasets, for example, by incorporating more recent satellite measurements with better calibration and spatial resolution (e.g., van der Werf et al. 2010; 2017), biomass-burning aerosol emissions still have large uncertainty, and thus are still poorly constrained in models at global and regional levels (e.g., Lioussé et al., 2010; Kaiser et al., 2012; Petrenko et al., 2012, 2017; Bond et al., 2013; Zhang et al., 2014; Pan et al., 2015; Ichoku et al., 2016a; Reddington et al., 2016; Pereira et al., 2016). Specifically, large uncertainty exists in the description of the magnitude, patterns, and drivers of wildfires and types of biomass burning (e.g., Hyer et al., 2011). For instance, a global enhancement of particulate matter BB emission by a factor of 3.4 was

**Deleted:** Biomass burning (BB) is estimated to contribute about 62% of the global particulate organic carbon (OC) and 27% of black carbon (BC) emissions annually (Wiedinmyer et al., 2011), thereby significantly affecting, not only air quality by acting as a major source of particulate matter (PM), but also the climate system by modulating solar radiation and cloud properties.

**Deleted:** With the advent of satellite remote sensing of active fire and burned area products in the last couple of decades, a number of global BB emission datasets based on these observations have become available (e.g., Ichoku et al., 2012), for example, two BB datasets based on burned area approaches, namely, the Global Fire Emissions Database (GFED, van der Werf et al., 2006, 2010, 2017) and the Fire INventory from NCAR (FINN, Wiedinmyer et al., 2011), and three BB emissions datasets based on fire radiative power (FRP) approaches, namely, the Global Fire Assimilation System (GFAS, Kaiser et al., 2012), which was developed in the European Centre for Medium-Range Weather Forecasts (ECMWF), and two National Aeronautics and Space Administration (NASA) products, i.e., the Fire Energetics and Emissions Research algorithm (FEER, Ichoku and Ellison, 2014) and the Quick Fire Emissions Dataset (QFED, Darmenov and da Silva, 2015). The aforementioned BB datasets will be compared in this study.

**Deleted:** other

recommended for GFAS by Kaiser et al. (2012) to match the observed aerosol loading. [Andreae \(2019\)](#) commented that “In contrast to gaseous compounds, which are chemically well defined, aerosols are complex and variable mixtures of organic and inorganic species and comprise particles across a wide range of sizes. This affects in particular the measurements of organic aerosol, black/elemental carbon, and size fractionated aerosol mass”.

A recent analysis with multiple models has been conducted under the auspices of the Aerosol Comparisons between Observations and Models (AeroCom) Phase III biomass burning emission experiments using the GFED version 3.1 (GFED3.1) as input to several models (hereinafter, “[The AeroCom multi-model study](#)”, <https://wiki.met.no/aerocom/phase3-experiments>) (Petrenko et al., manuscript in preparation). [The AeroCom Multi-model study](#) concluded that the modelled aerosol optical depth (AOD) from different models exhibits large diversity in most regions, i.e. some models overestimate while other models underestimate. However, over two major biomass burning dominated regions, South America and southern hemisphere Africa, all models consistently underestimate AOD. This result suggests that the underestimation of AOD in these two regions was more likely attributable to the GFED3.1 biomass burning emission dataset rather than the model configurations.

Our study aims to explore multiple BB emission datasets, including GFED3.1, GFED version 4 with small fires (GFED4s), FINN version 1.5, GFAS version 1.2, QFED version 2.4, and FEER version 1.0, in order to investigate the discrepancies between these six BB emission datasets by comparing them at both regional and global levels. Such a comparative evaluation of BB emission datasets would show the differences between them as well as how these differences propagate through the physical processes of related aerosols in models, e.g., dry and wet deposition, transport, atmospheric abundance, and the resulting AOD. Our study is expected to provide further insight into the development of possible mitigation for the current large uncertainties in BB emissions. The similar comparative studies of multiple BB aerosol emission datasets have been previously conducted at regional scales, e.g., by Zhang et al. (2014) in the northern sub-Saharan African region, Pereira et al. (2016) in South America, and Reddington et al. (2016) in the entire tropical region. The current study not only provides for the first time a global assessment and analysis of these six BB emission datasets to provide a world-wide perspective, but also examines their performance within 14 regions (Fig. 1). The 14 regions were previously defined for a series GFED-based studies (e.g., Van der Werf et al., 2006, 2010, and 2017).

In the rest of this paper, we first describe these six BB emission datasets, the GEOS model configuration and experimental designs, and observations in Sect. 2, then we show comparisons of the biomass burning emissions datasets and the resulting model simulated AOD in Sect. 3. We discuss possible attributions of the differences between the six BB emission datasets to the sources of uncertainty associated with the biomass burning emissions and the aerosol modeling in Sect. 4. Conclusions and recommendations are presented in Sect. 5.

Formatted: Font color: Text 1

Formatted: Font color: Text 1

Formatted: Font color: Text 1

Formatted: Font color: Text 1

Formatted: Font color: Text 1

Deleted: of

Deleted: ,

Deleted: but

Deleted: at

Formatted: Font color: Text 1

Deleted: i

Deleted: from

Formatted: Font color: Text 1

Deleted: this

Deleted: (i.e., GFED3.1)

Deleted: such as

Deleted: The

Deleted: Such detailed diagnosis

Deleted: measures

Deleted: It is noted that

Formatted: Font color: Text 1

Deleted: ,

Formatted: Font color: Text 1

Deleted: while t

Formatted: Font color: Text 1

Formatted: Font color: Text 1

Deleted: of 14 sub-regions

Deleted: to

Formatted: Font color: Text 1

Deleted:

Formatted: Font color: Text 1

Deleted: d

Deleted: ed

Deleted: the

Deleted: among the

Deleted: ed

Deleted: the

Deleted: s

Deleted: , and

Deleted: as well as

Deleted: we

## 2. Methodology

### 2.1 Six BB emission datasets

General information about each of the six biomass burning emission datasets investigated in this study, namely GFED3.1, GFED4s, FINN1.5, GFAS1.2, FEER1.0, and QFED2.4, is given below. Their main attributes, such as their spatial and temporal resolutions, the methods used to estimate burned area (where applicable), the method to derive emission coefficients (where applicable), and the references ~~for~~ the emission factors, are compared in Table 1. Overall, all datasets provide daily global biomass burning emissions since 2003.

#### 2.1.1 GFED3.1

The total dry matter consumed ~~by~~ biomass burning in GFED3.1 (van der Werf et al., 2010) is estimated by the multiplication of the MODIS burned area product at 500-m spatial resolution (Giglio et al. 2010, for the MODIS era) and fuel consumption per unit burned area, the latter being the product of the fuel loads per unit area and combustion completeness. This estimation is conducted using the Carnegie–Ames–Stanford approach (CASA) biogeochemical modeling framework that provides estimates of biomass in various carbon “pools” including leaves, grasses, stems, coarse woody debris, and litter. Fuel loads in CASA are estimated according to carbon input information on vegetation productivity, and carbon outputs through heterotrophic respiration, herbivory, fires, and tree mortality (Giglio et al., 2010; van der Werf et al., 2010). Then, the biomass burning emission of a ~~given~~ species is calculated by multiplying the total consumed dry matter with an emission factor of that species (*EF*, with a unit of g species per kg dry matter burned). ~~The *EF* used in GFED3.1 (and most of the other datasets) is mainly chosen from Andreae and Merlet (2001) and/or Akagi et al. (2011), but may also be obtained from various other sources.~~ The GFED3.1 dataset can be accessed through the link: [https://daac.ornl.gov/VEGETATION/guides/global\\_fire\\_emissions\\_v3.1.html](https://daac.ornl.gov/VEGETATION/guides/global_fire_emissions_v3.1.html).

#### 2.1.2 GFED4s

Compared to GFED3.1, the latest GFED version, GFED4s, has a few significant upgrades as described in detail by van der Werf et al. (2017), including (1) additional burned area associated with small fires which were previously omitted by the burned area product but now are compensated by including the active fires to augment the burned area product MCD64A1 (Giglio et al., 2013; Randerson et al., 2012); (2) a revised fuel consumption parameterization optimized using field observations (e.g., van Leeuwen et al., 2014); (3) partitioning of the extratropical forest category into temperate and boreal forests; (4) further dividing forest into temperate and boreal forest ecosystems and applying different sets of emission factors. Among the existing BB emission datasets, GFED4s has hitherto been the most widely used by modeling communities, such as the Coupled Model Intercomparison Project phase 6 (CMIP6, Van Marle et al., 2017) and AeroCom phase 3 experiment (<https://wiki.met.no/aerocom/phase3-experiments>). The link to the GFED4s dataset is <http://www.globalfiredata.org>.

#### 2.1.3 FINN1.5

The FINN1.5 biomass burning emission dataset is developed from its previous version FINN1 (Wiedinmyer et al., 2011) with several updates. It uses satellite observation of

Deleted: of

Deleted: from

Deleted: ; Randerson et al., 2012

Deleted: certai

Deleted: is applicable to other BB emission datasets as well but may be from various sources,

Deleted: Among the existing BB emission datasets, GFED3.1 has hitherto been the most widely used by modeling communities, such as by the Coupled Model Intercomparison Project (CMIP, Van Marle et al., 2017) and AeroCom (Petrenko 2017).

Formatted: Font color: Text 1

Formatted: Font color: Text 1

active fire (with confidence level greater than 20%) and land cover from the MODIS instruments onboard the NASA Terra and Aqua polar orbiting satellites, together with the estimated fuel consumption to derive biomass burning emissions. The burned area in each active fire pixel is assumed as 1 km<sup>2</sup>, except for grasslands and savannas where it is assigned a value of 0.75 km<sup>2</sup>. The fuel consumption at each fire pixel is estimated according to its generic land use/land cover type (LULC) which is assigned using values updated from Table 2 of Hoelzemann et al. (2004) in the various world regions based on Global Wildland Fire Emission Model (GWEM). With the estimated burned area, fuel consumption, and *EF* of individual species, the daily global open biomass burning emissions of each species are then calculated at a 1 km spatial resolution. The FINN1.5 emissions dataset is archived at: <http://bai.acom.ucar.edu/Data/fire/>.

#### 2.1.4 GFAS1.2

The GFAS1.2 (Kaiser et al., 2012) estimates biomass burning emission rates by multiplying FRP with the conversion factors (Units: kg species per MJ). The global distribution of FRP observations are obtained from the MODIS instruments onboard the Terra and Aqua satellites and then are assimilated into the GFAS system. The gaps in FRP observations, which are mostly due to cloud cover and spurious FRP observations of volcanoes, gas flares and other industrial activity, are corrected or filtered in the GFAS system. Eight biome-specific conversion factors are calculated by linear regressions between the GFAS FRP and the dry matter combustion rate of GFED3.1 in each biome (see Table 2 and Fig. 3 in Kaiser et al., 2012). Therefore, the biomass burning emission calculated by GFAS1.2 is close to that of GFED3.1. Then the biomass burning emission from a certain aerosol species is converted by multiplying the total consumed dry matter with the *EF* of that species. More information on the latest GFAS product can be found at <https://confluence.ecmwf.int/display/CKB/CAMS++Global+Fire+Assimilation+System+%28GFAS%29+data+documentation>.

#### 2.1.5 FEER1.0

The FEER1.0 (Ichoku and Ellison, 2014) multiplies its emission coefficients  $C_e$  (Units: kg species per MJ) with MODIS FRP data that have been preprocessed and gridded in the GFAS1.2 analysis system (Kaiser et al., 2012) to derive aerosol biomass burning emission rates. The  $C_e$  in FEER1.0 for smoke aerosol total particulate matter (TPM) is derived through zero-intercept regression of the emission rate of smoke aerosol (i.e.,  $R_{sa}$ ) against the corresponding FRP (Ichoku and Kaufman, 2005; Ichoku and Ellison, 2014) at pixel-level within each grid.  $C_e$  corresponds to the slope of the linear regression fitting. In the FEER methodology,  $R_{sa}$  is estimated through a spatio-temporal analysis of MODIS AOD data along with wind fields from the NASA Modern-Era Retrospective Analysis for Research and Applications (MERRA) reanalysis dataset (Rienecker et al., 2011). The smoke aerosol  $C_e$  in FEER1.0 is available at 1°×1° spatial resolution global grid, and covers most of the land areas where fires have been detected by MODIS for at least 30 times during the period 2003–2010 (Ichoku and Ellison, 2014) to ensure statistical representativeness. In the current version of FEER1.0 emission dataset,  $C_e$  for other smoke constituents, say OC, at each grid cell are obtained by scaling the  $C_e$  of smoke aerosol according to the ratio of their emission factors, such as  $EF_{oc}$  to  $EF_{sa}$  (i.e., ratio of

Formatted: Font color: Text 1

Formatted: Font color: Text 1

Deleted: eight biome-specific

Deleted: which were previously found to link FRP with the fuel combustion rate (Wooster et al., 2005) and smoke aerosol emission rate quantitatively (Ichoku and Kaufman, 2005).

Deleted: In GFAS1.2,

Deleted: t

Deleted: is

Deleted: (Kaiser et al., 2012)

Deleted: The e

Deleted: .

Deleted:

[https://confluence.ecmwf.int/display/CKB/CAMS++Global+Fire+Assimilation+System+\(GFAS\)+data+documentation](https://confluence.ecmwf.int/display/CKB/CAMS++Global+Fire+Assimilation+System+(GFAS)+data+documentation). The GFAS1.2 dataset can be downloaded at <https://apps.ecmwf.int/datasets/data/cams-gfas/>.

Formatted: Font color: Text 1

Formatted: Font color: Text 1

Formatted: Font color: Text 1

Formatted: Font color: Text 1

Deleted: uses

Deleted: from

Deleted: multiplied by emission coefficient  $C_e$  (Units: kg species per MJ)

Deleted: ; however, the way how  $C_e$ , which is known as scaled conversion factor in GFAS1.2 (by Kaiser et al., 2012), is derived in FEER1.0 is more sophisticated than that in GFAS1.2

Deleted: (Kaiser et al., 2012)

Formatted: Font color: Text 1

Formatted: Font color: Text 1

Formatted: Font color: Text 1

Formatted: Font color: Text 1

emission factor for OC to that for total smoke aerosol). The FEER1.0 dataset is available at <http://feer.gsfc.nasa.gov/data/emissions/>.

#### 2.1.6 QFED2.4

The earlier version of QFED (Darmenov and da Silva 2015) estimated biomass burning emissions by multiplying level 2 MODIS FRP with an emission coefficient  $C_e$  which is the product of the initial constant value  $C_0$  (1.37 kg per MJ, reported by Kaiser et al., 2009) and a scaling factor, with the scaling factor calculated by regressing the carbon monoxide (CO) BB emission (product of FRP,  $C_0$  and CO emission factor) to that in the GFED version 2. The scaling factor used by the QFED 2.4, the version used in this study, was obtained by further regressing the Goddard Earth Observing System (GEOS) Model simulated AOD to the MODIS AOD in 46 sub-regions, and then the resulting scaling factors in the 46 sub-regions were aggregated into four major fire-prone biomes, i.e., savanna, grassland, tropical forests, and extratropical forests, as values of 1.8, 1.8, 2.5, and 4.5, respectively. The QFED2.4 also used a sequential model with temporally damped emissions to estimate the emissions in cloudy areas. The real-time QFED2.4 fire emission is produced on a daily basis and used in the operational GEOS data assimilation system. In addition to the near real-time emissions, a longer historical record dataset, which is what we have used, is stored at <https://portal.nccs.nasa.gov/datashare/ies/a/aerosol/emissions/QFED/v2.4r6/>.

## 2.2 Application of the BB emission datasets in the NASA GEOS model

### 2.2.1 Description of the NASA GEOS model

The GEOS model consists of an atmospheric general circulation model, a catchment-based land surface model, and an ocean model, all coupled together using the Earth System Modeling Framework (ESMF, Rienecker et al., 2011; Molod et al., 2015). Within the GEOS model architecture, several interactively coupled atmospheric constituent modules have been incorporated, including an aerosol and carbon monoxide (CO) module based on the Goddard Chemistry Aerosol Radiation and Transport model (GOCART, Chin et al., 2000, 2002, 2009, 2014; Colarco et al., 2010; Bian et al., 2010) and a radiation module from the Goddard radiative transfer model (Chou and Suarez, 1999; Chou et al., 2001). The GOCART module used in this study includes representations of dust, sea salt, sulfate, nitrate, and black and organic carbon aerosol species. A conversion factor of 1.4 is used to scale organic carbon mass to organic aerosol (OA), which is on the low end of current estimates (Simon and Bhawe, 2012).

In this study the GEOS model (Heracles-5.2 version) was run globally on a cubed-sphere horizontal grid (c180, ~50 km resolution) and with 72 vertical hybrid-sigma levels extending from the surface to ~85 km for the year 2008. The model was run in a “replay” mode, where the winds, pressure, moisture, and temperature are constrained by the MERRA-2 reanalysis meteorological data (Gelaro et al., 2017), a configuration that allows a similar simulation of real events as in a traditional off-line chemistry transport model (CTM) but exercises the full model physics for, e.g., radiation, and moist physics processes. We used the HTAP2 anthropogenic emissions (Janssens-Maenhout et al., 2015) that provides high-spatial resolution monthly emissions. The BB emissions are

Field Code Changed

Formatted: None

Deleted: also maintained based on data from the MODIS Adaptive Processing System (MODAPS) Service (<http://modaps.nascom.nasa.gov/services/>)

Formatted: Font color: Text 1

Formatted: Font color: Text 1

Formatted: Font color: Auto



uniformly distributed within the boundary layer without considering the specific injection height of each plume. All six BB emissions are daily emissions with the diurnal cycle prescribed in the model: the maximum is around local noon, which is more prominent in the tropics, and is gradually weakened in the extra-tropics (Randles et al., 2017). The natural aerosols are either generated by the model itself (i.e., wind-blown dust and sea salt) or from prescribed emission files (i.e., volcanic and biogenic aerosols).

## 2.2.2 Experiment design

In order to investigate the sensitivity of the modelled AOD to different BB emission datasets, seven experiments were conducted with the GEOS model, differing only in the source of biomass burning emissions. The first six runs are GFED3.1, GFED4s, FINN1.5, GFAS1.2, FEER1.0, and QFED2.4, using the corresponding biomass burning datasets described above in Section 2.1. A seventh run is called “NOBB,” where the model is run without including biomass burning emissions.

## 2.4. AOD Observations

### 2.4.1 MISR retrievals

We evaluated the simulated monthly AOD with the half-degree monthly level 3 Multiangle Imaging SpectroRadiometer version 23 (MISR v23, with the filename tagged as F15\_0032) total AOD data at 558 nm wavelength on board the EOS-Terra satellite (Kalashnikova and Kahn, 2006; Kahn et al., 2010). The data can be downloaded from the website: [https://eosweb.larc.nasa.gov/project/misr/mil3mae\\_table](https://eosweb.larc.nasa.gov/project/misr/mil3mae_table).

### 2.4.2 AERONET sites

We also evaluated the modelled 3 hourly and monthly AOD at 550nm and Angström Exponent (AE, 440–870 nm) with that from the ground-based AErosol RObotic NETwork (AERONET, Holben et al., 1998) sites situated in biomass burning source regions. AERONET Version 3 Level 2.0 data, which are cloud-screened and quality-assured aerosol products with a 0.01 uncertainty (Giles et al., 2019), were used in this study. The data can be downloaded from the websites: [https://aeronet.gsfc.nasa.gov/new\\_web/download\\_all\\_v3\\_aod.html](https://aeronet.gsfc.nasa.gov/new_web/download_all_v3_aod.html). The AERONET AOD at 550nm is interpolated from the measurements at 440 and 675nm. AE is calculated with AOD at 440 and 870nm. We compared model simulations with AERONET data at 14 selected sites, each representing the spatiotemporal characteristics at different biomass burning regions shown in Fig. 1. The 14 regions are defined previously by the GFED studies (e.g., Van der Werf et al., 2006, 2010, and 2017). Since some regions, such as Northern Hemisphere South America (NHSA) and Equatorial Asia (EQAS), have no AERONET sites with data measured in 2008, we also used the average of multiple years or climatology of AERONET AOD at each site for reference. Locations of these 14 selected AERONET sites are represented by the numbered magenta dots in Fig. 1.

## 3. Results

### 3.1 Inter-comparison of the six biomass burning emission datasets

The biomass burning OC emissions were compared throughout this study, since OC is the major constituent in fresh biomass burning smoke particles, with mass fractions ranging

Deleted: ODIS

Formatted: Font color: Text 1

Formatted: Font color: Text 1

Formatted: Font color: Text 1

Formatted: Font color: Text 1

Formatted: Font color: Text 1

Deleted: We

Formatted: Font color: Text 1

Deleted: used the AOD retrieved from the MODIS collection 6 products from both the Terra and Aqua satellites with the combination of Dark Target (DT) aerosol algorithm (Remer et al., 2005; Levy et al., 2010), which was designed for aerosol retrievals over dark land (mostly vegetated) and ocean surfaces in the visible (VIS) to shortwave infrared (SWIR) parts of the spectrum, and the Deep Blue aerosol algorithm (Sayer et al., 2014), which was designed for aerosol retrieval over bright surfaces (e.g., desert).

Formatted: Font color: Text 1

Deleted: Angstrom

Formatted: Font color: Text 1

Formatted: Font color: Text 1

Formatted: Font color: Text 1

Deleted: Angstrom Exponent (

Deleted: )

Deleted: that

Formatted: Font color: Text 1

Deleted: i.e., Northern Hemisphere South America (NHSA) and Equatorial Asia (EQAS),

Deleted: thus

Deleted: show

Deleted: OC

from 37% to 67% ~~subject to~~ fuel type (e.g., grassland/savanna, forests, or others), according to various studies based on thermal evolution techniques (Reid et al., 2005, part II, Table 2). These inter-comparisons were carried out in terms of both annual and seasonal variations in Sect. 3.1.1 and Sect. 3.1.2, respectively.

### 3.1.1 Annual total

Figure 2 shows the spatial distributions of annual total biomass burning OC emissions in 2008 from the six BB emission datasets. The ~~regions with high emission of OC~~ in Africa, boreal Asia, and South America were pronounced in all six BB emission datasets, albeit to different degrees. The regional differences of the annual ~~total~~ biomass burning OC emissions in different BB emission datasets can be appreciated more quantitatively in Fig. 3. Relevant statistics for the six BB emission datasets in the 14 regions ~~are~~ also listed at the top of the panel ~~in Fig. 3~~, with the mean averaged over the six BB emission datasets in the first row (*mean*). We used three different measures to quantify the spread of ~~the annual total from~~ the six BB emission datasets: (1) standard deviation (*std*), (2) ratio of maximum to minimum (*max/min*), and (3) the coefficient of variation (*cv*, defined as the ratio of the *std* to the *mean*). The rank of *cv* for each of the 14 regions ~~is~~ also listed in Fig. 3 (e.g., a ranking of 1 means that this region shows the least spread among the six BB emission datasets, while a ranking of 14 indicates that this region has the largest spread). The best agreements among the six emission datasets occurred in Northern Hemisphere Africa (NHAF), Equatorial Asia (EQAS), Southern Hemisphere Africa (SHAF), and Southern Hemisphere South America (SHSA), which have the top *cv* ranks (1-4) and relatively low *max/min* ratio (a factor of 3-4). The worst agreements occurred in ~~the~~ Middle East (MIDE), Temperate North America (TENA), Boreal North America (BONA) and Europe (EURO), which have the bottom *cv* ranks (14-11) and large *max/min* ratio (a factor of 66-10). This diversity was mostly driven by the QFED2.4 emission dataset, which estimated the largest emission amount for almost all regions (except EQAS), especially in MIDE where ~~the~~ BB emission from QFED2.4 is more than 50 times higher than ~~those from the two GFED versions~~. Globally, the QFED2.4 dataset showed the highest OC emission of 51.93 Tg C in 2008, which was nearly four times that of GFED4s ~~at~~ 13.76 Tg C (the lowest among the six BB datasets).

Overall, two FRP-based BB emissions, QFED2.4 and FEER1.0, were a factor of 2-4 larger than ~~the~~ other BB datasets. ~~This result~~ is consistent with the findings of Zhang et al. (2014) over sub-Saharan Africa. It is worth noting that the BB emission amount of GFAS1.2 was close to that of GFED3.1, ~~reflecting the fact~~ that GFAS1.2 is tuned to GFED3.1 (described in Sect. 2.1.4). Globally, FINN1.5 yielded more OC emissions than the two GFED and GFAS1.2 datasets (e.g., 40% larger than GFED4s). Regionally, FINN1.5 was generally comparable to the two GFED datasets in most ~~of the~~ regions, but was higher than them in the tropical regions, such as EQAS, Southeast Asia (SEAS), Central America (CEAM) and ~~Northern Hemisphere South America (NHSA)~~. Interestingly, FINN1.5 was even the largest among all six datasets over ~~the~~ EQAS region, which might be associated with its assumption of continuation of burning into the second day ~~in that region~~ (to be discussed in section 4.1.2). The global OC emissions from GFED4s were lower than those from its GFED3.1 counterpart, although higher in several ~~other~~ regions, such as TENA, CEAM, NHSA, Boreal Asia (BOAS) and Central Asia

- Deleted: ,
- Deleted: depending on
- Deleted:
- Formatted: Font color: Text 1
- Deleted:
- Formatted: Font color: Text 1
- Deleted: OC
- Deleted: hot spots
- Formatted: Font color: Text 1
- Formatted: Font color: Text 1
- Deleted: OC
- Formatted: Font color: Text 1
- Formatted: Font color: Text 1
- Deleted: we
- Deleted: in Fig. 3
- Formatted: Font color: Text 1
- Deleted: annual
- Formatted: Font color: Text 1
- Deleted: of the annual mean
- Deleted: wa
- Formatted: Font color: Text 1
- Deleted: at
- Deleted: other emission datasets
- Deleted: of
- Deleted: ,
- Deleted: which
- Deleted:
- Deleted: confirm
- Deleted: the
- Deleted: NHSA
- Deleted: the
- Deleted: (i.e., the Tropical Asia)
- Deleted: over there
- Deleted: they
- Deleted: Central America (
- Deleted: )
- Deleted: Northern Hemisphere South America (
- Deleted: )

(CEAS). Possible explanations for these differences among the six global BB emissions datasets are provided in Sect. 4.1.

### 3.1.2 Seasonal variation

Biomass burning is generally characterized by distinct seasonal variations in each of the 14 regions and globally, as shown in Fig. 4. Overall, there were four peak fire seasons across the regions: (1) During the boreal spring (March-April-May), fires peak in BOAS mainly because of forest fires (see the contribution of different fire categories in Table 3 of van der Werf et al., 2017), in CEAM, NHSA, and SEAS because of savanna and deforestation fires, and in Central Asia (CEAS) mainly due to the agricultural waste burning to prepare the fields for spring crops. (2) During the boreal summer (June-July-August), fires peak in BONA and TENA, mostly due to wildfires that occur under the prevailing dry and hot weather, in EURO probably associated with the burning of agricultural waste. In addition, we found that fire peaked in MIDE in three FRP-based datasets, i.e., QFED2.4, FEER1.0 and GFAS1.2. It might be associated with the failure to filter out the gas flares from the FRP fire product, in particular in QFED2.4 (Darmenov and da Silva 2015). (3) During the austral spring (September-October-November), fires peak in the southern hemispheric regions of SHSA, SHAF and AUST, associated with savanna burning (in addition to deforestation fires in SHSA). In SHSA, two GFED versions peaked in August, one month early than the rest. (4) During the boreal winter (December and January), fires peak in NHAF, particularly along the sub-Sahel belt (Fig. 2), where savanna fires are associated with agricultural management and pastoral practices across that region (e.g., Ichoku et al., 2016b). Overall, all six BB emission datasets exhibited similar seasonal variations, although they differed in magnitude. In particular, it is noteworthy that in EQAS, the annual OC emissions from GFED4s was lower than that of GFED3.1 by 18%, but higher by a factor of two in the month of August when peatland burning is predominant.

For reference, biomass burning black carbon (BC) emissions were also shown, but in the supplement (Fig. S1, S2 for annual total and Fig. S3 for seasonal variation), which exhibited similar features as OC. The amounts of biomass burning BC emission were almost proportional to their OC counterparts (about 1/10 to 1/15 of OC).

### 3.2 Comparison of model-simulated AOD with remote sensing data

As in other similar situations where several different datasets are available to be chosen from (e.g. Bian et al., 2007), a question that invariably comes to mind is: which BB emission dataset is the most accurate or should be used in a given situation? In fact, it is difficult to give a conclusive answer, as it is often challenging to measure the emission rate of an active fire in real time or to disentangle the contribution of smoke aerosols from the total atmospheric aerosol loading/concentration in observations. Therefore, in this study we have implemented all six global BB emission datasets separately in the GEOS model, and evaluated their respective simulated aerosol loadings. More specifically, we compared the simulated AOD with the satellite-retrieved AOD data from MISR (primarily to examine the spatial coverage) as well as with ground-based measurements from AERONET sites near biomass burning source regions to examine the seasonal variation. Our analysis was focused on the regional biomass burning peak

Deleted: sub-

Deleted: SEAS,

Deleted: and

Formatted: Font color: Text 1

Deleted: , and

Formatted: Font color: Text 1

Deleted: , although the seasonal maximum in QFED may have been

Formatted: Font color: Text 1

Deleted: significantly influenced by

Formatted: Font color: Text 1

Formatted: Font color: Text 1

Deleted: emissions

Deleted: from

Formatted: Font color: Text 1

Deleted: and other activities

Formatted: Font color: Text 1

Formatted: Font color: Text 1

Deleted: April

Deleted: by a factor of two

Deleted: mean

Formatted: Font color: Text 1

Deleted: evaluated the simulated aerosol loading associated with each BB emission dataset instead

Deleted: MODIS

Formatted: Font color: Text 1

Formatted: Font color: Text 1

Deleted: during

seasons, when smoke aerosol emissions dominate those from other sources, such as pollution or dust. With such an effort to evaluate the sensitivity of the simulated AOD to the different BB emission datasets, the results from this study may shed some light on answering the aforementioned question, i.e., which BB dataset is the most accurate or should be used in a given situation? We acknowledge that although the result from a particular model (e.g., GEOS in this case) can potentially introduce additional uncertainty through various complicated and non-linear procedures employed to calculate the AOD, such as the modelled relative humidity and the related aerosol's hygroscopic growth (Bian et al., 2009; Pan et al., 2015), still, evaluation of the model-simulated AOD has proven to be a feasible approach to compare various BB emission datasets in reference to the currently available observations (e.g., Petrenko et al. 2012; Zhang et al., 2014).

Aiming to evaluate the sensitivity of the modelled AOD to different BB emissions datasets, we compared the spatial distribution of the GEOS model-simulated AOD with MISR-retrieved AOD in Sect. 3.2.1 and with the AERONET measured AOD at 14 AERONET sites in Sect. 3.2.2. We also conducted an in-depth study at two AERONET sites, Alta Floresta (in the southern hemisphere South America, SHSA) and Mongu (in the southern hemisphere Africa, SHAF), as discussed in Sect. 3.3.

### 3.2.1 Global spatial distribution

Comparisons for September and April in 2018 are shown in Fig. 5 and Fig. 6 respectively, representing the peak biomass burning months in the southern hemisphere, and many regions in the northern hemisphere, respectively. The MISR AOD is displayed on the top left panel and the model biases (model minus MISR) from seven individual experiments are shown on the rest of panels.

In September 2008, the high AOD observed from MISR (Fig. 5a) in the southern hemisphere was mostly attributable to biomass burning. A large fraction of the southern hemisphere Africa (SHAF) were featured with high AOD (greater than 0.5). The area-averaged AOD over the entire SHAF was 0.331 (see Table S1 for the area-averaged MISR AOD in each region). The observed AOD peaked in the southern Congo (nearly 1.0) and gradually decreased westwards. Large negative model bias (-0.283) was found in the NOBB run over the region of SHAF (greenish shading in Fig. 5b; see Table S1 for the area-averaged model biases in each region). The negative bias was reduced most significantly in the QFED2.4 run (see Fig. 5h), to -0.044, followed by the FEER1.0 run (see Fig. 5g), to -0.079, but the least in GFED4s and GFAS1.2 (see Fig. 5d and f, respectively), still as large as -0.208.

In the southern hemisphere South America (SHSA), where the area-averaged MISR AOD was 0.188, the maximum AOD was ~0.7 in the central Brazil (Fig. 5a). The negative bias averaged over SHSA was a value of -0.132 in the NOBB run (Fig. 5b). It was reduced most significantly in the FEER1.0 run to -0.021 (Fig. 5g), but overcorrected in the QFED2.4 run to 0.020 (see reddish shading in Fig. 5h). The reduction of negative bias was the least again in the GFED4s run (Fig. 5d) and the GFAS1.2 run (Fig. 5f), still as large as -0.081 and -0.080, respectively.

Deleted: s

Deleted: focusing on

Formatted: Font color: Text 1

Deleted: OE

Formatted: Font color: Text 1

Deleted: MODIS

Formatted: Font color: Text 1

Formatted: Font color: Text 1

Deleted: N

Formatted: Font color: Text 1

Deleted: ing

Deleted: hemisphere and

Formatted: Font color: Text 1

Deleted: MODIS-Aqua

Deleted: relative to it

Deleted: MODIS

Formatted: Font color: Text 1

Deleted: other

Formatted: Font color: Text 1

Deleted: in each of the two cases

Formatted: Font color: Text 1

Formatted: Font color: Text 1

Formatted: Font color: Text 1

Deleted: In September 2008, the high AOD observed from MODIS-Aqua (i.e., MODIS-a) in the Southern hemisphere (Fig. 5a) was mostly attributable to biomass burning. The observed AOD peaked in the region of SHAF with an area-averaged value as of 0.351 (see the area-averaged value for each region in Table S1) and the adjacent eastern South Atlantic Ocean (>1.0), and gradually decreased westwards. The observed AOD was 0.199 averaged over SHSA with a maximum value of nearly 0.4 in western Brazil (Fig. 5a). Large negative biases of -0.301 and -0.140 in the regions of SHAF and SHSA, respectively, are found in the NOBB run (see Fig. 5b, Table S1 shows the area-averaged values). These negative biases were reduced to the largest degree most significantly in the QFED2.4 run, i.e., to -0.059 and 0.004 in these two regions, respectively (See Fig. 5h), followed by the FEER1.0 run to -0.094 and -0.034 respectively (Fig. 5g). The reductions of negative biases were the least in GFED4s, only to -0.226 and -0.093, respectively (Fig. 5d), followed by GFAS1.2 (Fig. 5f).



Being mixed with and often surpassed by other aerosol types, however, the contribution of biomass burning aerosols to the total AOD is hardly distinguishable from those of other sources in the peak months in certain regions, such as April (Fig. 6) in the regions of Southeast Asia (SEAS), Central Asia (CEAS), and Boreal Asia (BOAS). Such complicated situations lead to the difficulties in evaluating the BB emission datasets with the AOD observations, in particular when the background AOD represented by the NOBB run was already overestimated in latter two regions.

### 3.2.2 Seasonal variations of AOD at AERONET sites

In order to better quantify the sensitivity of the simulated AOD to the six different BB emission datasets, we further compared the simulated monthly AOD with the ground-based AOD observations from AERONET stations by choosing one representative station in each region (see Fig. 7, and the panels representing the AERONET stations in Fig. 7 were arranged in a way that their placements correspond to those of their respective regions in Fig. 4 for easy reference). The exception is in two regions NHSA and EQAS, where there are no valid AERONET observations during 2008. Thus, we used the multi-year climatology of AOD at Medellin and Palangkaraya to represent NHSA and EQAS, respectively. We also included the climatology of AERONET AOD in the other 12 AERONET sites for reference. As shown in Fig. 7, the annual cycle of AOD in 2008 at available sites (brown thin bars) were similar to their respective climatology (light gray thick bars) to within 0.05. The MISR AOD was plotted for reference as green diamond. In this section, the modelled monthly mean AOD was calculated by averaging over the modelled instantaneous AOD in each month; while the monthly AOD of AERONET and MISR are simply calculated by averaging over available observations in each month.

Contributions from non-BB emissions to the total AOD are represented by NOBB experiment (black line in Fig. 7). Runs with different BB emission datasets showed almost identical AOD during non-biomass burning seasons at each selected AERONET station in each region, thereby allowing their differences to be noticeable during the biomass burning peak seasons. At Alta Floresta in Brazil (Fig. 7.5), Mongu in Zambia (Fig. 7.9), and Chiang Mai Met Sta in Thailand (Fig. 7.12), where the biomass burning emissions dominated the peak AOD, almost all experiments underestimated AOD during the respective peak biomass burning seasons. However, the fact is that the contribution of non-BB AOD was usually more than that of BB AOD during the burning seasons at most of the selected AERONET sites, except at three sites above. Therefore, it is difficult to disentangle the effect of biomass burning on the total AOD in most situations, especially when the model has difficulty representing the non-BB AOD, leading, for example, to overestimation at three high-latitude ( $> 55^{\circ}\text{N}$ ) AERONET sites (the three panels in the top row of Fig. 7), i.e., Fort McMurray in Canada (Fig. 7.1), Toraverre in Estonia (Fig. 7.6), and Moscow MSU MO in Russia (Fig. 7.10). However, it is apparent that the simulated AOD with QFED2.4 were overestimated during October and November at Fort McMurray in USA, indicating that QFED2.4 overestimated BB organic carbon emission during these two months. In general, at most of AERONET sites, the simulated AOD based on QFED2.4 were the highest and closest to AERONET AOD during the

**Deleted:** In April 2008 (Fig. 6), biomass burning emissions peaked in the regions of Southeast Asia (SEAS), Central Asia (CEAS), Boreal Asia (BOAS), Central America (CEAM), and Northern Hemisphere South America (NHSA). FINN1.5 and QFED2.4 had the best agreement with MODIS-a in regions of SEAS and CEAM (see Table S1). ...eing mixed with,...and often surpassed by, ... [1]

**Formatted:** ... [2]

**Deleted:** , however, the contribution of biomass burning aerosols to the total AOD are hardly distinguishable in this month, especially if the simulated background AOD in NOBB (simulation without biomass burning emission) was already biased high relative to MODIS (e.g., in EURO-Europe).

**Formatted:** Font color: Text 1

**Deleted:** occurred during most of other months (not shown),...leading...to the difficulties in evaluating the BB emission datasets with the AOD observations, in particular when the background AOD represented by the NOBB run was already overestimated in latter two regions.. ... [3]

**Formatted:** Font color: Text 1

**Deleted:** (country indicated in parentheses)

**Deleted:** with its country of origin indicated in parentheses

**Formatted:** Font color: Text 1

**Deleted:** ).

**Formatted:** ... [4]

**Deleted:** , ... Tt ... [5]

**Formatted:** Font color: Text 1

**Deleted:** MODIS-t (Terra) and MODIS-a (Aqua)...ISR [6]

**Deleted:** In general, r

**Deleted:** leav

**Deleted:** The larger spread of the seven runs at each ... [7]

**Formatted:** Font color: Text 1

**Deleted:** Meanwhile... the fact is that contributions from [8]

**Formatted:** Font color: Text 1

**Deleted:** of

**Deleted:** M...del simulations ...asd...difficulty ... [9]

**Formatted:** ... [10]

**Deleted:** almost year around... i.e., Fort McMurray in [11]

**Formatted:** Font color: Text 1

**Deleted:** EURO

**Formatted:** Font color: Text 1

**Deleted:** BOAS (three panels in the top row of Fig. 7)

**Formatted:** Font color: Text 1

**Deleted:** apparently

**Formatted:** Font color: Text 1



corresponding peak of the biomass burning seasons, followed by FEER1.0 and FINN1.5, and then GFED3.1, GFEDv4 and GFAS1.2.

### 3.3 Case studies in biomass burning dominated regions

In order to investigate the relationship between AOD and biomass burning emission in the context of daily variation, we focused on two AERONET stations, namely, Alta Floresta in Brazil and Mongu in Zambia during September, for the in-depth analysis in this section. Biomass burning emissions are known to be dominant at such locations and month as estimated by Chin et al. (2009), who found that 50-90% of the AOD was attributable to biomass burning emissions according to GOCART model simulations. Based on other previous studies also, e.g., Pereira et al. (2016) in southern hemisphere South America, Reddington et al. (2016) in tropical regions including southern hemisphere South America and Africa, and the AeroCom Multi-model study lead by Dr. Petrenko mentioned earlier in the introduction part, there appears to be a general consensus that the simulated AOD is consistently underestimated over southern hemisphere South America and Africa in many models with different BB emission datasets. In this study, we calculated the 3-hourly AOD by sorting the instantaneous AOD from both AERONET and model outputs for each day into eight time-steps, namely, 0, 3, 6, 9, 12, 15, 18, and 21Z. The modelled monthly mean AOD was calculated by averaging over the modelled 3-hourly AOD, which coincided with 3-hourly AERONET AOD in that month. The detailed analyses are discussed below.

#### 3.3.1 Alta Floresta in Brazil (Southern Hemisphere South America)

The monthly averaged AOD observed from AERONET at Alta Floresta is 0.47 during September 2008 (Fig. 8a). It shows that the simulated AOD from all six experiments captured the sustained aerosol episode observed in the AERONET dataset during September 13-14 (AOD about 1.0-1.5). The simulation with QFED2.4 BB emission produced the closest agreement with the AERONET-observed AOD with an average ratio of 1.00. In contrast, the simulated AOD with FEER1.0 (ratio=0.73), FINN1.5 (ratio=0.55), GFAS1.2 (ratio=0.42), GFED3.1 (ratio=0.40), and GFED4s (ratio=0.36) tended to underestimate for most of the time. All experiments showed relatively low skill of capturing the temporal variability of the observed AOD at Alta Floresta (corr=0.24-0.60). The Angström Exponent (AE; an indicator of particle size) from AERONET is 1.66 (not shown), indicating that small particles, most likely those from smokes, dominated the total aerosol loading at Alta Floresta (Eck et al., 2001). All experiments matched the observed AE (not shown).

The OC column mass loading (Fig. 8b) resembled the corresponding AOD (Fig. 8a), implying that the day-to-day variation of OC column mass loading in this dry season dominates the change of AOD in the model, rather than other factors such as relative humidity (RH). The OC column mass loading is determined by the regional scale of emission, transport, and removal processes of aerosols, the latter two processes of which are the same across the six experiments given the same model configurations were used. Therefore, the differences of OC column mass loading and thus AOD across the six experiments are attributed to the different choices of biomass burning emission datasets. Figure 8c shows the local biomass burning OC emissions in different biomass burning

- Deleted: during September... we focused on two AERONET stations, namely, Alta Floresta in BrazilSHSA [12]
- Deleted: SHAF
- Formatted: Font color: Text 1
- Formatted: Font color: Text 1
- Deleted: in the context of daily variation during September... Biomass burning emissions are known to be [13]
- Deleted: , based on
- Deleted: using a
- Formatted: Font color: Text 1
- Deleted: SHSA
- Formatted: Font color: Text 1
- Deleted: ,
- Deleted: and
- Formatted: Font color: Text 1
- Deleted: SHSA and SHAF
- Formatted: Font color: Text 1
- Deleted: these two regions
- Formatted: Font color: Text 1
- Deleted: W
- Formatted: Font color: Text 1
- Deleted: on
- Deleted: In this section, ...t ... [14]
- Formatted: Font color: Text 1
- Formatted ... [15]
- Deleted: . Figure 8a
- Formatted: Font color: Text 1
- Deleted: in the middle of September, on
- Deleted: emissions
- Formatted: Font color: Text 1
- Moved (insertion) [1]
- Deleted: , with GFED4s having the largest negative bias [16]
- Deleted: (
- Deleted: smoke particles are from burning of both forests [17]
- Formatted: Font color: Text 1
- Deleted: w
- Deleted: There was a large contrast of local biomass.. [18]
- Formatted ... [19]
- Deleted: Nevertheless, t...e OC column dry ...ass loading [20]
- Formatted: Font color: Text 1
- Deleted: of using

emission datasets (i.e., at the  $0.5^\circ \times 0.5^\circ$  grid box where this site is located). We found that there was a large contrast in the local biomass burning OC emission between September 24-25 (as high as  $1-2 \mu\text{g m}^{-2} \text{s}^{-1}$ ) and the other days (close to zero) across the six experiments, in spite of the differences in magnitude. Similar emission patterns are found when averaged over nine or 25 surrounding grid boxes (not shown). Such sharp contrast was completely absent in the simulated OC column mass density (Fig. 8b) and AOD (Fig. 8a).

All of this evidence, therefore, collectively suggest that the temporal variations of AOD (and aerosol mass loading) in Alta Floresta during the burning season do not directly respond to the local BB emission at the daily and sub-daily time scales, but to the regional emission. The regional emission is adjusted by the processes determining the residence time of aerosols (typically a few days), such as the regional scale transport and removal of aerosols. The MODIS-Terra true color image overlaid with active fire detections (red dots) on September 13, 2008 (Fig. 8d) confirms that there were no active fires (represented by red dots) detected at Alta Floresta (blue circle), and thus the dense smoke over there was transported from the upwind areas instead from local BB emissions during this peak aerosol episode. Therefore, accurate estimation of both the magnitude and spatial pattern of regional emissions are rather important.

### 3.3.2 Mongu in Zambia (Southern Hemisphere Africa)

The case at Mongu is different from that at Alta Floresta. There were numerous active fire detections (represented by the red dots in this MODIS-Aqua true color image) at and close to Mongu (blue circle), as revealed by Fig. 9d on September 12, 2008, one of peak aerosol episodes. The visibility over the entire region was apparently low due to smoke aerosols. Figure 9a shows that the simulated AOD from all six experiments captured two peak aerosol episodes observed from the AERONET dataset during September 2-3 and September 11-12 (AOD about 1.0), albeit underestimated. But all experiments failed to capture the sustained aerosol episode after September 20 (the observed AOD is about 0.5). All model experiments almost reproduced the AERONET AE value of 1.80 throughout September at this site (not shown), confirming that the dominance of the fine-mode aerosol particles in smoke aerosols is captured by the model irrespective of the BB emission dataset used.

The biomass burning OC emissions averaged over the grid box of Mongu exhibited distinct daily variations in each BB dataset (Fig. 9c). Similar emission patterns are found when averaged over nine or 25 surrounding grid boxes (not shown). At this site, the day-to-day variations of AOD still cannot be totally explained by the corresponding local emission at Mongu. For example, emission from FEER1.0 on September 17 is six times higher than that on September 2 (Fig. 9c), but the simulated AOD on September 17 is twice lower than that on September 2 (Fig. 9a). However, the magnitude of AOD at Mongu in each experiment corresponded to the magnitude of BB emission at the regional scale, since it is apparent that overall higher regional BB emissions still resulted in higher column mass loading and thus AOD. For instance, FEER1.0 and QFED2.4, which have the largest monthly total biomass burning OC emission over the region of SHAF among the six BB emission datasets during September ( $2.27$  and  $2.92 \text{ Tg mon}^{-1}$ , respectively, as

Deleted: theces in

Formatted ... [21]

Formatted: Font color: Text 1

Deleted: contrast of

Deleted: difference

Formatted ... [22]

Deleted: in common

Formatted ... [23]

Moved up [1]: All experiments showed relatively low skill of capturing the temporal variability of the observed AOD at Alta Floresta ( $\text{corr}=0.24-0.60$ ).

Deleted: ese...evidences ... [24]

Formatted ... [25]

Deleted: . O...her...processes which ...etermininge...the residence time of aerosols (typically a few days), such as the regional scale transport and removal of aerosols, likely play critical roles in determining the local aerosol loading... The MODIS-Terra true color image overlaid with active fire detections fire hotspots ...red dots) on on ... [26]

Formatted: Font color: Text 1

Deleted: dense smoke over ...lta Floresta (blue circle), and thus the ... [27]

Deleted: from the ...ransported smoke ... [28]

Deleted: (Fig. 8d)... Thus...Therefore, accurate estimation of both the magnitude and spatial pattern of regional emissions and representations of regional scale transport and removal ... [29]

Formatted ... [30]

Deleted: of...Alta Floresta. There were numerous active fire detectionsfire hot spots...(represented by the red dots in this MODIS-Aqua true color image) at and close to Mongu (blue circle), as revealed by Fig. 9d on September 12, 2008, one of peak aerosol episodes. The visibility over the entire region was apparently low due to smoke aerosols. Accordingly, the biomass burning OC emissions averaged over the grid box of Mongu exhibited distinct daily variations in each BB dataset (Fig. 9b). Similar emission patterns are found when averaged over nine or 25 surrounding grid boxes (not shown). ... [31]

Deleted: in...uring September 2-3 and September 11-12 (AOD about 1.0), although ... [32]

Deleted: of the

Deleted: ...1.80 throughout September at this site (not shown), confirming that the dominance of the fine-mode aerosol particles in smoke aerosols that ... [33]

Deleted: b..., ... [34]

Formatted: Font color: Text 1

Deleted: in

shown in Fig. 4), corresponded to the highest AOD (ratio=49% and 46%, respectively, as shown in Fig. 9a); while FINN1.5 and GFED4s, which represent the lowest monthly mean biomass burning OC emission over the region of SHAF (0.87 and 0.85 Tg mon<sup>-1</sup>, respectively, as shown in Fig.4), corresponded to very low AOD (15% and 19% of the observed, respectively).

Although the temporal variation of the ambient RH may partially contribute to the day-to-day changes of the emission-AOD relationship, the close resemblance between the model simulated AOD and column OC mass loading (Fig. 9b) excludes such possibility. This evidence therefore suggest again that the temporal variations of AOD (and aerosol mass loading) in Mongu, where local emissions were present, do not also directly respond to the local BB emission at the daily and sub-daily time scales during the burning season, further confirming the importance of accurate estimation of both the magnitude and spatial pattern of regional emissions as mentioned in the case of Alta Floresta. Therefore, over southern hemisphere Africa and southern hemisphere South America, except for QFED2.4, enhancement of regional BB emission amounts in all the other BB emission datasets (although to different degrees) is suggested by this study in order to reproduce the observed AOD level.

#### 4. Discussion

The simulated AOD is biased low in biomass burning dominated regions and seasons across all six BB emission datasets as demonstrated in this study. More explanations on differences among the six BB emissions datasets are discussed in Sect. 4.1. Basically, the uncertainty of the simulated AOD could be attributable to two main sources: (1) BB emissions-related biases; (2) Model-related biases. They are discussed in Sections 4.2 and 4.3, respectively.

#### 4.1 The possible explanations of differences among the six BB emission datasets

##### 4.1.1 Higher BB emissions estimated from QFED2.4 and FEER1.0

This study has shown that the QFED2.4 and FEER1.0 BB emission datasets are consistently higher than the others, with QFED2.4 being the highest overall. Some of the possible reasons responsible for this difference include:

**Constraining with MODIS AOD.** The emission coefficients ( $C_e$ ) used to derive biomass burning emissions in both QFED2.4 and FEER1.0 are constrained by the MODIS AOD, although in different ways (detailed in Sec.2.1.6 and 2.1.5, respectively). This is not the case for other BB emission datasets, especially GFAS1.2, although it also uses the same FRP products as FEER1.0 in deriving dry mass combustion rate (it is tuned to that of GFED3.1 instead). QFED2.4 applied four biome-dependent scaling factors to the initial constant value  $C_0$  when deriving its  $C_e$ , by minimizing the discrepancy between the AOD simulated by the GEOS model and that from MODIS in the respective biomes. The resulting QFED2.4 scaling factors are 1.8 for savanna and grassland fires, 2.5 for tropical forests, and 4.5 for extratropical forests (Darmenov and da Silva 2015). This partially explains its very high emission over the extratropical regions of TENA, BONA and BOAS relative to the other emission datasets (Fig. 2-4). However, the high BB emission estimated by QFED2.4 is questionable during October and November of 2008 in the

Deleted: dry

Deleted: c

Deleted: All model experiments almost reproduced the [35]

Deleted: ese

Deleted: s

Formatted ... [36]

Deleted: and representations of regional scale transport [38]

Deleted: afore

Formatted ... [37]

Deleted: [ ... [39]

Deleted: t

Deleted: in

Deleted: over in the region of Mongusouthern ... [40]

Deleted:

Deleted: are

Deleted: based on the results

Deleted: of

Deleted: The similar suggestion is applicable to the region [41]

Deleted: ,

Formatted ... [42]

Deleted: , which

Formatted ... [43]

Deleted: s

Deleted: g

Formatted ... [44]

Formatted ... [45]

Deleted:

Deleted:

Formatted ... [46]

Deleted:

Deleted: which

Formatted ... [47]

Formatted ... [48]

Deleted: as FEER1.0

Deleted: but

Deleted:

Formatted ... [49]

Deleted: the

Deleted: dry matter combustion rate instead

Formatted ... [50]

Deleted: the

Deleted: AOD

region of BONA (Fig. 4) according to the evaluation of its resulting AOD relative to the AERONET AOD at the Fort McMurray site (Fig. 7.1). As for FEER1.0, the process of deriving  $C_e$  involved calculating the near-source smoke-aerosol column mass with the MODIS AOD (total minus the background) for individual plumes, thereby limiting influence from other emission sources (Ichoku and Ellison, 2014).

**Fuel consumption.** In general, the FRP-based estimation approaches, such as GFAS1.2, QFED2.4 and FEER1.0, may enable more direct estimates of fuel consumption from energy released from fires, without being affected by the uncertainties associated with the estimates of fuel loads and combustion completeness (e.g., Kaufman et al., 1998; Wooster et al., 2003, 2005; Ichoku and Kaufman, 2005; Ichoku et al., 2008; Jordan et al., 2008). However, FRP from non-BB sources, such as the gas flare, could be mistakenly identified as BB sources. One example is over bare land in the eastern border of Algeria in MIDE (refer the land type to the website: <http://maps.elie.ucl.ac.be/CCI/viewer/index.php>) by QFED2.4 (see Fig. 2f), thus additional screening of FRP fire product is required.

#### 4.1.2 Features of FINN1.5

Globally, the FINN1.5 dataset is lower than QFED2.4 and FEER1.0, but larger than GFAS1.2, GFED3.1 and GFED4s (Fig. 3). Although FINN1.5 can capture the location of the large wildfires using the active fire products, the estimation of burned area is rather simple without the complicated spatial and temporal variability in the amount of burned area per active fire detection or variability in fuel consumption within biomes. For example, it estimates 1 km<sup>2</sup> burned area per fire pixel for all biomass types except for savanna and grassland where 0.75 km<sup>2</sup>/fire pixel is estimated instead. That might partially explain why the FINN1.5 is extremely low in AUST, as suggested by Wiedinmyer et al. (2011). Additionally, the FINN1.5 dataset is the least over boreal regions, such as in regions of BOAS and BONA, where FINN1.5 is only 1/3 and 3/5 of GFED4s, respectively. Large forest fires dominate in BOAS and BONA, such that the direct mapping of burned area as done in GFED4s and GFED3.1 produces more biomass burning emissions (van der Werf et al., 2017). On the other hand, the BB emission in FINN1.5 dataset is relatively large near the equator. For instance, it is the largest among the six datasets over the region EQAS, and the second largest over the regions of CEAM and SEAS (see Fig. 3). This might be attributed to the smoothing of the fire detections in these tropical regions to compensate for the limited daily coverage by the MODIS instruments due to gaps between adjacent swaths and higher chances of cloud coverage in tropical regions (Wiedinmyer et al., 2011). Thus, in FINN1.5, each fire detected in the equatorial region only is counted for a 2-day period by assuming that fire continues into the next day but at half of its original size.

#### 4.1.3 Difference between GFED4s and GFED3.1

Globally and in some regions, biomass burning OC emission in GFED4s is lower than that in GFED3.1 (see Fig. 2-4), although the former has 11% higher global carbon emissions and includes small fires. There are a few possible reasons: 1) For aerosols, the implementation of lower EF for certain biomes in GFED4s than in GFED3.1 reduces the aerosol biomass burning emissions. As for the savanna and grassland, for instance, the

Deleted: site

Deleted:

Formatted: Font color: Text 1

Formatted: Font color: Text 1

Formatted: Font color: Text 1

Deleted: (

Deleted: o

Formatted: Font color: Text 1

Deleted: the possible misidentification of fires in MIDE

Formatted: Font color: Text 1

Field Code Changed

Formatted: Font color: Text 1

Formatted: Font color: Text 1

Formatted: Font color: Text 1

Deleted: requiring

Formatted: Font color: Text 1

Deleted: the

Deleted: the

Deleted: o

Deleted: the

Deleted: has

Formatted: Font color: Text 1

Deleted: lack of

Deleted: the higher chance of presences of

Deleted: ):

Deleted: for

Deleted: , a fire

Deleted: in FINN1.5,

Deleted: OC



GFED4s dataset mainly applies *EF* value recommended by Akagi et al. (2011), which is 2.62 g OC per kg dry matter burned, 18% lower than the *EF* from Andreae and Merlet (2001) used in GFED3.1, which is 3.21 g OC per kg dry matter burned (see Table 2). The new estimation of *EF* is  $3.0 \pm 1.5$  g OC per kg dry matter burned as suggested by Andreae (2019). With it, the OC emissions in savanna and grassland can be slightly enhanced, but would still be lower than those in GFED3.1; 2) In addition, the improvement in including small fires in GFED4s over GFED3.1 is offset by the occasional optimization of fuel consumption using field observations for overall carbon emissions. For instance, the turnover rates of herbaceous leaf (e.g., savanna) are increased in GFED4s, leading to the lower fuel loading and thus lower consumption for this land-cover type in GFED4s (van Leeuwen et al., 2014; van der Werf et al., 2017). Therefore, the biomass burning OC emissions are lower in GFED4s over SHAF, NHAf, and AUST (Fig. 3 and 4), where ~88% of carbon emission is from savanna and grassland (van der Werf et al., 2017).

On the other hand, there are regions in the northern hemisphere where GFED4s is higher than GFED3.1, for example, over CEAS and EURO, where small fires associated with burning of agricultural residues contribute to 43.6% and 58.6% of the carbon emissions, respectively (van der Werf et al., 2017). In spite of the 30% reduction of the *EF* in these two regions, the effect of including small fires in GFED4s is greater, resulting in the biomass burning OC emission from GFED4s being twice as high as that from GFED3.1. Another example is in BOAS where the biomass burning OC emissions are 10% higher in GFED4s than in GFED3.1. This is likely attributable to the higher *EF* used in the former BB dataset than in the latter one for boreal forest fires (9.60 vs. 9.14 g OC per kg dry matter, see Table 2), where 86.5 % of the carbon emission is from the Siberian forest (van der Werf et al., 2017).

It is interesting that the yearly total biomass burning OC emission from GFED4s is 20% lower than that from GFED3.1 in EQAS (Fig. 4), even though the small fires are included and the *EF* of peatland and tropical forest are higher in the former (Table 2). By examining the monthly variations over EQAS (Fig. 4), however, we found that GFED4s is actually higher than GFED3.1 in August by a factor of two when peatland burning is predominant, but equal to or lower than GFED3.1 in other months, particularly in May, leading to the overall lower annual total value in GFED4s.

#### 4.2 Sources of the uncertainty associated with biomass burning emissions

Uncertainty in any of the six BB emissions datasets considered in this study could have been introduced from a variety of measurement and/or analysis procedures, including: detection of fire or area burned, retrieval of FRP, emission factors (see Table 1), land cover maps, and fuel consumption estimates, some of which are explained in detail below.

**Fire detection.** Most of the current global estimations of biomass burning emissions are heavily dependent on polar-orbiting satellite measurements from MODIS on Terra and Aqua (e.g., MCD14DL, MOD14A1, MYD14A1, and MCD14ML as listed in Table 1). The temporal and spatial resolutions of these measurements impose limitations on their ability to detect and characterize the relevant attributes of fires, such as the locations and timing of active fires and the extent of the burned areas. Each of the two MODIS sensors,

Deleted: s

Deleted: are

Deleted: (

Deleted: using

Formatted: Font color: Text 1

Formatted: Font: Italic, Font color: Text 1

Formatted: Font color: Text 1

Formatted: Font color: Text 1

Deleted: were used in GFED4s

Formatted: Font color: Text 1

Formatted: Font color: Text 1

Deleted: the

Deleted: its

Formatted: Font color: Text 1

Deleted: on inclusion

Deleted: of

Deleted: OC

Deleted: exceeds

Deleted: twice as high OC

Deleted: OC

Deleted: is

Deleted: It

Deleted: a

Deleted: in BOAS

Deleted: hot spots



from which all of the major BB datasets derive their inputs, can only possibly observe a given fire location twice in 24 hours, which leaves excessive sampling gaps in the diurnal cycle of fire activity (Saide et al., 2015). Even for these few times that MODIS makes observations at its nominal spatial resolution of 1 km at nadir, it has the potential to miss a significant number of smaller fires (e.g. Hawbaker et al., 2008, Burling et al, 2011, Yokelson et al., 2011), as well as to miss fires obstructed by clouds, those located in the gaps between MODIS swaths in the tropics (Hyer et al., 2009; Wang et al., 2018). In addition, MODIS fire detection sensitivity is reduced at MODIS off nadir views, with increasing view zenith angles especially toward the edge of scan, where its ground pixel size is almost a factor of 10 larger (Peterson and Wang, 2013; Roberts et al., 2009; Wang et al., 2018), resulting in dramatic decreases in the total number of detected fire pixels and total FRP (Ichoku et al., 2016b; Wang et al., 2018). Moreover, all operational remote sensing fire products have difficulty accounting for understory fires or fires with low thermal signal or peatland fires such as those in Indonesia, where smoldering can last for months (Tansey et al, 2008). These issues can propagate into the uncertainties of the emissions datasets that are dependent on active fire detection products, especially those based on FRP, e.g., GFAS1.2 (Kaiser et al., 2012), FEER1.0 (Ichoku and Ellison, 2014), and QFED2.4 (Darmenov and da Silva, 2015). This issue also affects FINN1.5 (Wiedinmyer et al., 2011), which derives the burned area by assuming each active fire pixel to correspond to a burned area of 1 km<sup>2</sup> for most biome types (see details in Sect. 2.1.3), and GFED4s, which uses burned area product for large fires but derives burned areas for small fires using the MODIS active fire product.

On the other hand, although the sparse diurnal sampling frequency may not necessarily be an issue for the MODIS burned area product, upon which some of the emission datasets are based (e.g., GFED3.1), burned area product may not account for small fires due to its low spatial resolution of 500-m, which may limit the identification of small burned scars such as those generated by small fires from crop lands (fire size < 21 ha). In addition, the estimation of biomass burning emission based on the burned area product, e.g., GFED, is subject to the uncertainty associated with the estimation of fuel load and combustion completeness as mentioned earlier.

**Emission factor (EF).** The EF, used for deriving individual particulate or gaseous species of smoke emissions from burned dry matter in all major BB emission datasets, heavily depends on the two papers by Andreae and Merlet (2001) and Akagi et al. (2011). The authors of these two studies made significant contributions by compiling the values of EFs from hundreds of papers. However, the EFs can have significant uncertainties (Andreae, 2019), because each EF results from a particular experiment or field campaign. Some EFs are derived from lab-based studies whereby samples of fuels are burned in combustion chambers (e.g., Christian et al., 2003; Freeborn et al., 2008), where the combustion characteristics can be very different from those of large-scale open biomass burning and wildfires, and some EFs are derived from field campaigns, where the measurement locations are often not close enough to the biomass burning source due to personnel safety and other logistic factors (Aurell et al., 2019).

Formatted: Font color: Text 1

Deleted: and

Formatted: Font color: Text 1

Deleted:

Formatted: Font color: Text 1

**Deleted:** These issues can propagate into the uncertainties of the emissions datasets that are dependent on active fire detection products, especially those based on FRP, e.g., GFAS1.2 (Kaiser et al., 2012), FEER1.0 (Ichoku and Ellison, 2014), QFED2.4 (Darmenov and da Silva, 2015), as well as FINN1.5 (Wiedinmyer et al., 2011) which does not use FRP product but uses active fire product to correspond to to derive burned area, and even GFED4s which does not use FRP either but uses active fire product to derive burned areas for small fire the MODIS.

On the other hand, although the sparse diurnal sampling frequency may not necessarily be an issue for the MODIS burned area product, upon which some of the emission datasets are based (e.g., GFED3.1), burned area product may not account for small fires due to its low spatial resolution of 500-m, which may limit the identification of small burned scars such as those generated by small fires from crop lands (fire size < 21 ha).

Formatted: Font color: Text 1

Deleted: s

Deleted: literature compiled

Formatted: Font: Italic, Font color: Text 1

Formatted: Font color: Text 1

Deleted: .

Deleted: dispersed

Deleted: deals with

Deleted: The EF can have significant uncertainties. In general, most

Deleted: very few

Deleted: i.

Deleted: s.

It is somewhat surprising that the aerosol emissions from GFED4s are lower than those from GFED3.1 in most of the savanna regions (e.g., SHAF, NHAf, and SHSA), even though the former includes smaller fires and has 11% higher global carbon emissions. This discrepancy between GFED4s and GFED3.1 can be partially explained by the fact that different emission factors were used to derive these two products, with the lower EF used for savanna in the former dataset taken from Andreae and Merlet (2001), whereas the higher EF used in the latter dataset was obtained from Akagi et al. (2011) (see Table 2). This situation will not change much even if the EF value from the latest estimation by Andreae (2019) were used, as explained earlier in Sect. 4.1.3.

**Burning stages.** Most current BB emission datasets do not distinguish the different burning stages, such as the flaming and smoldering stages that have distinctive emission characteristics. Typically, flaming dominates the earlier stage of the fire while smoldering dominates the later part. In the case of boreal forest fires, for example, about 40% of combustion originates from the flaming phase while 60% comes from the smoldering phase (Reid et al., 2005). In addition, smoldering combustion produces more OC and CO than flaming combustion; whereas flaming combustion produces more BC and carbon dioxide (CO<sub>2</sub>) than smoldering (e.g., Freeborn et al., 2008).

#### 4.3 Sources of the uncertainty associated with aerosol modeling

The model-related biases in the GEOS model, which other models most probably also suffer from, include, for example, inaccurate representations of horizontal and vertical transport of aerosol with wind, fire emission plume height, estimation of aerosol removal in models. Modeling of AOD properties such as optical properties and water uptake probably generates additional uncertainty. The ratio of OA to OC is 1.4 in this study, as first determined by White and Roberts (1977). However, this OA/OC ratio of 1.4 is at the low end of the generally suggested range of 1.2–2.5 (Turpin and Lim, 2001; Zhang et al., 2005; Bae et al., 2006; El-Zanan et al., 2006; Aiken et al., 2008; Chan et al., 2010). Observations suggest that OA/OC values of  $1.6 \pm 0.2$  should be used for urban aerosols and  $2.1 \pm 0.2$  for non-urban aerosols (Turpin and Lim, 2001). Enhancing this ratio can obviously increase the resulting AOD, but a more accurate measurement of this ratio during biomass burning is needed. Furthermore, the production of secondary organic aerosol (SOA) in biomass burning plumes, which has been observed in lab studies and ambient plumes (e.g., Bian et al., 2017; Ahern et al., 2019), are missing in these GEOS simulations. In addition, Ge et al. (2017) have shown that the choice of different meteorological fields, such as those from ECMWF and National Centers for Environmental Prediction (NCEP), can yield a factor of two difference in the resulting surface PM<sub>2.5</sub> concentration during the fire season of September in the Maritime continents.

#### 5. Conclusions and recommendations

In this study, we compared six global biomass burning aerosol emission datasets in 2008, i.e., GFED3.1, GFED4s, FINN1.5, and GFAS1.2, FEER1.0 and QFED2.4. We also have examined the sensitivity of the modelled AOD to the different BB emission datasets in the NASA GEOS model globally and in 14-subregions. The main results are summarized as follows:

**Formatted:** Automatically adjust right indent when grid is defined, Adjust space between Latin and Asian text, Adjust space between Asian text and numbers

**Deleted:** a

**Deleted:** used

**Deleted:** based on

**Deleted:** a

**Deleted:** based on

**Deleted:** as explained earlier in Sect. 4.1.3

**Deleted:** be

**Deleted:** d

**Deleted:** using

**Deleted:** Furthermore, most of

**Deleted:** , and other model assumptions

**Deleted:** which is

**Deleted:** ),

**Deleted:** which is

**Deleted:** 4

**Formatted:** Font: (Asian) Times New Roman, 12 pt, Font color: Text 1, (Asian) Chinese (China)

**Formatted:** Font color: Text 1

**Deleted:** 3

**Deleted:** O

**Deleted:** respectively

**Deleted:** ; Aiken et al., 2008

**Deleted:** choose

- 1507 a. The biomass burning OC emissions derived from GFED3.1, GFED4s, FINN1.5,  
 1508 GFAS1.2, FEER1.0, and QFED2.4 can differ by up to a factor of 3.8 on an annual  
 1509 average, with values of 15.65, 13.76, 19.48, 18.22, 28.48, and 51.93 Tg C in 2008,  
 1510 respectively. The biomass burning BC emissions can differ by up to a factor of 3.4 on  
 1511 an annual average, with values of 1.76, 1.65, 1.83, 1.99, 3.66, and 5.54 Tg C in 2008,  
 1512 respectively. In general, higher biomass burning OC and BC emissions are estimated  
 1513 from QFED2.4 globally and regionally, followed by FEER1.0.
- 1514 b. The best agreement among the six emission datasets occurred in Northern  
 1515 Hemisphere Africa (NHAF), Equatorial Asia (EQAS), Southern Hemisphere Africa  
 1516 (SHAF), and South Hemisphere South America (SHSA), where the biomass burning  
 1517 emissions are predominant in determining aerosol loading, with the top coefficient of  
 1518 variation ranks (1-4) and relatively low *max/min* ratio (a factor of 3-4). The least  
 1519 agreement occurred in the Middle East (MIDE), Temperate North America (TENA),  
 1520 Boreal North America (BONA), and Europe (EURO), with the bottom coefficient of  
 1521 variation ranks (14-11) and large *max/min* ratios (a factor of 66-10), as these are  
 1522 regions where biomass burning is either not dominant in total aerosol loading or  
 1523 QFED2.4 is extremely large. It seems that the diversity among the six BB emission  
 1524 datasets is largely driven by QFED2.4, which estimates the largest emission amount  
 1525 for almost all regions (except for equatorial Asia).
- 1526 c. In Southern Hemisphere Africa (SHAF) and Southern Hemisphere South America  
 1527 (SHSA) during September 2008, where and when biomass burning aerosols are  
 1528 dominant over other aerosol types, the amounts of biomass burning OC emissions  
 1529 from QFED2.4 and FEER1.0 are at least double those from the remaining four BB  
 1530 emission datasets. The AOD simulated by the NASA GEOS based on these two BB  
 1531 emission datasets are the closest to those from MISR and AERONET, but still biased  
 1532 low. In particular, at Alta Floresta in SHSA, they can account for 36%-100% of the  
 1533 observed AOD, and at Mongu in SHAF, the AOD simulated with the six biomass  
 1534 burning emission datasets only account for 15%-49% of the observed AOD. Overall,  
 1535 during the biomass burning peak seasons at most of the representative AERONET  
 1536 sites selected in each region, the AOD simulated with QFED2.4 is the highest and  
 1537 closest to AERONET and MISR observations, followed by that of FEER1.0.  
 1538 Considering that regional scale transport and removal processes as well as wind fields  
 1539 are the same across the six BB emission experiments since they were run under the  
 1540 same model configurations except for BB emission, it is evident that enhancement of  
 1541 BB emission amounts in all six BB emission datasets except for QFED2.4 (although  
 1542 to different degrees) will be needed for the model AOD simulations to match  
 1543 observations, particularly in SHAF (Mongu) and SHSA (Alta Floresta). Although the  
 1544 result of this study is partially model-dependent, nevertheless, it sheds some light on  
 1545 our understanding of the uncertainty of the simulated AOD associated with the choice  
 1546 of biomass burning aerosol emission datasets.

1548 Based on the results of the current study, it is appropriate to make some  
 1549 recommendations for future studies on improving BB emission estimation. Our  
 1550 understanding of the complexity, variability, and interrelationships between different fire  
 1551 characteristics (behavior, energetics, emissions) still need to be improved (Hyer et al,  
 1552 2011). More accurate estimation of emission factors (EF) for different ecosystem types

Deleted: 3.8

Formatted: Font color: Text 1

Deleted: for OC

Deleted: ;

Deleted: and t

Deleted: the

Deleted: OC

Deleted: MODIS

Formatted: Font color: Text 1

Formatted: Font color: Text 1

Deleted: AOD

Deleted: by

Deleted: ODIS

Deleted: therefore,

Deleted: and representation of spatial distribution

Deleted:

Formatted: Font color: Text 1

Formatted: Font color: Text 1

Deleted: in

Deleted: the regions of

Deleted: are suggested by this study based on the results of AOD

Deleted: We acknowledge that

Deleted: aerosol

Formatted: Don't adjust right indent when grid is defined, Don't adjust space between Latin and Asian text, Don't adjust space between Asian text and numbers

Deleted: from

Formatted: Font color: Text 1

Deleted: For example,

Deleted: m

and burning stages would greatly improve the emission overall, as demonstrated by the discrepancy between GFED3.1 and GFED4s (see Sect. 4.1.3). The global BB emission datasets driven by fire remote sensing and retrievals of FRP and burned-area products, which have hitherto depended heavily on MODIS, can be augmented with products from higher resolution sensors such as Visible Infrared Imaging Radiometer Suite (VIIRS), and the global suite of geostationary meteorological satellites such as Meteosat (covering Europe, Africa and the Indian Ocean), Geostationary Operational Environmental Satellite (GOES, covering North, Central, and South America) and Himawari (covering east Asia, southeast Asia, and Australia). Also, measurements from the recent field campaigns such as WE-CAN ([https://www.eol.ucar.edu/field\\_projects/we-can](https://www.eol.ucar.edu/field_projects/we-can)) and FIREX-AQ (<https://www.esrl.noaa.gov/csd/projects/firex-aq/science/motivation.html>) are expected to contribute toward advancing our knowledge of biomass burning emissions in North America. The evaluation in this study has been solely based on remote sensing AOD data, including retrievals from both satellite (MISR) and ground-based (AERONET) sensors. Continuous mass concentration measurements are needed to validate the fire-generated aerosol loading in specific contexts, such as in analyzing collocated surface and vertical aerosol concentrations and composition, at least in the major BB regions.

#### Data availability

The GFED3.1 biomass burning dataset can be accessed through the link: [https://daac.ornl.gov/VEGETATION/guides/global\\_fire\\_emissions\\_v3.1.html](https://daac.ornl.gov/VEGETATION/guides/global_fire_emissions_v3.1.html). The link to the GFED4s dataset is <http://www.globalfiredata.org>. The FINN1.5 emissions dataset is archived at: <http://bai.acom.ucar.edu/Data/fire/>. The GFAS1.2 emissions dataset is downloaded at: <https://apps.ecmwf.int/datasets/data/cams-gfas/>. The FEER1.0 dataset is available at <http://feer.gsfc.nasa.gov/data/emissions/>. The QFED2.4 can be downloaded from the website: <https://portal.nccs.nasa.gov/datashare/ies/aerosol/emissions/QFED/v2.4r6/>. MISR level 3 AOD data can be downloaded from website: [https://eosweb.larc.nasa.gov/project/misr/mil3mae\\_table](https://eosweb.larc.nasa.gov/project/misr/mil3mae_table). AERONET Version 3 Level 2.0 data can be downloaded from the websites: [https://aeronet.gsfc.nasa.gov/new\\_web/download\\_all\\_v3\\_aod.html](https://aeronet.gsfc.nasa.gov/new_web/download_all_v3_aod.html). The GEOS model results can be provided by contacting with the corresponding author.

#### Author contribution

CI, MC, and XP conceived this project. XP conducted the data analysis and the model experiments. XP and CI wrote the majority of this manuscript, and all other authors participated in the writing process and interpretation of the results. HB, AD, PC and AS helped on model set-up. CI, AD, and LE provided the biomass burning emission datasets and interpretation of these datasets. TK, JW, and GC provided the help to apply the biomass burning emission datasets in the model. CI and MC provided funding supports.

#### Acknowledgement

MISR AOD data were obtained from the NASA Langley Research Center Atmospheric Science Data Center. We thank the AERONET networks for making their data available. Site PIs and data managers of those networks are gratefully acknowledged. We acknowledge the use of imagery from the NASA Worldview application (<https://worldview.earthdata.nasa.gov>), part of the NASA Earth Observing System Data and Information System (EOSDIS). Computing resources

**Deleted:** The evaluation in this study is solely based on remote sensing AOD data. More global dense and continuous surface measurements are needed to validate the fire-generated aerosol loading in specific contexts, including surface and vertical aerosol concentrations and aerosol compositions, especially in the major BB regions.

**Deleted:** The fire detection techniques

**Deleted:** investigated

**Formatted:** Font color: Text 1

**Formatted:** Font color: Text 1

**Formatted:** Font color: Text 1

**Formatted:** Font color: Text 1

**Deleted:** will

**Formatted:** Font color: Text 1

**Formatted:** Default Paragraph Font

**Field Code Changed**

**Formatted:** No underline, Font color: Text 1

**Field Code Changed**

**Formatted:** No underline

**Formatted:** No underline

**Field Code Changed**

**Formatted:** No underline, Font color: Text 1

**Formatted:** Font color: Text 1

**Formatted:** Default Paragraph Font, Font color: Text 1

**Field Code Changed**

**Formatted:** No underline, Font color: Text 1

**Field Code Changed**

**Formatted:** No underline

**Formatted:** No underline

**Formatted:** Font color: Text 1

**Deleted:** ¶

**Deleted:** We thank the

**Formatted:** Font: 11 pt, Font color: Text 1

**Deleted:** Goddard Earth Science Data and Information Services Center for providing gridded satellite products of MODIS through their Giovanni website

**Formatted:** Font color: Text 1

supporting this work were provided by the NASA High-End Computing (HEC) Program through the NASA Center for Climate Simulation (NCCS) at Goddard Space Flight Center. We also thank the providers of biomass burning emission datasets of GFED, FINN, and GFAS. We acknowledge supports from various NASA earth science programs, including the NASA Atmospheric Composition Modeling, Analysis, and Prediction Program (ACMAP), the Modeling, Analysis, and Prediction program (MAP), the Interdisciplinary Studies Program (IDS), and Carbon Cycle Science program. CI is also grateful for partial support received during the preparation of this article from the Educational Partnership Program of the National Oceanic and Atmospheric Administration (NOAA), U.S. Department of Commerce, under Agreement No. #NA16SEC4810006. TO is supported by NASA under Grant No. NNX14AM76G. We appreciate the constructive comments from two reviewers, which help us to improve the quality of this manuscript. XP also acknowledges the valuable suggestions from Dr. Dongchul Kim. The contents of this article are solely the responsibility of the authors and do not represent the official views of any agency or institution.

## Reference

- Ahern, A. T., Robinson, E. S., Tkacik, D. S., Saleh, R., Hatch, L. E., Barsanti, K. C., et al. Production of secondary organic aerosol during aging of biomass burning smoke from fresh fuels and its relationship to VOC precursors. *Journal of Geophysical Research: Atmospheres*, 124. <https://doi.org/10.1029/2018JD029068>, 2019.
- Aiken, A. C., Decarlo, P. F., Kroll, J. H., Worsnop, D. R., Huffman, J. A., Docherty, K. S., Ulbrich, I. M., Mohr, C., Kimmel, J. R., Sueper, D., Sun, Y., Zhang, Q., Trimborn, A., Northway, M., Ziemann, P. J., Canagaratna, M. R., Onasch, T. B., Alfarra, M. R., Prevot, A. S. H., Dommen, J., Duplissy, J., Metzger, A., Baltensperger, U., and Jimenez, J. L.: O/C and OM/OC ratios of primary, secondary, and ambient organic aerosols with high-resolution time-of-flight aerosol mass spectrometry, *Environ. Sci. Technol.*, 42, 4478–4485, doi:10.1021/es703009q, 2008.
- Akagi, S. K., Yokelson, R. J., Wiedinmyer, C., Alvarado, M. J., Reid, J. S., Karl, T., Crounse, J. D., and Wennberg, P. O.: Emission factors for open and domestic biomass burning for use in atmospheric models, *Atmos. Chem. Phys.*, 11, 4039–4072, <https://doi.org/10.5194/acp-11-4039-2011>, 2011.
- Andreae, M. O.: Emission of trace gases and aerosols from biomass burning – an updated assessment, *Atmos. Chem. Phys.*, 19, 8523–8546, <https://doi.org/10.5194/acp-19-8523-2019>, 2019.
- Andreae, M. O. and Merlet, P.: Emission of trace gases and aerosols from biomass burning, *Global Biogeochem. Cy.*, 15, 955–966, <https://doi.org/10.1029/2000GB001382>, 2001.
- Aurell, J., Mitchell, B., Greenwell, D., Holder, A., Tabor, D., Kiros, F., and Gullett, B.: Measuring Emission Factors from Open Fires and Detonations. *AWMA Air Quality Measurement Methods and Technology*, Durham, North Carolina, April 02 - 04, 2019.



- Bae, M. S., Demerjian, K. L., and Schwab, J. J.: Seasonal estimation of organic mass to organic carbon in PM<sub>2.5</sub> at rural and urban locations in New York state, *Atmos. Environ.*, 40, 7467–7479, 2006.
- Bian, H., M. Chin, R. Kawa, B. Duncan, A. Arellano Jr., and R. Kasibhatla, Uncertainty of global CO simulations constraint by biomass burning emissions. *J. Geophys. Res.*, 112, D23308, doi:10.1029/2006JD008376, 2007.
- Bian, H., Chin, M., Rodriguez, J. M., Yu, H., Penner, J. E., and Strahan, S.: Sensitivity of aerosol optical thickness and aerosol direct radiative effect to relative humidity, *Atmos. Chem. Phys.*, 9, 2375–2386, https://doi.org/10.5194/acp-9-2375-2009, 2009.
- Bian, H., M. Chin, S. R. Kawa, H. Yu, T. Diehl, Multi-scale carbon monoxide and aerosol correlations from MOPITT and MODIS satellite measurements and GOCART model: implication for their emissions and atmospheric evolutions, *J. Geophys. Res.*, 115, D07302, doi:10.1029/2009JD012781, 2010.
- Bian, H., P. Colarco, M. Chin, G. Chen, J.M. Rodriguez, Q. Liang, et al. Investigation of source attributions of pollution to the Western Arctic during the NASA ARCTAS field campaign. *Atmos. Chem. and Phys.*, 13, 4707–4721, doi:10.5194/acp-13-4707-2013, 2013.
- Bian, Q., Jathar, S. H., Kodros, J. K., Barsanti, K. C., Hatch, L. E., May, A. A., Kreidenweis, S. M., and Pierce, J. R.: Secondary organic aerosol formation in biomass-burning plumes: theoretical analysis of lab studies and ambient plumes, *Atmos. Chem. Phys.*, 17, 5459–5475, https://doi.org/10.5194/acp-17-5459-2017, 2017.
- Bond, T., Doherty, S. J., Fahey, D. W., Forster, P. M., Berntsen, T., DeAngelo, B. J., Flanner, M. Ghan, Kärcher, B., Koch, D., Kinne, S., Kondo, Y., Quinn, P. Sarofim, M. C., Schultz, M., Schulz, M., Venkataraman, C., Zhang, H., Zhang, S., Bellouin, N. Guttikunda, S. Hopke, P. K., Jacobson, M. Z., Kaiser, J. W., Klimont, Z., Lohmann, U., Schwarz, J. P., Shindell, D., Storelvmo, T., Warren, S. G., and Zender, C. S.: Bounding the role of black carbon in the climate system: A scientific assessment, *J. Geophys. Res.*, 118, 5380–5552, doi:10.1002/jgrd.50171, 2013.
- Buchard, V., C. A. Randles, A. da Silva, A. S. Darmenov, et al. The MERRA-2 Aerosol Reanalysis, 1980-onward, Part II: Evaluation and Case Studies. *Journal of Climate*, doi:10.1175/jclid-16-0613.1, 2017.
- Burling, I. R., Yokelson, R. J., Akagi, S. K., Urbanski, S. P., Wold, C. E., Griffith, D. W. T., Johnson, T. J., Reardon, J., and Weise, D. R.: Airborne and ground-based measurements of the trace gases and particles emitted by prescribed fires in the United States, *Atmos. Chem. Phys. Discuss.*, 11, 18677–18727, doi:10.5194/acpd-11-18677-2011, 2011.
- Chan, T. W., Huang, L., Leaitch, W. R., Sharma, S., Brook, J. R., Slowik, J. G., Abbatt, J. P. D., Brickell, P. C., Liggio, J., Li, S.-M., and Moosmüller, H.: Observations of

1729 [OM/OC and specific attenuation coefficients \(SAC\) in ambient fine PM at a rural site in](#)  
1730 [central Ontario, Canada, \*Atmos. Chem. Phys.\*, 10, 2393-2411,](#)  
1731 <https://doi.org/10.5194/acp-10-2393-2010>, 2010.

1732

1733 Chin, M., R. B. Rood, S.-J. Lin, J.-F. Müller, and A. M. Thompson, Atmospheric sulfur  
1734 cycle in the global model GOCART: Model description and global properties, *J. Geophys.*  
1735 *Res.*, 105, 24,661-24,687, 2000.

1736

1737 Chin, M., P. Ginoux, S. Kinne, O. Torres, B. N. Holben, B. N. Duncan, R. V. Martin, J.  
1738 A. Logan, A. Higurashi, and T. Nakajima, Tropospheric aerosol optical thickness from  
1739 the GOCART model and comparisons with satellite and sun photometer measurements, *J.*  
1740 *Atmos., Sci.*, 59, 461-483, 2002.

1741

1742 Chin, M., T. Diehl, O. Dubovik, T. F. Eck, B. N. Holben, A. Sinyuk, and D. G. Streets,  
1743 Light absorption by pollution, dust and biomass burning aerosols: A global model study  
1744 and evaluation with AERONET data, *Ann. Geophys.*, 27, 3439-3464, 2009.

1745

1746 Chin, M., T. Diehl, Q. Tan, J. M. Prospero, R. A. Kahn, L. A. Remer, H. Yu, A. M.  
1747 Sayer, H. Bian, I. V. Geogdzhayev, B. N. Holben, S. G. Howell, B. J. Huebert, N. C.  
1748 Hsu, D. Kim, T. L. Kucsera, R. C. Levy, M. I. Mishchenko, X. Pan, P. K. Quinn, G. L.  
1749 Schuster, D. G. Streets, S. A. Strode, O. Torres, and X.-P. Zhao, Multi-decadal variations  
1750 of atmospheric aerosols from 1980 to 2009: a perspective from observations and a global  
1751 model, *Atmos. Chem. Phys.*, 14, 3657-3690, 2014.

1752

1753 Chou, M.-D. and M. J. Suarez, A solar radiation parameterization for atmospheric  
1754 studies, NASA/TM-1999- 104606, Vol. 15, 1999.

1755

1756 Chou, M.-D., M. J. Suarez, X.-Z. Liang, and M.-H. Yan, A thermal infrared radiation  
1757 parameterization for atmospheric studies. NASA Tech. Memo. 104 606, 55 pp, 2001.

1758

1759 Christian, T., Kleiss, B., Yokelson, R. J., Holzinger, R., Crutzen, P. J., Hao, W. M.,  
1760 Saharjo, B. H., and Ward, D. E.: Comprehensive laboratory measurements of biomass-  
1761 burning emissions: 1. Emissions from Indonesian, African, and other fuels, *J. Geophys.*  
1762 *Res.*, 108(D23), 4719, doi:10.1029/2003JD003704, 2003.

1763

1764 Colarco, P. R., A. da Silva, M. Chin, T. Diehl. Online simulations of global aerosol  
1765 distributions in the NASA GEOS-4 model and comparisons to satellite and ground-based  
1766 aerosol optical depth, *J. Geophys. Res.*, 115, D14207, doi:10.1029/2009JD012820, 2010.

1767

1768 Darmenov, A. and da Silva, A. The quick fire emissions dataset (QFED)—documentation  
1769 of versions 2.1, 2.2 and 2.4, NASA Technical Report Series on Global Modeling and  
1770 Data Assimilation, NASA TM-2015-104606, 38, 2015.

1771

1772 Eck, T. F., Holben, B. N., Ward, D. E., Dubovik, O., Reid, J. S., Smirnov, A., et al..  
1773 Characterization of the optical properties of biomass burning aerosols in Zambia during

1774 the 1997 ZIBBEE field campaign. *Journal of Geophysical Research*, 106(D4), 3425–  
1775 3448. <https://doi.org/10.1029/2000JD900555>, 2001.

1776

1777 [El-Zanan, H. S., Lowenthal, D. H., Zielinska, B., Chow, J. C., and Kumar, N.:](#)  
1778 [Determination of the organic aerosol mass to organic carbon ratio in IMPROVE samples,](#)  
1779 [Chemosphere](#), 60, 485–496, 2005.

1780

1781 Freeborn, P. H., M. J. Wooster, W. M. Hao, C. A. Ryan, B. L. Nordgren, S. P. Baker, and  
1782 C. Ichoku. Relationships between energy release, fuel mass loss, and trace gas and  
1783 aerosol emissions during laboratory biomass fires, *J. Geophys. Res.*, 113, D01301,  
1784 doi:10.1029/2007JD008679, 2008.

1785

1786 Ge, C., J. Wang, J. S. Reid, D. Posselt, P. Lynch, E. Hyer, Mesoscale modeling of smoke  
1787 transport from equatorial Southeast Asian Maritime Continent to the Philippines: First  
1788 comparison of ensemble analysis with in situ observations, *J. Geophys. Res.-Atmos.*,  
1789 122, 5380–5398, 2017.

1790

1791 Gelaro, R., W. McCarty, M. J. Suárez, R. Todling, A. Molod, L. Takacs, C. A. Randles, A.  
1792 Darmenov, M. G. Bosilovich, R. Reichle, K. Wargan, L. Coy, R. Cullather, C. Draper, S.  
1793 Akella, V. Buchard, A. Conaty, A. M. da Silva, W. Gu, G. Kim, R. Koster, R. Lucchesi,  
1794 D. Merkova, J. E. Nielsen, G. Partyka, S. Pawson, W. Putman, M. Rienecker, S. D.  
1795 Schubert, M. Sienkiewicz, and B. Zhao: The Modern-Era Retrospective Analysis for  
1796 Research and Applications, Version 2 (MERRA-2). *J. Climate*, 30, 5419–5454,  
1797 <https://doi.org/10.1175/JCLI-D-16-0758.1>, 2017.

1798

1799 Giglio, L., Randerson, J. T., van der Werf, G. R., Kasibhatla, P. S., Collatz, G. J., Morton,  
1800 D. C., and DeFries, R. S.: Assessing variability and long-term trends in burned area by  
1801 merging multiple satellite fire products, *Biogeosciences*, 7, 1171–1186,  
1802 <https://doi.org/10.5194/bg-7-1171-2010>, 2010.

1803

1804 Giglio, L., Randerson, J. T., and van der Werf, G. R.: Analysis of daily, monthly, and  
1805 annual burned area using the fourth-generation global fire emissions database (GFED4),  
1806 *J. Geophys. Res.-Biogeo.*, 118, 317–328, <https://doi.org/10.1002/jgrg.20042>, 2013.

1807

1808 Giles, D. M., Sinyuk, A., Sorokin, M. G., Schafer, J. S., Smirnov, A., Slutsker, I., Eck, T.  
1809 F., Holben, B. N., Lewis, J. R., Campbell, J. R., Welton, E. J., Korkin, S. V., and  
1810 Lyapustin, A. I.: Advancements in the Aerosol Robotic Network (AERONET) Version 3  
1811 database – automated near-real-time quality control algorithm with improved cloud  
1812 screening for Sun photometer aerosol optical depth (AOD) measurements, *Atmos. Meas.*  
1813 *Tech.*, 12, 169–209, <https://doi.org/10.5194/amt-12-169-2019>, 2019.

1814

1815 Hawbaker, T. J., Radeloff, V. C., Syphard, A. D., Zhu, Z. L., and Steward, S. I.:  
1816 Detection rates of the MODIS active fire product in the United States. *Remote Sens.*  
1817 *Environ.*, 112(5) 2656–2664, 2008.

1818

1819 Hoelzemann, J. J., Schultz, M. G., Brasseur, G. P., Granier, C., and Simon, M.: Global  
 1820 Wildland Fire Emission Model (GWEM): Evaluating the use of global area burnt satellite  
 1821 data, *J. Geophys. Res.*, 109, D14S04, doi:10.1029/2003JD003666, 2004.  
 1822  
 1823 Holben, B. N., Eck, T. F., Slutsker, I., Tanre, D., Buis, J. P., Setzer, A., Vermote, E.,  
 1824 Reagan, J. A., Kaufman, Y. J., Nakajima, T., Lavenu, F., Jankowiak, I., and Smirnov, A.:  
 1825 AERONET – a federated instrument network and data archive for aerosol  
 1826 characterization, *Remote Sens. Environ.* 66, 1–16, 1998.  
 1827  
 1828 Hyer, E. J., and J. S. Reid. Baseline uncertainties in biomass burning emission models  
 1829 resulting from spatial error in satellite active fire location data, *Geophys. Res. Lett.*, 36,  
 1830 L05802, doi:10.1029/2008GL036767, 2009.  
 1831  
 1832 Hyer, E. J., J. S. Reid, and J. Zhang: An over-land aerosol optical depth data set for data  
 1833 assimilation by filtering, correction, and aggregation of MODIS collection 5 optical depth  
 1834 retrievals, *Atmos. Meas. Tech.*, 4, 379–408, doi:10.5194/amt-4-379-2011, 2011.  
 1835  
 1836 Ichoku, C., and Ellison, L. Global top-down smoke-aerosol emissions estimation using  
 1837 satellite fire radiative power measurements. *Atmospheric Chemistry and Physics*, 14(13),  
 1838 6643-6667. doi:10.5194/acp-14-6643-2014, 2014.  
 1839  
 1840 Ichoku, C., Ellison, L. T., Yue, Y., Wang, J., & Kaiser, J. W. Fire and Smoke Remote  
 1841 Sensing and Modeling Uncertainties. *Natural Hazard Uncertainty Assessment: Modeling*  
 1842 *and Decision Support*, 215-230, doi: 10.1002/9781119028116.ch14, 2016a.  
 1843  
 1844 Ichoku, C., Ellison, L. T., Willmot, K. E., Matsui, T., Dezfuli, A. K., Gatebe, C. K., Wang,  
 1845 J., Wilcox, E. M., Lee, J., Adegoke, J. and Okonkwo, C. Biomass burning, land-cover  
 1846 change, and the hydrological cycle in Northern sub-Saharan Africa. *Environmental*  
 1847 *Research Letters*, 11(9), p.095005, 2016b.  
 1848  
 1849 Ichoku, C., L. Giglio, M. J. Wooster, and L. A. Remer. Global characterization of  
 1850 biomass-burning patterns using satellite measurements of fire radiative energy. *Remote*  
 1851 *Sensing of Environment*, 112 (6): 2950-2962 [10.1016/j.rse.2008.02.009], 2008.  
 1852  
 1853 Ichoku, C., R. Kahn, and M. Chin. Satellite contributions to the quantitative  
 1854 characterization of biomass burning for climate modeling, *Atmos. Res.*, 111, 1–28, 2012.  
 1855  
 1856 Ichoku, C., and Y. Kaufman. A method to derive smoke emission rates from MODIS fire  
 1857 radiative energy measurements. *IEEE Trans on Geosc & Rem Sens*, 43 (11): 2636-2649  
 1858 [10.1109/TGRS.2005.857328], 2005.  
 1859  
 1860 Janssens-Maenhout, G., Crippa, M., Guizzardi, D., Dentener, F., Muntean, M., Pouliot,  
 1861 G., Keating, T., Zhang, Q., Kurokawa, J., Wankmüller, R., Denier van der Gon, H.,  
 1862 Kuenen, J. J. P., Klimont, Z., Frost, G., Darras, S., Koffi, B., and Li, M.: HTAP\_v2.2: a  
 1863 mosaic of regional and global emission grid maps for 2008 and 2010 to study

hemispheric transport of air pollution, *Atmos. Chem. Phys.*, 15, 11411–11432, <https://doi.org/10.5194/acp-15-11411-2015>, 2015.

Jordan, N., Ichoku, C., and Hoff, R.: Estimating smoke emissions over the U.S. Southern Great Plains using MODIS fire radiative power and aerosol observations, *Atmos. Env.*, 42, 2007–2022, 2008.

Kahn, R.A., Gaitley B.J., Garay M.J., Diner D.J., Eck T., Smirnov A., and Holben B.N.: Multiangle Imaging SpectroRadiometer global aerosol product assessment by comparison with the Aerosol Robotic Network. *J. Geophys. Res.* 115, D23209, doi: 10.1029/2010JD014601, 2010.

Kalashnikova O. V., and Kahn R.A.: Ability of multiangle remote sensing observations to identify and distinguish mineral dust types: Part 2. Sensitivity over dark water *J. Geophys. Res.*, D11207, 111 10.1029/2005JD006756, 2006.

Kaiser, J. W., Heil, A., Andreae, M. O., Benedetti, A., Chubarova, N., Jones, L., Morcrette, J.-J., Razinger, M., Schultz, M. G., Suttie, M., and van der Werf, G. R.: Biomass burning emissions estimated with a global fire assimilation system based on observations of fire radiative power, *Biogeosciences*, 9, 527–554, doi:10.5194/bg-9-527-2012, 2012.

Kaiser, J.W., Flemming, J., Schultz, M. G., Suttie, M., and Wooster, M. J.: The MACC Global Fire Assimilation System: First Emission Products (GFASv0), Tech. Memo. 596, ECMWF, Reading, UK, 2009.

Kaufman, Y. J., C. O. Justice, L. P. Flynn, J. D. Kendall, E. M. Prins, L. Giglio, D. E. Ward, W. P. Menzel, and A. W. Setzer. Potential global fire monitoring from EOS-MODIS, *J. Geophys. Res.*, 103(D24), 32,215–32,238, doi:10.1029/98JD01644, 1998.

Liousse, B., Guillaume, J. M., Grégoire, M., Mallet, C., Galy, C., Pont, V., Akpo, A., Bedou, M., Castéra, P., Dungall, L., Gardrat, E., Granier, C., Konaré, A., Malavelle, F., Mariscal, A., Mieville, A., Rosset, R., Serça, D., Solmon, F., Tummon, F., Assamoi, E., Yoboué, V., and Van Velthoven, P.: Updated African biomass burning emission inventories in the framework of the AMMAIDAF program, with an evaluation of combustion aerosols, *Atmos. Chem. Phys.*, 10, 7347–7382, doi:10.5194/acp-10-7347-2010, 2010.

Molod, A. M., L. L. Takacs, M. J. Suarez, and J. Bacmeister. Development of the GEOS atmospheric general circulation model: evolution from MERRA to MERRA2. " *Geosci. Model Dev.* 8 1339–1356 [10.5194/gmd-8-1339-2015], 2015.

Pan, X., Chin, M., Gautam, R., Bian, H., Kim, D., Colarco, P. R., Diehl, T. L., Takemura, T., Pozzoli, L., Tsigaridis, K., Bauer, S., and Bellouin, N.: A multi-model evaluation of aerosols over South Asia: common problems and possible causes, *Atmos. Chem. Phys.*, 15, 5903–5928, <https://doi.org/10.5194/acp-15-5903-2015>, 2015.



**Formatted:** Don't adjust right indent when grid is defined, Space After: 6 pt, No widow/orphan control, Don't adjust space between Latin and Asian text, Don't adjust space between Asian text and numbers

**Formatted:** Font color: Auto

**Deleted:** Levy, R.C., Remer, L.A., Kleidman, R.G., Mattoo, S., Ichoku, C., Kahn, R. and Eck, T.F. Global evaluation of the Collection 5 MODIS dark-target aerosol products over land. *Atmospheric Chemistry and Physics*, 10(21), pp.10399-10420, 2010.



1917 Pan, X., Chin, M., Ichoku, C. M., & Field, R. D. Connecting Indonesian fires  
 1918 and drought with the type of El Niño and phase of the Indian Ocean dipole during 1979–  
 1919 2016. *Journal of Geophysical Research: Atmospheres*, 123.  
 1920 <https://doi.org/10.1029/2018JD028402>, 2018.  
 1921  
 1922 Peterson, D., & Wang, J. A Sub-pixel-based calculate of fire radiative power from  
 1923 MODIS observations: 2. Sensitivity analysis and potential fire weather application.  
 1924 *Remote Sensing of Environment*, 129, 231–249, 2013.  
 1925  
 1926 Peterson, D. A., J. R. Campbell, E. J. Hyer, M. D. Fromm, G. P. Kablick, J. H. Cossuth,  
 1927 and M. T. DeLand. Wildfire-driven thunderstorms cause a volcano-like stratospheric  
 1928 injection of smoke. *npj Climate and Atmospheric Science*, **1**, 30, 2018.  
 1929  
 1930 Petrenko, M., R. Kahn, M. Chin, A. Soja, T. Kucsera, and Harshvardhan. The use of  
 1931 satellite-measured aerosol optical depth to constrain biomass burning emissions source  
 1932 strength in the global model GOCART, *J. Geophys. Res.*, 117, D18212,  
 1933 doi:10.1029/2012JD017870, 2012.  
 1934  
 1935 Petrenko, M., Kahn, R., Chin, M., & Limbacher, J. Refined use of  
 1936 satellite aerosol optical depth snapshots to constrain biomass burning emissions  
 1937 in the GOCART model. *Journal of Geophysical Research: Atmospheres*, 122, 10,983–  
 1938 11,004. <https://doi.org/10.1002/2017JD026693>, 2017.  
 1939  
 1940 Pereira, G., Siqueira, R., Rosário, N. E., Longo, K. L., Freitas, S. R., Cardozo, F. S.,  
 1941 Kaiser, J. W., and Wooster, M. J.: Assessment of fire emission inventories during the  
 1942 South American Biomass Burning Analysis (SAMBBA) experiment, *Atmos. Chem.*  
 1943 *Phys.*, 16, 6961–6975, doi:10.5194/acp-16-6961-2016, 2016.  
 1944  
 1945 Randerson, J. T., Chen, Y., van der Werf, G. R., Rogers, B. M., and Morton, D. C.:  
 1946 Global burned area and biomass burning emissions from small fires, *J. Geophys. Res.-*  
 1947 *Biogeo.*, 117, G04012, <https://doi.org/10.1029/2012JG002128>, 2012.  
 1948  
 1949 Randles, C. A., A. da Silva, V. Buchard, et al. 2017: The MERRA-2 Aerosol Reanalysis,  
 1950 1980-onward, Part I: System Description and Data Assimilation Evaluation. *J Clim*, doi:  
 1951 10.1175/jclid-16-0609.1  
 1952  
 1953 Reddington, C. L., Spracklen, D. V., Artaxo, P., Ridley, D. A., Rizzo, L. V., and Arana,  
 1954 A.: Analysis of particulate emissions from tropical biomass burning using a global  
 1955 aerosol model and long-term surface observations, *Atmos. Chem. Phys.*, 16, 11083–  
 1956 11106, <https://doi.org/10.5194/acp-16-11083-2016>, 2016.  
 1957  
 1958 Reid, J. S., R. Koppmann, T. F. Eck, and D. P. Eleuterio. A review of biomass burning  
 1959 emissions part II: Intensive physical properties of biomass burning particles, *Atmos.*  
 1960 *Chem. Phys.*, 5, 799–825, 2005.  
 1961

**Deleted:**   
 Remer, L. A., et al. (2005), The MODIS aerosol algorithm,  
 products, and validation, *J. Atmos. Sci.*, 62(4), 947–973. 

1965 Reid, C.E.; Brauer, M.; Johnston, F.H.; Jerrett, M.; Balmes, J.R.; Elliott, C.T. Critical  
 1966 Review of Health Impacts of Wildfire Smoke Exposure. *Environ. Health Perspect*, 124,  
 1967 1334–1343, 2016.  
 1968  
 1969 Rienecker, M. M., M. J. Suarez, R. Gelaro, R. Todling, J. Bacmeister, E. Liu, M. G.  
 1970 Bosilovich, S. D. Schubert, L. Takacs, G.-K. Kim, S. Bloom, J. Chen, D. Collins, A.  
 1971 Conaty, A. da Silva, W. Gu, J. Joiner, R. D. Koster, R. Lucchesi, A. Molod, T. Owens, S.  
 1972 Pawson, P. Pegion, C. R. Redder, R. Reichle, F. R. Robertson, A. G. Ruddick, M.  
 1973 Sienkiewicz, J. Woollen, MERRA - NASA's Modern-Era Retrospective Analysis for  
 1974 Research and Applications. *J. Climate*, 24, 3624–3648, 2011.  
 1975  
 1976 Roberts, G., Wooster, M., & Lagoudakis, E. Annual and diurnal African biomass burning  
 1977 temporal dynamics. *Biogeosciences*, 6, 2009.  
 1978  
 1979 [Saide, P. E., et al.: Revealing important nocturnal and day-to-day variations in fire smoke](#)  
 1980 [emissions through a multiplatform inversion, \*Geophys. Res. Lett.\*, 42, 3609–](#)  
 1981 [3618, doi:10.1002/2015GL063737, 2015.](#)  
 1982  
 1983 Simon, H. and Bhawe, P. V.: Simulating the Degree of Oxidation in Atmospheric Organic  
 1984 Particles, *Environ. Sci. Technol.*, 46, 331–339, doi:10.1021/es202361w, 2012.  
 1985  
 1986 [Tansey, K., J. Beston, A. Hoscilo, S. E. Page, and C. U. Paredes Hernandez, Relationship](#)  
 1987 [between MODIS fire hotspot count and burned area in a degraded tropical peat swamp](#)  
 1988 [forest in Central Kalimantan, Indonesia, \*J. Geophys. Res.\*, 113, D23112,](#)  
 1989 [doi:10.1029/2008JD010717, 2008.](#)  
 1990  
 1991 Turpin, B. J. and Lim, H. J.: Species contributions to PM<sub>2.5</sub> mass concentrations:  
 1992 Revisiting common assumptions for estimating organic mass, *Aerosol Sci. Tech.*, 35,  
 1993 602–610, doi:10.1080/02786820152051454, 2001.  
 1994  
 1995 van der Werf, G. R., Randerson, J. T., Giglio, L., Collatz, G. J., Kasibhatla, P. S., and  
 1996 Arellano Jr., A. F.: Interannual variability in global biomass burning emissions from 1997  
 1997 to 2004, *Atmos. Chem. Phys.*, 6, 3423–3441, [https://doi.org/10.5194/acp-6-3423-](https://doi.org/10.5194/acp-6-3423-2006)  
 1998 [2006, 2006.](#)  
 1999  
 2000 van der Werf, G. R., Randerson, J. T., Giglio, L., Collatz, G. J., Mu, M., Kasibhatla, P.  
 2001 S., Morton, D. C., DeFries, R. S., Jin, Y., and van Leeuwen, T. T.: Global fire emissions  
 2002 and the contribution of deforestation, savanna, forest, agricultural, and peat fires (1997–  
 2003 2009), *Atmos. Chem. Phys.*, 10, 11707–11735, [https://doi.org/10.5194/acp-10-11707-](https://doi.org/10.5194/acp-10-11707-2010)  
 2004 [2010, 2010.](#)  
 2005  
 2006 van der Werf, G. R., Randerson, J. T., Giglio, L., van Leeuwen, T. T., Chen, Y., Rogers,  
 2007 B. M., Mu, M., van Marle, M. J. E., Morton, D. C., Collatz, G. J., Yokelson, R. J., and  
 2008 Kasibhatla, P. S.: Global fire emissions estimates during 1997–2016, *Earth Syst. Sci.*  
 2009 *Data*, 9, 697–720, <https://doi.org/10.5194/essd-9-697-2017>, 2017.  
 2010

**Deleted:** ¶

Sayer, A. M., L. A. Munchak, N. C. Hsu, R. C. Levy, C. Bettenhausen, and M.-J. Jeong. MODIS Collection 6 aerosol products: Comparison between Aqua's e-Deep Blue, Dark Target, and "merged" data sets, and usage recommendations, *J. Geophys. Res. Atmos.*, 119, 13,965–13,989, doi:10.1002/2014JD022453, 2014. ¶

**Deleted:** ¶

2019 van Leeuwen, T. T., van der Werf, G. R., Hoffmann, A. A., Detmers, R. G., Ruecker, G.,  
 2020 French, N. H. F., Archibald, S., Carvalho, J. A. J., Cook, G. D., de Groot, W. J., Hely, C.,  
 2021 Kasischke, E. S., Kloster, S., McCarty, J. L., Pettinari, M. L., Savadogo, P., Alvarado, E.  
 2022 C., Boschetti, L., Manuri, S., Meyer, C. P., Siegert, F., Trollope, L. A. and Trollope, W.  
 2023 S. W.: Biomass burning fuel consumption rates: a field measurement database,  
 2024 Biogeosciences, 11(24), 7305–7329, doi:10.5194/bg-11-7305-2014, 2014.  
 2025  
 2026 van Marle, M. J. E., Kloster, S., Magi, B. I., Marlon, J. R., Daniau, A.-L., Field, R. D.,  
 2027 Arneth, A., Forrest, M., Hantson, S., Kehrwald, N. M., Knorr, W., Lasslop, G., Li, F.,  
 2028 Mangeon, S., Yue, C., Kaiser, J. W., and van der Werf, G. R.: Historic global biomass  
 2029 burning emissions for CMIP6 (BB4CMIP) based on merging satellite observations with  
 2030 proxies and fire models (1750–2015), Geosci. Model Dev., 10, 3329–3357,  
 2031 <https://doi.org/10.5194/gmd-10-3329-2017>, 2017.  
 2032  
 2033 Wang, J., C. Ge, Z. Yang, E. J. Hyer, J. S. Reid, B.-N. Chew, M. Mahmud, Y. Zhang, and  
 2034 M. Zhang, Mesoscale modeling of smoke transport over the Southeast Asian Maritime  
 2035 Continent: interplay of sea breeze, trade wind, typhoon, and topography, Atmospheric  
 2036 Research, 122, 486–503, doi: 10.1016/j.atmosres.2012.05.009, 2013.  
 2037  
 2038 Wang, J., S.A. Christopher, U.S. Nair, J.S. Reid, E.M. Prins, J. Szykman, and J.L. Hand,  
 2039 Mesoscale modeling of Central American smoke transport to the United States, 1: "top-  
 2040 down" assessment of emission strength and diurnal variation impacts, J. Geophys. Res.,  
 2041 11, D05S17, doi:10.1029/2005JD006416, 2006.  
 2042  
 2043 Wang, J., Yue, Y., Wang, Y., Ichoku, C., Ellison, L., & Zeng, J. Mitigating  
 2044 satellite-based fire sampling limitations in deriving biomass burning emission  
 2045 rates: Application to WRF-Chem model over the Northern sub-Saharan African  
 2046 Region. Journal of Geophysical Research: Atmospheres, 123, 507–528. [https://doi.](https://doi.org/10.1002/2017JD026840)  
 2047 [org/10.1002/2017JD026840](https://doi.org/10.1002/2017JD026840), 2018.  
 2048  
 2049 [White, W. H. and Roberts, P. T.: On the nature and origins of visibility-reducing aerosols](#)  
 2050 [in the Los Angeles air basin, Atmos. Environ., 11, 803–812, 1977.](#)  
 2051  
 2052 Wiedinmyer, C., Akagi, S. K., Yokelson, R. J., Emmons, L. K., Al-Saadi, J. A., Orlando,  
 2053 J. J., and Soja, A. J. The Fire Inventory from NCAR (FINN): a high resolution global  
 2054 model to estimate the emissions from open burning, Geosci. Model Dev., 4, 625–  
 2055 641, doi:10.5194/gmd-4-625-2011, 2011.  
 2056  
 2057 Wooster, M. J., G. Roberts, G. L. W. Perry, and Y. J. Kaufman. Retrieval of biomass  
 2058 combustion rates and totals from fire radiative power observations: FRP derivation and  
 2059 calibration relationships between biomass consumption and fire radiative energy release,  
 2060 J. Geophys. Res., 110, D24311, doi:10.1029/2005JD006318, 2005.  
 2061  
 2062 Wooster, M. J., B. Zhukov, and D. Oertel. Fire radiative energy for quantitative study of  
 2063 biomass burning: Derivation from the BIRD experimental satellite and comparison to  
 2064 MODIS fire products, Remote Sens. Environ., 86(1), 83–107, doi:10.1016/S0034-  
 2065 4257(03)00070-1, 2003.

Deleted: ¶

2067  
 2068 Yang, Z., J. Wang, C. Ichoku, E. Hyer, and J. Zeng, Mesoscale modeling and satellite  
 2069 observation of transport and mixing of smoke and dust particles over northern sub-  
 2070 Saharan African region, *J. Geophys. Res. Atmos.*, 118, 12,139-12,157,  
 2071 doi:10.1002/2013JD020644, 2013.  
 2072  
 2073 Yokelson, R. J., Burling, I. R., Urbanski, S. P., Atlas, E. L., Adachi, K., Buseck, P. R.,  
 2074 Wiedinmyer, C., Akagi, S. K., Toohey, D. W., and Wold, C. E.: Trace gas and particle  
 2075 emissions from open biomass burning in Mexico, *Atmos. Chem. Phys.*, 11, 6787–  
 2076 6808, doi:10.5194/acp-11-6787-2011, 2011.  
 2077  
 2078 Zhang, F., J. Wang, C. M. Ichoku, et al.. Sensitivity of mesoscale modeling of smoke  
 2079 direct radiative effect to the emission inventory: a case study in northern sub-Saharan  
 2080 African region. *Environmental Research Letters*, 9 (7): 075002 (14 pp) [10.1088/1748-  
 2081 9326/9/7/075002], 2014.  
 2082  
 2083 [Zhang, Q., Worsnop, D. R., Canagaratna, M. R., and Jimenez, J. L.: Hydrocarbon-like](#)  
 2084 [and oxygenated organic aerosols in Pittsburgh: insights into sources and processes of](#)  
 2085 [organic aerosols, \*Atmos. Chem. Phys.\*, 5, 3289–3311, 2005b, \[http://www.atmos-chem-\]\(http://www.atmos-chem-phys.net/5/3289/2005/\)](#)  
 2086 [phys.net/5/3289/2005/.](#)  
 2087  
 2088 Zhu, J., X. Xia, J. Wang, C. Wiedinmyer, J. A. Fisher, C. A. Keller. Impact of Southeast  
 2089 Asian smoke on aerosol properties in Southwest China: first comparison of model  
 2090 simulations with satellite and ground observation, *J. Geophys. Res.-Atmos.*, 122, 3904–  
 2091 3919, 2017.  
 2092

Deleted: ¶

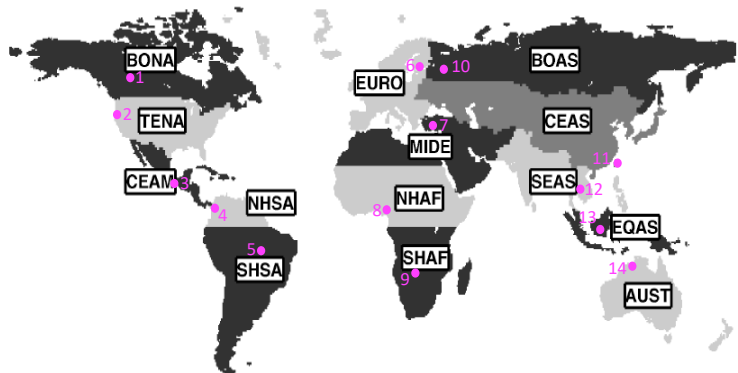
Deleted: ¶

Deleted: ¶

Formatted: Font color: Text 1

2096  
2097  
2098  
2099  
2100

FIGURES



BONA	Boreal North America	NHAF	Northern Hemisphere Africa
TENA	Temperate North America	SHAF	Southern Hemisphere Africa
CEAM	Central America	BOAS	Boreal Asia
NHSA	Northern Hemisphere South America	CEAS	Central Asia
SHSA	Southern Hemisphere South America	SEAS	Southeast Asia
EURO	Europe	EQAS	Equatorial Asia
MIDE	Middle East	AUST	Australia and New Zealand

2101  
2102  
2103  
2104

Figure 1. Map showing the 14 regions used in this study, following GFED regionalization defined by Giglio et al. (2006) and van der Werf et al. (2006; 2017). The fourteen AERONET sites selected for detailed analysis in the respective regions are represented by the numbered magenta dots. These AERONET sites and the included data years (in parentheses) for calculating aerosol climatology are: 1-Fort McMurray (2005-2018), 2-Monterey (2002-2018), 3-Tuxtla Gutierrez (2005-2010), 4-Medellin (2012-2016), 5-Alta Floresta (1993-2018), 6-Toravere (2002-2017), 7-IMS METU ERDEMLI (1999-2017), 8-Ilorin (1998-2018), 9-Mongu (1997-2010), 10-Moscow MSU MO (2001-2017), 11-EPA NCU (2004-2018), 12-Chiang Mai Met Sta (2007-2017), 13-Palangkaraya (2012-2017), 14-Lake Argyle (2001-2017).



## OC biomass burning emission for 2008

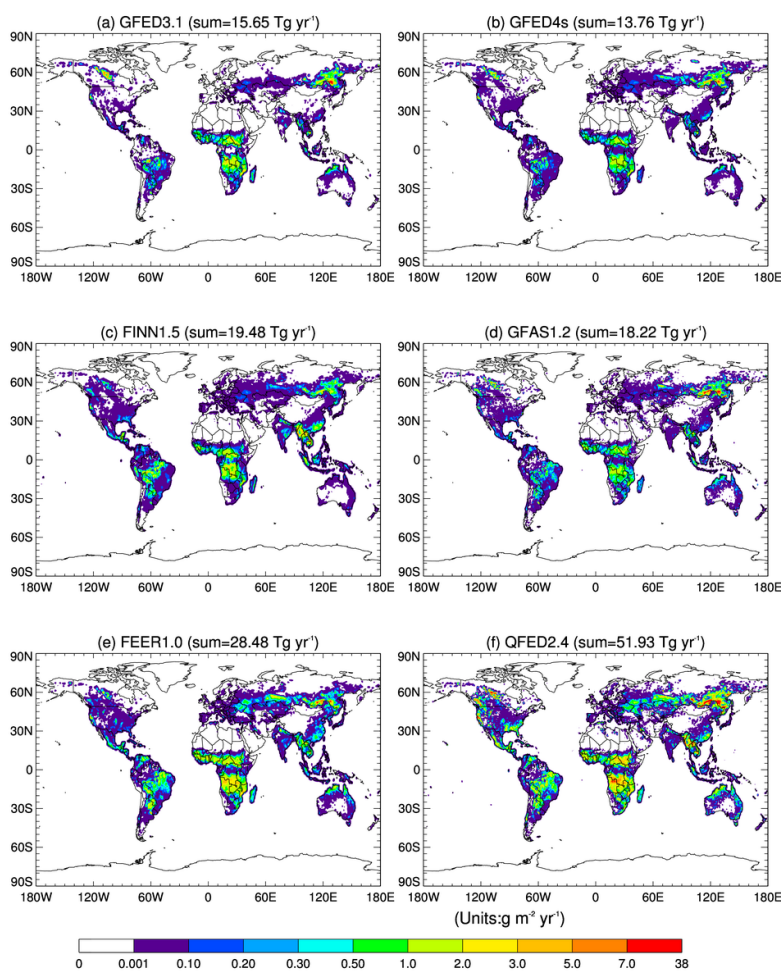
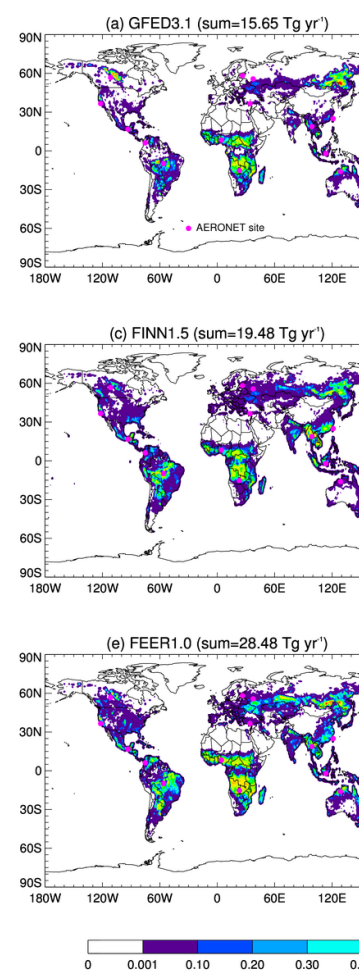


Figure 2. The spatial distribution of annual total organic carbon biomass burning emissions for 2008 estimated by six biomass burning emission datasets (units: g m<sup>-2</sup> yr<sup>-1</sup>). The global total amount is indicated in the parentheses.

## OC biomass burr



Deleted:

Formatted: Superscript

Formatted: Superscript

Deleted: The fourteen selected AERONET sites are indicated as magenta dots.

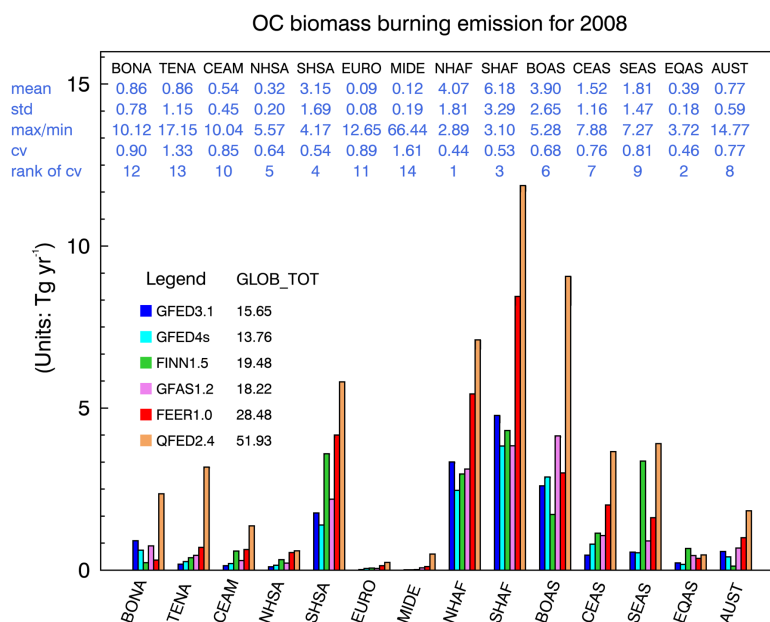


Figure 3. The regional annual **total** organic carbon biomass burning emissions for 2008 in six biomass burning emission datasets in 14 regions (units: Tg yr<sup>-1</sup>). The global annual total amount is listed after the name of each dataset (GLOB\_TOT). Relevant statistics for the six BB emission datasets in each region are also listed under the short name of each region on the top of the panel in blue, with the mean of the six BB emission datasets in the first row. Three different methods to measure the spread of the six BB emission datasets are shown as well: one absolute method, i.e., the standard deviation (std) in the second row, and two relative methods, i.e., the ratio of max to min (i.e., maximum/minimum) shown in the third row, and the coefficient of variation (cv), defined as the ratio of the std to the mean, in the fourth row. The rankings of the regions regarding the spread of the BB emissions datasets according to cv are shown in the fifth row (i.e., a ranking of 1 means that this region shows the least spread among the six BB emissions datasets, while a ranking of 14 indicates that this region has the largest spread among the 14 regions).

Deleted: total

Deleted: -

Deleted: !

Deleted: R

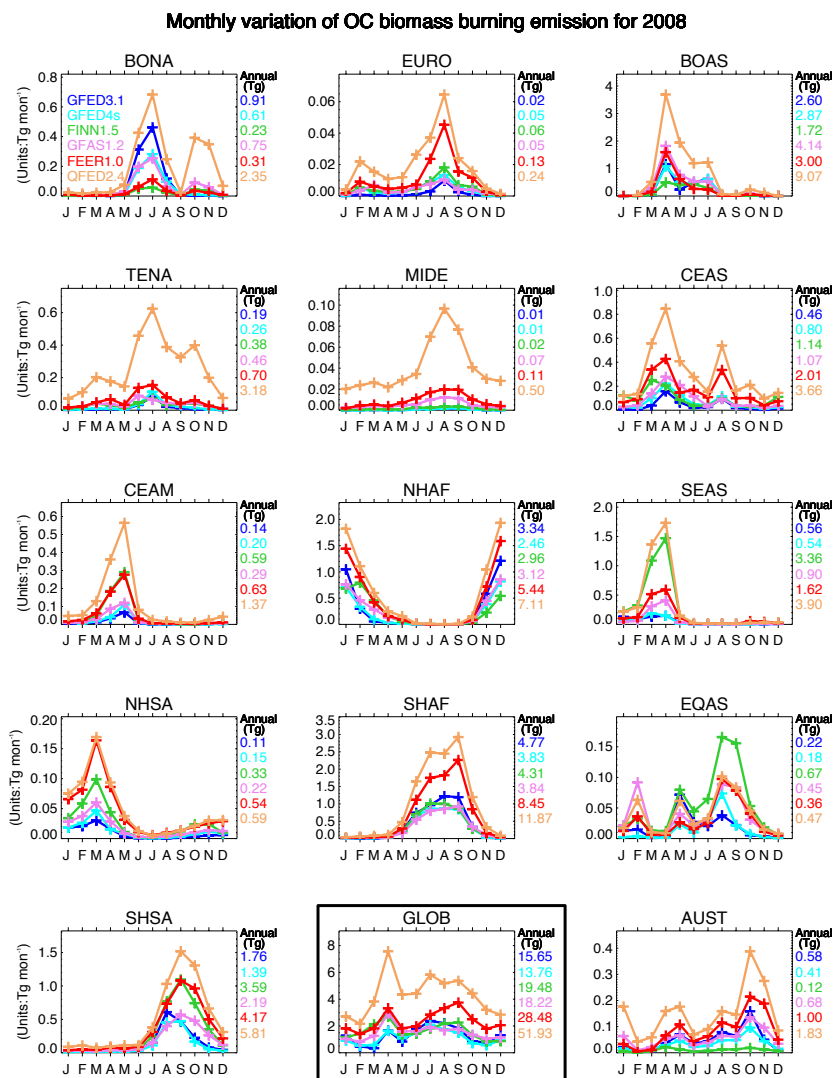


Figure 4. Monthly variation of organic carbon biomass burning emissions for 2008 in six biomass burning emission datasets in 14 regions and the globally (i.e., GLOB, highlighted with a black box). The annual total emission is listed on the right side of each panel.

Deleted: total

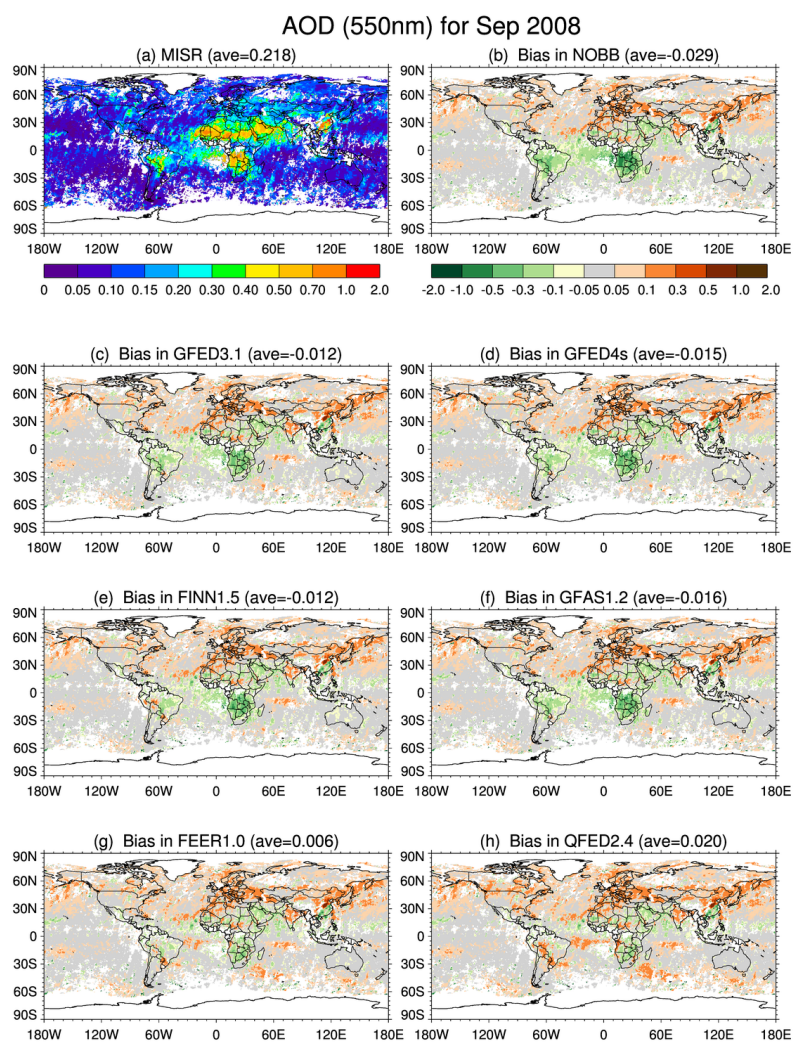
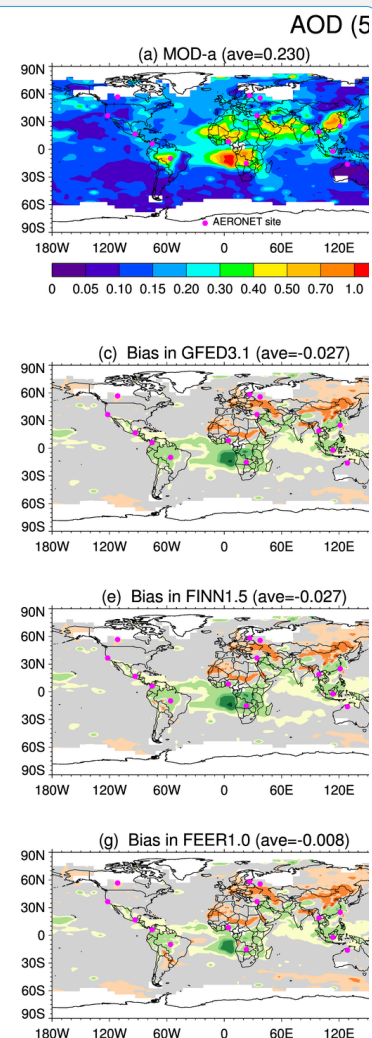


Figure 5. (a) The spatial distribution of monthly mean AOD at 558nm for September 2008 from MISR with the white color representing missing value. The global averaged value (ave) is shown in the parentheses. (b)-(h) are for GEOS model biases (i.e., model at 550nm minus MISR at 558nm) in seven model experiments, i.e., bias in (b) NOBB, (c) GFED3.1, (d) GFED4s, (e) FINN1.5, (f) GFAS1.2, (g) FEER1.0, (h) QFED2.4, respectively.



**Deleted:**

**Deleted:** 0

**Deleted:** MODIS-aqua (i.e., MOD-a)

**Deleted:** The fourteen selected AERONET stations are labeled as magenta dots.

**Deleted:** ODIS-a



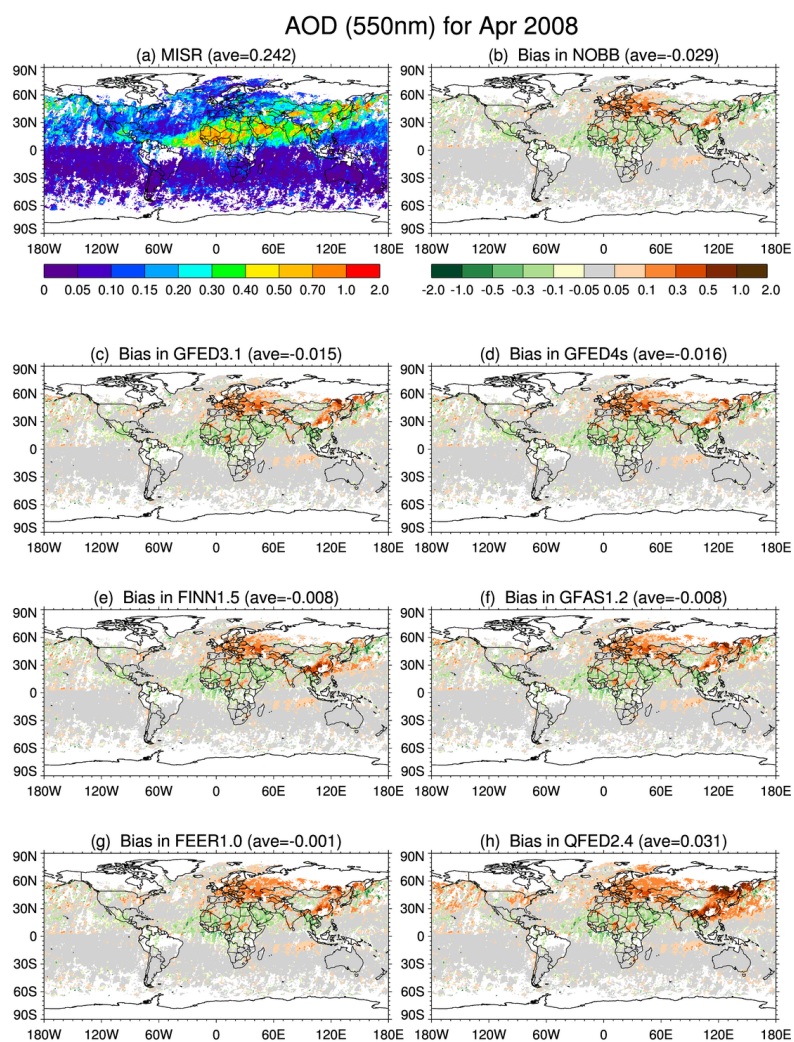
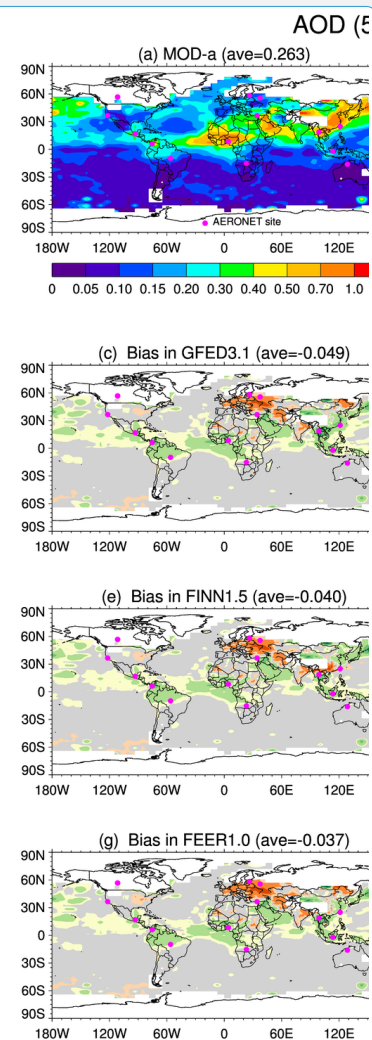


Figure 6. Same as Figure 5 except for April 2008.



Deleted:



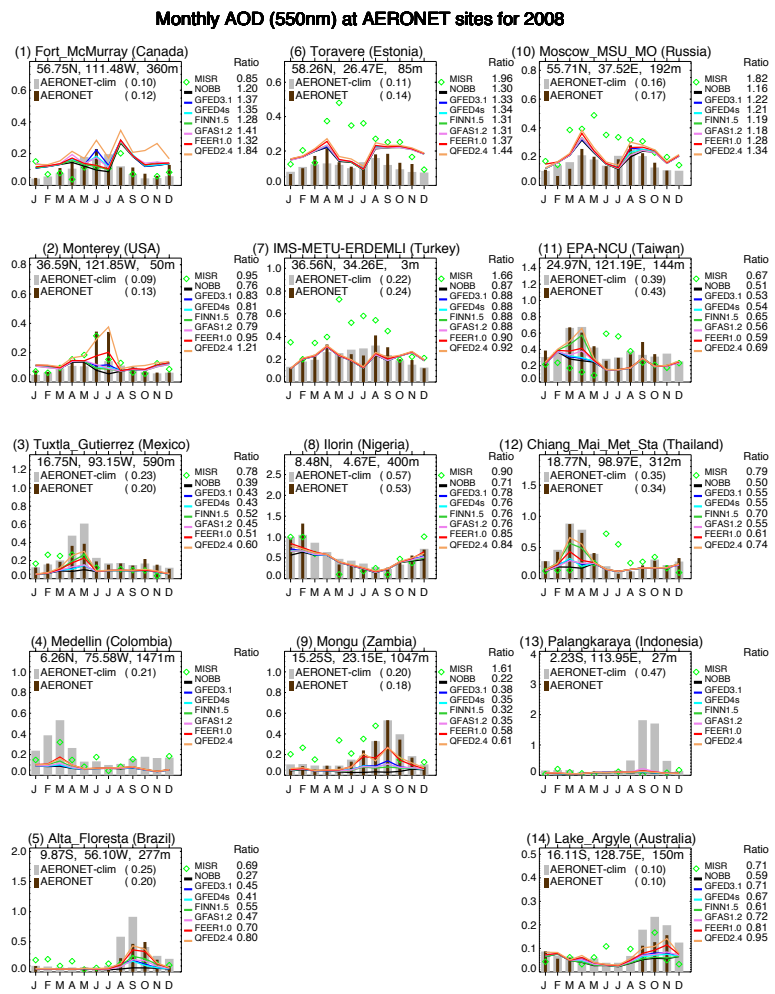
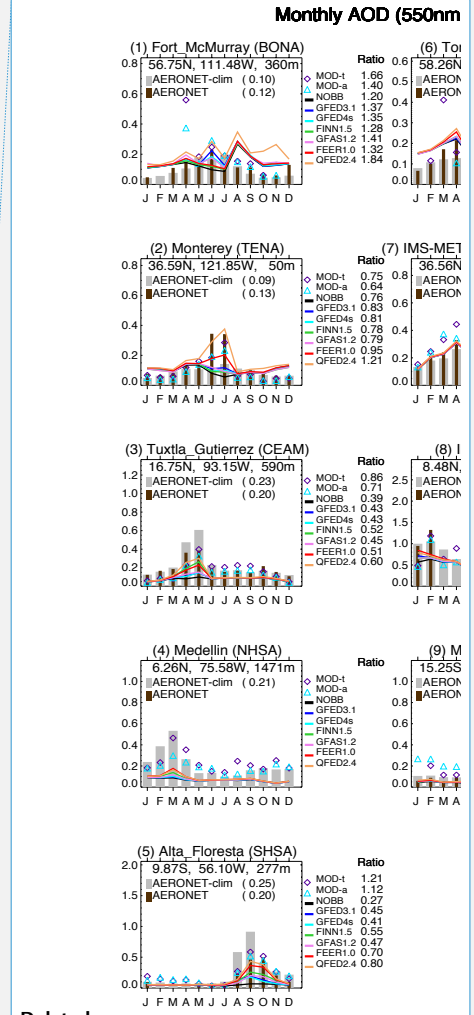


Figure 7. Monthly variation of AOD (at 550nm wavelength) for 2008 over 14 AERONET sites selected from the respective 14 regions (with its country indicated in parentheses). The climatology of AERONET AOD (i.e., AERONET-clim) is represented by light gray thick bars with yearly mean value shown in the parenthesis after its name, along with the monthly AERONET AOD represented by the brown thin bars. MISR is represented by the green diamond, and seven GEOS experiments with different biomass burning emission options are represented by the lines in different colors. The annual ratio (Ratio=model/AERONET) listed on the right hand is estimated by averaging over monthly ratio.



Deleted:  
Deleted: ir  
Deleted: , as  
Deleted: MODIS-Terra (MOD-T), MODIS-Aqua (MOD-a) are  
Deleted: purple diamond and blue triangle  
Deleted: respectively,  
Deleted: line

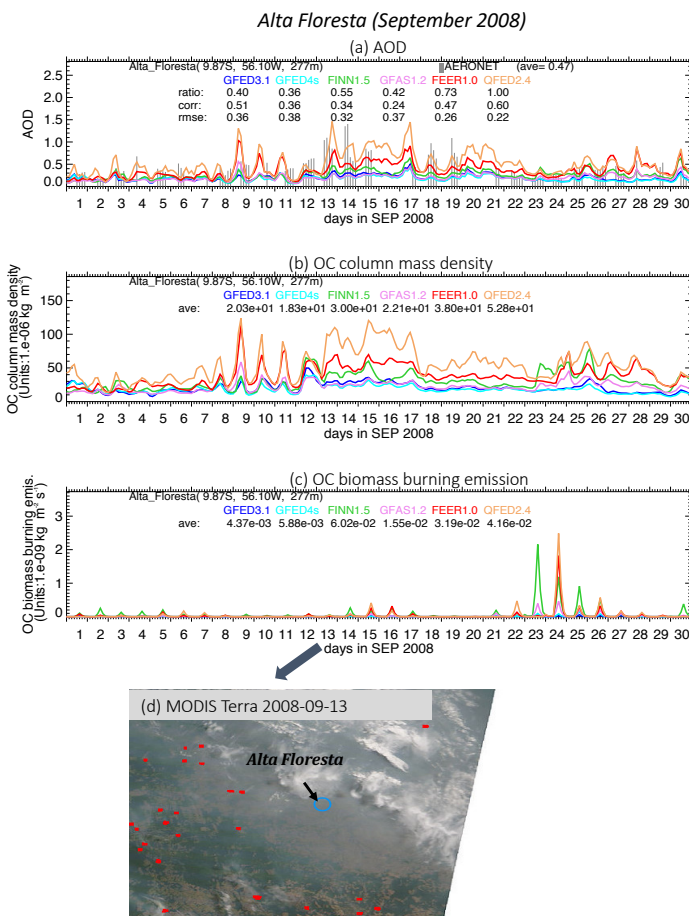
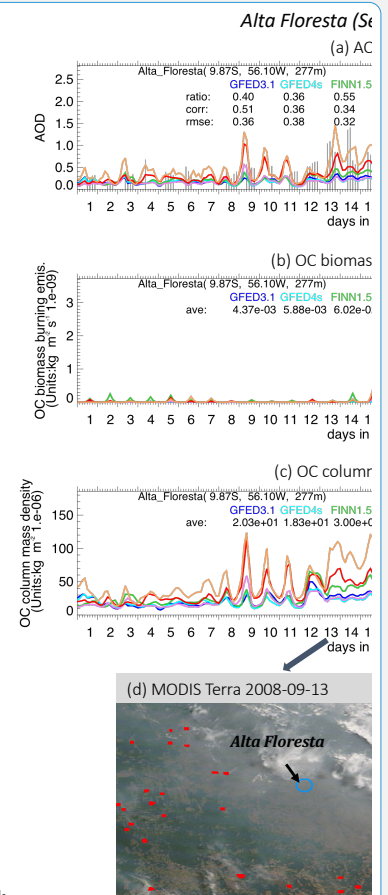


Figure 8. Characteristics of the observed and the simulated aerosols at Alta Floresta during September 2008: (a) The 3-hourly time series of AOD at 550nm. The AERONET is represented by vertical gray bars, and the outputs from the six model experiments are represented by the color curves. The relevant statistics are listed: *ave* is the monthly average, *ratio* is the fraction of the simulated to the observed AOD at all observed hours, *corr* is correlation between the observed and the simulated AOD, and *rmse* is root mean square error. (b) The 3-hourly time series of OC column mass density over the grid box where Alta Floresta is located (units:  $1.e-06 \text{ kg m}^{-2}$  or  $\text{mg m}^{-2}$ ). (c) Same as (b) but biomass burning OC emission rate (units:  $1.e-09 \text{ kg m}^{-2} \text{ s}^{-1}$  or  $\mu\text{g m}^{-2} \text{ s}^{-1}$ ). (d) MODIS-Terra true color image around Alta Floresta on September 13, 2008, overlaid with the active fire detections in red dots (Image credit: [https://aeronet.gsfc.nasa.gov/cgi-bin/bamgomass\\_interactive](https://aeronet.gsfc.nasa.gov/cgi-bin/bamgomass_interactive) and <https://worldview.earthdata.nasa.gov>).



Deleted:

- Deleted: local biomass burning OC emission rate averaged
- Formatted: Superscript
- Formatted: Superscript
- Deleted: OC column mass density
- Deleted: near and at
- Deleted: hot spots

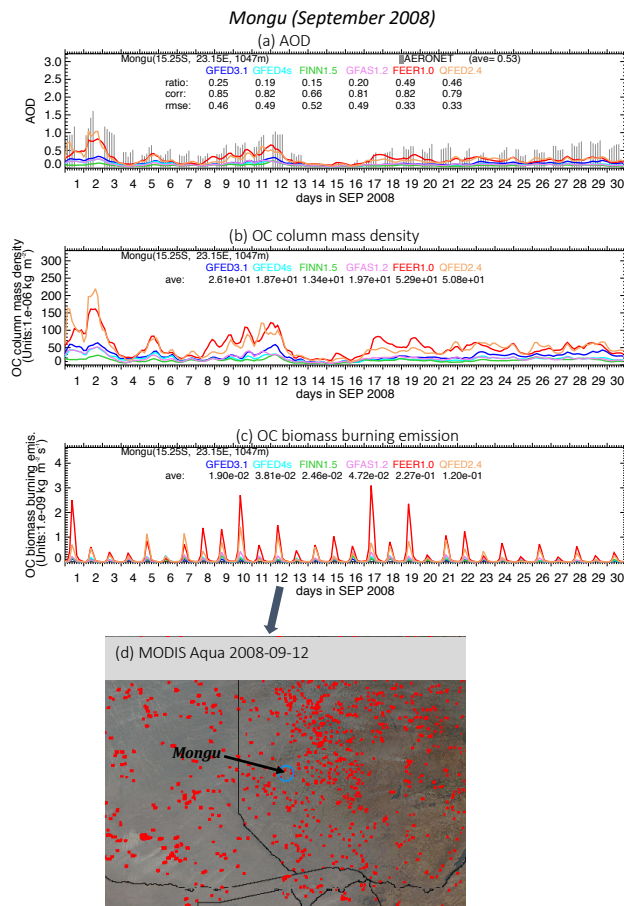
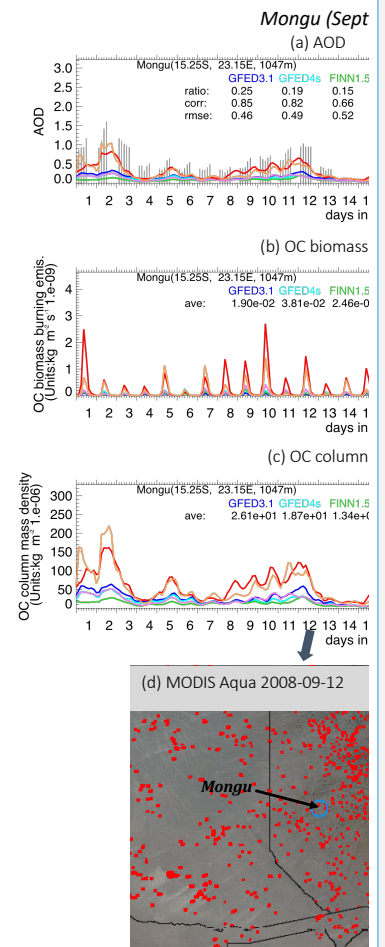


Figure 9. Characteristics of the observed and the simulated aerosols at Mongu during September 2008: (a) The 3-hourly time series of AOD at 550nm. The AERONET is represented by vertical gray bars, and the outputs from the six model experiments are represented by the color curves. The relevant statistics are listed: *ave* is the monthly average, *ratio* is the fraction of the simulated to the observed AOD at all observed hours, *corr* is correlation between the observed and the simulated AOD, and *rmse* is root mean square error. (b) The 3-hourly time series of OC column mass density over the grid box where Mongu is located (units:  $1.e-06 \text{ kg m}^{-2}$  or  $\text{mg m}^{-2}$ ). (c) Same as (b) but biomass burning OC emission rate (units:  $1.e-09 \text{ kg m}^{-2} \text{ s}^{-1}$  or  $\mu\text{g m}^{-2} \text{ s}^{-1}$ ). (d) MODIS-Aqua true color image around Mongu on September 12, 2008, overlaid with the active fire detections in red dots (Image credit: [https://aeronet.gsfc.nasa.gov/cgi-bin/bamgomass\\_interactive](https://aeronet.gsfc.nasa.gov/cgi-bin/bamgomass_interactive) and <https://worldview.earthdata.nasa.gov>).



Deleted:

Deleted: (b) The 3-hourly time series of local biomass burning OC emission rate averaged over one grid box where Mongu is located. (c) Same as (b) but OC column mass density.

Deleted: near and at

Deleted: hot spots

2216 **Table 1.** Summary of six biomass burning emission datasets during MODIS-era (i.e., 2000-present)

a. Burned area based approaches						
BB Emission Dataset	Original Grid	Time-Frame/Frequency	Burned Area	Active Fire Product	Fuel Consumption	Emission Factor
GFED3.1	0.5°×0.5° (lon×lat)	2000-2012/ 3-hourly, daily, monthly	MOD09GHK and/or MYD09GHK	Gridded composite L3 fire product MOD14A1 and/or MYD14A1	Estimated in CASA by product of fuel load and combustion completeness	Mainly from Andreae and Merlet (2001) with annual updates
GFED4s	0.25°×0.25° (lon×lat)	2000-2016/ 3-hourly, daily, monthly	Daily MCD64A1 product in Collection 5.1 at 500m spatial resolution	L3 MOD14A1 and MYD14A1; fire location product MCD14ML	Revised CASA by optimizing parameterization, reorientation of fuel consumption in frequently burned landscapes	Mainly from Akagi et al. (2011), supplemented by Andreae and Merlet (2001) and other
FINN1.5	1km <sup>2</sup>	2002-2015/ daily	Estimated by active fire counts: 0.75 km <sup>2</sup> for savannas at each fire pixel, 1km <sup>2</sup> for other types	MODIS NRT active fire product (MCD14DL)	Assigned according to the global wildland fire emission model (Hoelzemann et al., 2004) with updates	Mainly from Andreae and Merlet (2001) and Akagi et al. (2011), with updates through 2015
b. FRP based approaches						
BB Emission Dataset	Original Grid	Time-Frame/Frequency	FRP	Emission Coefficient (C <sub>e</sub> )	Emission Factor	
GFAS1.2	0.1×0.1 (lon×lat)	2003-Present/daily	Assimilation of level 2 MOD14 and MYD14 FRP	Calculated by regression of FRP to dry matter combustion rate of GFED v3.1 in 8 biomes.	Mainly from Andreae and Merlet (2001) with updates from literatures through 2009	
FEER1.0	0.1×0.1 (lon×lat)	2003-Present/ daily, monthly	From GFASv1.2 (Kaiser et al., 2012, see above)	Calculated by linear regression between FRP and total particulate matter emission rate estimated from MODIS AOD at each grid	Andreae and Merlet (2001) with updates provided by Andreae in 2014	
QFED2.4	0.1×0.1 (lon×lat)	2000-Present/ daily, monthly	Level 2 fire products MOD14/MYD14	Calculated by regression of the GEOS simulated AOD to the MODIS AOD in 46 sub-regions and then aggregated into 4 biomes.	Andreae and Merlet (2001)	

CASA: Carnegie-Ames-Stanford-Approach biogeochemical

2223 **Table 2.** Comparison of emission factor (Units: g species per kg dry matter burned) used by GFED3.1<sup>1</sup> and GFED4s<sup>2</sup> (listed in the upper and lower part of the  
2224 cell respectively, bold if GFED4s is larger).

	Savanna and Grassland	Tropical Forest	Temperate Forest <sup>3</sup>	Boreal forest <sup>3</sup>	Peat Fires <sup>4</sup>	Agricultural Residues
<b>OC</b>	3.21 2.62	4.30 <b>4.71</b>	9.14 <b>9.60</b>	9.14 <b>9.60</b>	4.30 <b>6.02</b>	3.71 2.30
<b>BC</b>	0.46 0.37	0.57 0.52	0.56 0.50	0.56 0.50	0.57 0.04	0.48 <b>0.75</b>
<b>SO<sub>2</sub></b>	0.37 <b>0.48</b>	0.71 <b>0.40</b>	1.00 <b>1.10</b>	1.00 <b>1.10</b>	0.71 0.40	0.40 0.40
<b>PM<sub>2.5</sub></b>	<u>4.94</u> <b>7.20</b>	<u>9.05</u> <b>9.10</b>	<u>12.84</u> <b>12.90</b>	<u>12.84</u> <b>15.30</b>	<u>9.05</u> <b>9.10</b>	<u>8.25</u> <b>6.30</b>
<b>CO<sub>2</sub></b>	1646 <b>1686</b>	1626 <b>1643</b>	1572 <b>1647</b>	1572 1489	1703 1703	1452 <b>1585</b>
<b>CO</b>	61 <b>63</b>	101 93	106 88	106 <b>127</b>	210 210	94 <b>102</b>

2225 <sup>1</sup>. Mainly from Andreae and Merlet (2001) with annual updates

2226 <sup>2</sup>. Mainly from Akagi et al. (2011), supplemented by Andreae and Merlet (2001) and other sources

2227 <sup>3</sup>. GFED4s (van der Werf et al., 2017) further divides extra-tropical forest in GFED3 (van der Werf et al., 2010) into temperate forest and boreal forest.

2228 <sup>4</sup>. Based on Christian et al. (2003) for CO<sub>2</sub> and CO.

Deleted: ,



2233  
2234  
2235

**SUPPLEMENT**

# BC biomass burning emission for 2008

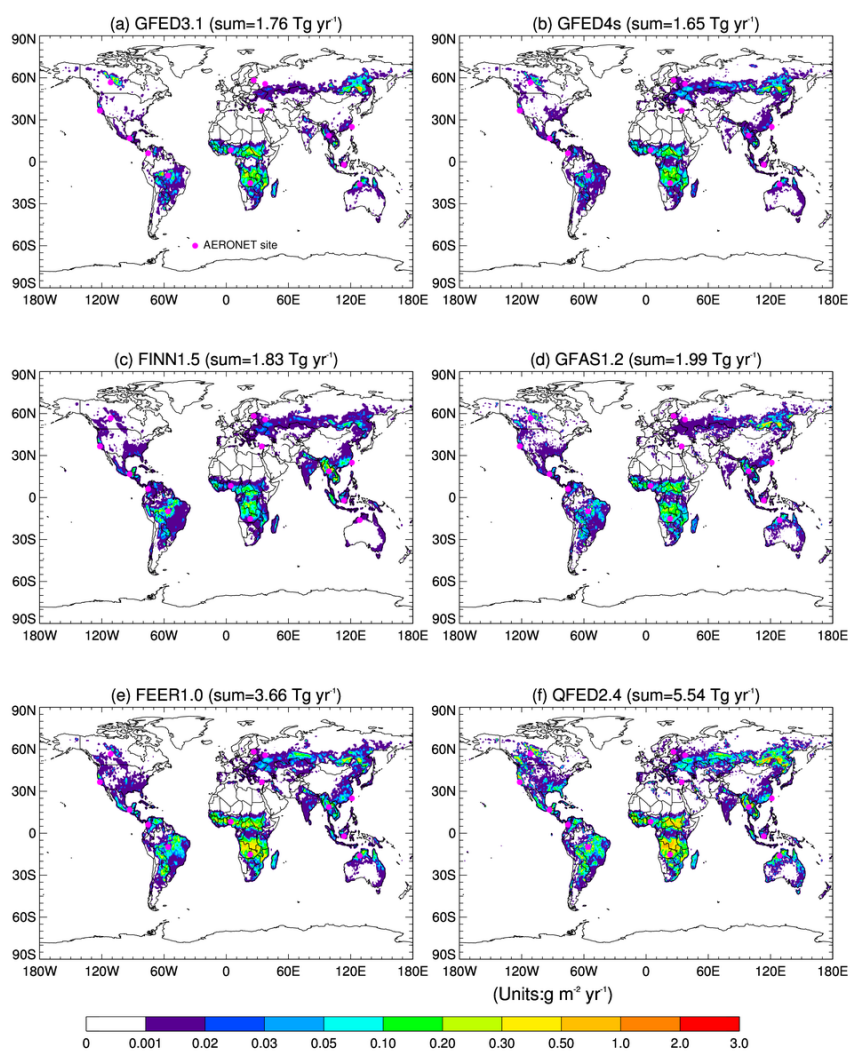


Figure S1. The spatial distribution of annual [total](#) black carbon biomass burning emissions for 2008 estimated by six biomass burning emission datasets. [The global total amount is indicated in the parentheses.](#) The fourteen selected AERONET sites are labeled as magenta dots.

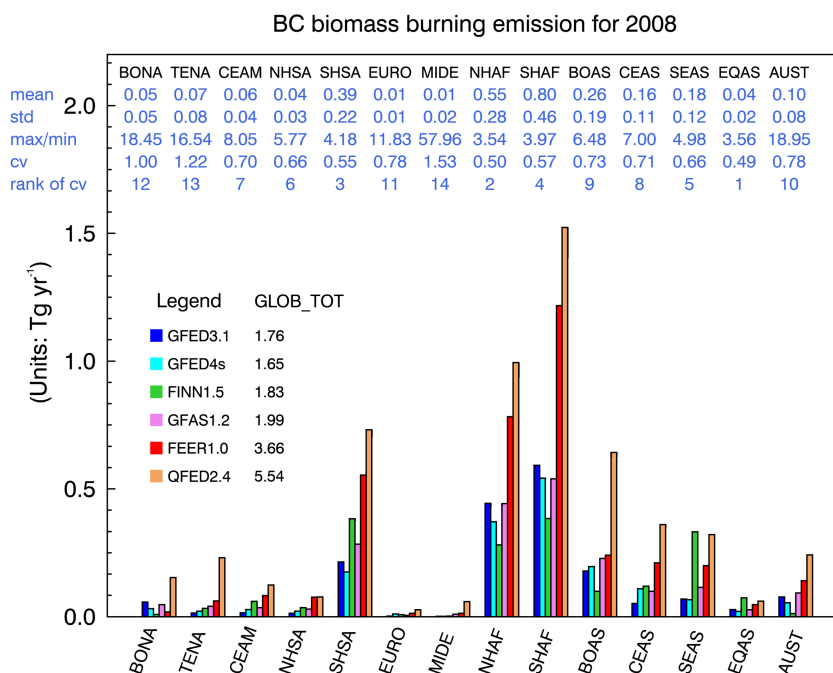


Figure S2. The regional annual total black carbon biomass burning emissions for 2008 in six biomass burning emission datasets in 14 regions (units:  $\text{Tg yr}^{-1}$ ). The global annual total amount is listed after the name of each dataset (GLOB\_TOT). Relevant statistics for the six BB emission datasets in each region are also listed under the short name of this region on the top of the panel in blue, with the mean of six BB emission datasets in the first row. Three different methods to measure the dispersion of the six BB emission datasets are shown as well: one absolute method, i.e., the standard deviation (std) in the second row, and two relative methods, i.e., the ratio of max (maximum) to min (minimum) shown in the third row, and the coefficient of variation (cv), defined as the ratio of the std to the mean, in the fourth row. The rankings of the regions regarding the dispersion of the BB emissions datasets according to cv are shown in the fifth row (i.e., a ranking of 1 means that this region shows the least spread among the six BB emissions datasets, while a ranking of 14 indicates this region has the largest spread in the 14 regions).

Deleted: total

Deleted: (units:  $\text{Tg yr}^{-1}$ )

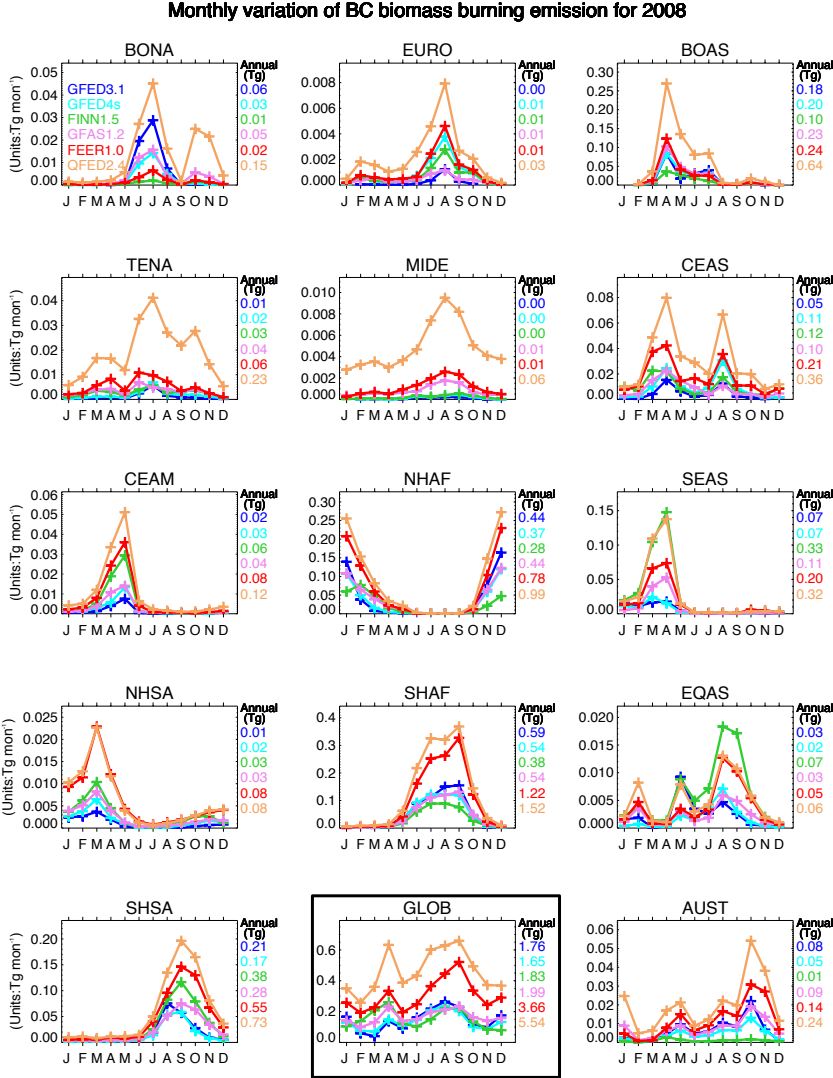


Figure S3. Monthly variation of black carbon biomass burning emissions for 2008 in six biomass burning emission datasets in 14 regions and the global (GLOB, highlighted with a black box). The annual total emission is listed in the right side of each panel.

Deleted: total

**Table S1.** The regional averaged monthly mean AOD at 550nm from MISR along with model biases (i.e., model minus MISR) in seven model experiments, i.e., NOBB, GFED3.1, GFED4s, FINN1.5, GFAS1.2, FEER1.0, and QFED2.4, for September and April 2008, respectively.

Dataset	BONA	TENA	CEAM	NHSA	SHSA	EURO	MIDE	NHAF	SHAF	BOAS	CEAS	SEAS	EQAS	AUST	GLOB
September 2008															
MISR	0.127	0.129	0.133	0.141	0.188	0.139	0.334	0.411	0.331	0.135	0.219	0.257	0.138	0.085	0.218
NOBB	0.04	0.011	-0.031*	-0.083	-0.132	0.084	-0.013	-0.05	-0.283	0.043	0.053	0.025	-0.047	-0.031	-0.029
GFED3.1	0.042	0.013	-0.031	-0.074	-0.078	0.085	-0.012	-0.046	-0.178	0.048	0.055	0.026	-0.039	-0.02	-0.012
GFED4s	0.044	0.014	-0.031	-0.075	-0.081	0.085	-0.012	-0.047	-0.208	0.047	0.056	0.025	-0.04	-0.023	-0.015
FINN1.5	0.041	0.013	-0.031	-0.07	-0.04	0.08	-0.013	-0.047	-0.21	0.045	0.05	0.016	-0.033	-0.025	-0.012
GFAS1.2	0.042	0.013	-0.031	-0.074	-0.08	0.08	-0.013	-0.047	-0.208	0.046	0.05	0.016	-0.029	-0.02	-0.016
FEER1.0	0.044	0.016	-0.03	-0.061	-0.021	0.088	-0.009	-0.039	-0.079	0.049	0.061	0.027	-0.032	-0.01	0.006
QFED2.4	0.058	0.04	-0.023	-0.058	0.02	0.097	-0.004	-0.035	-0.044	0.058	0.068	0.028	-0.029	-0.002	0.02
April 2008															
MISR	0.192	0.16	0.182	0.207	0.067	0.148	0.381	0.446	0.096	0.221	0.324	0.363	0.118	0.049	0.242
NOBB	-0.041	-0.016	-0.083	-0.086	-0.016	0.077	-0.059	-0.082	-0.042	-0.005	0.017	-0.074	-0.028	-0.004	-0.029
GFED3.1	-0.023	-0.008	-0.077	-0.082	-0.014	0.079	-0.058	-0.078	-0.04	0.104	0.055	-0.057	-0.027	-0.002	-0.015
GFED4s	-0.026	-0.008	-0.076	-0.081	-0.015	0.081	-0.057	-0.079	-0.039	0.095	0.05	-0.063	-0.027	-0.002	-0.016
FINN1.5	-0.031	-0.006	-0.056	-0.072	-0.013	0.075	-0.055	-0.068	-0.037	0.041	0.069	0.014	-0.024	-0.002	-0.008
GFAS1.2	-0.014	-0.005	-0.07	-0.075	-0.014	0.073	-0.057	-0.073	-0.039	0.164	0.07	-0.058	-0.025	-0.001	-0.008
FEER1.0	-0.017	0.003	-0.054	-0.059	-0.011	0.089	-0.053	-0.068	-0.036	0.162	0.083	-0.028	-0.024	0	-0.001
QFED2.4	0.018	0.027	-0.026	-0.054	-0.008	0.099	-0.047	-0.059	-0.032	0.329	0.17	0.038	-0.022	0.004	0.031

\*Highlighted in blue if negative bias.

**Deleted: Table S1.** The regional averaged monthly mean AOD at 550nm in MODIS-Aqua (i.e., MOD-a) along with model biases (i.e., model minus MODIS-a) in seven model experiments, i.e., NOBB, GFED3.1, GFED4s, FINN1.5, GFAS1.2, FEER1.0, and QFED2.4, for September and April 2008, respectively. ¶  
Dataset¶ ... [51]



Page 12: [1] Deleted	Xiaohua Pan	10/7/19 1:06:00 PM
Page 12: [1] Deleted	Xiaohua Pan	10/7/19 1:06:00 PM
Page 12: [1] Deleted	Xiaohua Pan	10/7/19 1:06:00 PM
Page 12: [2] Formatted	Xiaohua Pan	10/30/19 2:14:00 PM
Font color: Text 1		
Page 12: [2] Formatted	Xiaohua Pan	10/30/19 2:14:00 PM
Font color: Text 1		
Page 12: [2] Formatted	Xiaohua Pan	10/30/19 2:14:00 PM
Font color: Text 1		
Page 12: [3] Deleted	Xiaohua Pan	10/7/19 1:14:00 PM
Page 12: [3] Deleted	Xiaohua Pan	10/7/19 1:14:00 PM
Page 12: [3] Deleted	Xiaohua Pan	10/7/19 1:14:00 PM
Page 12: [4] Formatted	Xiaohua Pan	10/30/19 2:14:00 PM
Font color: Text 1		
Page 12: [4] Formatted	Xiaohua Pan	10/30/19 2:14:00 PM
Font color: Text 1		
Page 12: [5] Deleted	Ichoku, Charles	10/26/19 11:43:00 AM
Page 12: [5] Deleted	Ichoku, Charles	10/26/19 11:43:00 AM
Page 12: [6] Deleted	Xiaohua Pan	10/28/19 4:34:00 PM
Page 12: [6] Deleted	Xiaohua Pan	10/28/19 4:34:00 PM
Page 12: [6] Deleted	Xiaohua Pan	10/28/19 4:34:00 PM
Page 12: [6] Deleted	Xiaohua Pan	10/28/19 4:34:00 PM
Page 12: [6] Deleted	Xiaohua Pan	10/28/19 4:34:00 PM

Page 12: [7] Deleted Xiaohua Pan 10/11/19 10:41:00 AM

Page 12: [7] Deleted Xiaohua Pan 10/11/19 10:41:00 AM

Page 12: [8] Deleted Xiaohua Pan 10/11/19 10:50:00 AM

Page 12: [8] Deleted Xiaohua Pan 10/11/19 10:50:00 AM

Page 12: [8] Deleted Xiaohua Pan 10/11/19 10:50:00 AM

Page 12: [8] Deleted Xiaohua Pan 10/11/19 10:50:00 AM

Page 12: [8] Deleted Xiaohua Pan 10/11/19 10:50:00 AM

Page 12: [9] Deleted Xiaohua Pan 10/11/19 10:56:00 AM

Page 12: [9] Deleted Xiaohua Pan 10/11/19 10:56:00 AM

Page 12: [9] Deleted Xiaohua Pan 10/11/19 10:56:00 AM

Page 12: [9] Deleted Xiaohua Pan 10/11/19 10:56:00 AM

Page 12: [9] Deleted Xiaohua Pan 10/11/19 10:56:00 AM

Page 12: [10] Formatted Xiaohua Pan 10/30/19 2:14:00 PM

Font color: Text 1

Page 12: [10] Formatted Xiaohua Pan 10/30/19 2:14:00 PM

Font color: Text 1

Page 12: [11] Deleted Xiaohua Pan 10/11/19 10:59:00 AM

Page 12: [11] Deleted Xiaohua Pan 10/11/19 10:59:00 AM

Page 13: [12] Deleted Xiaohua Pan 10/31/19 2:14:00 PM

Page 13: [12] Deleted Xiaohua Pan 10/31/19 2:14:00 PM

Page 13: [13] Deleted	Ichoku, Charles	10/26/19 11:54:00 AM
-----------------------	-----------------	----------------------

Page 13: [13] Deleted	Ichoku, Charles	10/26/19 11:54:00 AM
-----------------------	-----------------	----------------------

Page 13: [14] Deleted	Xiaohua Pan	10/31/19 2:23:00 PM
-----------------------	-------------	---------------------

Page 13: [14] Deleted	Xiaohua Pan	10/31/19 2:23:00 PM
-----------------------	-------------	---------------------

Page 13: [15] Formatted	Xiaohua Pan	10/31/19 2:23:00 PM
-------------------------	-------------	---------------------

Font: Bold, Font color: Text 1

Page 13: [15] Formatted	Xiaohua Pan	10/31/19 2:23:00 PM
-------------------------	-------------	---------------------

Font: Bold, Font color: Text 1

Page 13: [15] Formatted	Xiaohua Pan	10/31/19 2:23:00 PM
-------------------------	-------------	---------------------

Font: Bold, Font color: Text 1

Page 13: [15] Formatted	Xiaohua Pan	10/31/19 2:23:00 PM
-------------------------	-------------	---------------------

Font: Bold, Font color: Text 1

Page 13: [16] Deleted	Xiaohua Pan	10/22/19 1:46:00 PM
-----------------------	-------------	---------------------

Page 13: [17] Deleted	Xiaohua Pan	10/31/19 2:30:00 PM
-----------------------	-------------	---------------------

Page 13: [18] Deleted	Xiaohua Pan	10/22/19 1:56:00 PM
-----------------------	-------------	---------------------

Page 13: [19] Formatted	Xiaohua Pan	10/30/19 2:14:00 PM
-------------------------	-------------	---------------------

Font color: Text 1

Page 13: [19] Formatted	Xiaohua Pan	10/30/19 2:14:00 PM
-------------------------	-------------	---------------------

Font color: Text 1

Page 13: [20] Deleted	Xiaohua Pan	10/22/19 1:48:00 PM
-----------------------	-------------	---------------------

Page 13: [20] Deleted	Xiaohua Pan	10/22/19 1:48:00 PM
-----------------------	-------------	---------------------

Page 13: [20] Deleted	Xiaohua Pan	10/22/19 1:48:00 PM
-----------------------	-------------	---------------------

Page 13: [20] Deleted	Xiaohua Pan	10/22/19 1:48:00 PM
-----------------------	-------------	---------------------

Page 13: [20] Deleted	Xiaohua Pan	10/22/19 1:48:00 PM
-----------------------	-------------	---------------------

Page 14: [21] Formatted	Xiaohua Pan	10/30/19 2:14:00 PM
-------------------------	-------------	---------------------

Font color: Text 1

▲ Page 14: [21] Formatted Xiaohua Pan 10/30/19 2:14:00 PM

Font color: Text 1

▲ Page 14: [21] Formatted Xiaohua Pan 10/30/19 2:14:00 PM

Font color: Text 1

▲ Page 14: [21] Formatted Xiaohua Pan 10/30/19 2:14:00 PM

Font color: Text 1

▲ Page 14: [22] Formatted Xiaohua Pan 10/30/19 2:14:00 PM

Font color: Text 1

▲ Page 14: [22] Formatted Xiaohua Pan 10/30/19 2:14:00 PM

Font color: Text 1

▲ Page 14: [23] Formatted Xiaohua Pan 10/30/19 2:14:00 PM

Font color: Text 1

▲ Page 14: [23] Formatted Xiaohua Pan 10/30/19 2:14:00 PM

Font color: Text 1

▲ Page 14: [24] Deleted Xiaohua Pan 10/25/19 10:49:00 AM

▲ Page 14: [24] Deleted Xiaohua Pan 10/25/19 10:49:00 AM

▲ Page 14: [25] Formatted Xiaohua Pan 10/30/19 2:14:00 PM

Font color: Text 1

▲ Page 14: [25] Formatted Xiaohua Pan 10/30/19 2:14:00 PM

Font color: Text 1

▲ Page 14: [26] Deleted Xiaohua Pan 10/11/19 1:37:00 PM

▲ Page 14: [26] Deleted Xiaohua Pan 10/11/19 1:37:00 PM

▲ Page 14: [26] Deleted Xiaohua Pan 10/11/19 1:37:00 PM

▲ Page 14: [26] Deleted Xiaohua Pan 10/11/19 1:37:00 PM

▲ Page 14: [26] Deleted Xiaohua Pan 10/11/19 1:37:00 PM

▲ Page 14: [26] Deleted Xiaohua Pan 10/11/19 1:37:00 PM

▲ Page 14: [26] Deleted Xiaohua Pan 10/11/19 1:37:00 PM

▲ Page 14: [26] Deleted Xiaohua Pan 10/11/19 1:37:00 PM

▲

Page 14: [27] Deleted	Xiaohua Pan	10/22/19 2:12:00 PM
Page 14: [27] Deleted	Xiaohua Pan	10/22/19 2:12:00 PM
Page 14: [28] Deleted	Ichoku, Charles	10/26/19 12:10:00 PM
Page 14: [28] Deleted	Ichoku, Charles	10/26/19 12:10:00 PM
Page 14: [29] Deleted	Xiaohua Pan	10/22/19 2:14:00 PM
Page 14: [29] Deleted	Xiaohua Pan	10/22/19 2:14:00 PM
Page 14: [29] Deleted	Xiaohua Pan	10/22/19 2:14:00 PM
Page 14: [30] Formatted	Xiaohua Pan	10/30/19 2:14:00 PM
Font color: Text 1		
Page 14: [30] Formatted	Xiaohua Pan	10/30/19 2:14:00 PM
Font color: Text 1		
Page 14: [31] Deleted	Xiaohua Pan	10/28/19 2:10:00 PM
Page 14: [31] Deleted	Xiaohua Pan	10/28/19 2:10:00 PM
Page 14: [31] Deleted	Xiaohua Pan	10/28/19 2:10:00 PM
Page 14: [32] Deleted	Ichoku, Charles	10/26/19 12:14:00 PM
Page 14: [32] Deleted	Ichoku, Charles	10/26/19 12:14:00 PM
Page 14: [33] Deleted	Ichoku, Charles	10/26/19 12:15:00 PM
Page 14: [33] Deleted	Ichoku, Charles	10/26/19 12:15:00 PM
Page 14: [34] Deleted	Xiaohua Pan	10/22/19 3:27:00 PM
Page 14: [34] Deleted	Xiaohua Pan	10/22/19 3:27:00 PM
Page 15: [35] Deleted	Xiaohua Pan	10/22/19 2:26:00 PM



Page 15: [36] Formatted Xiaohua Pan 10/30/19 2:14:00 PM

Font color: Text 1, Not Highlight

Page 15: [37] Formatted Xiaohua Pan 10/30/19 2:14:00 PM

Font color: Text 1

Page 15: [38] Deleted Xiaohua Pan 10/11/19 1:53:00 PM

Page 15: [39] Deleted Xiaohua Pan 10/22/19 3:52:00 PM

Page 15: [40] Deleted Ichoku, Charles 10/26/19 12:25:00 PM

Page 15: [41] Deleted Xiaohua Pan 10/22/19 3:52:00 PM

Page 15: [42] Formatted Xiaohua Pan 10/30/19 2:14:00 PM

Font color: Text 1

Page 15: [43] Formatted Xiaohua Pan 10/30/19 2:14:00 PM

Font color: Text 1

Page 15: [44] Formatted Xiaohua Pan 10/30/19 2:14:00 PM

Font: Not Bold, No underline, Font color: Text 1

Page 15: [45] Formatted Xiaohua Pan 10/30/19 2:14:00 PM

Font color: Text 1

Page 15: [46] Formatted Xiaohua Pan 10/30/19 2:14:00 PM

Font color: Text 1

Page 15: [47] Formatted Xiaohua Pan 10/30/19 2:14:00 PM

Font color: Text 1

Page 15: [48] Formatted Xiaohua Pan 10/30/19 2:14:00 PM

Font color: Text 1

Page 15: [49] Formatted Xiaohua Pan 10/30/19 2:14:00 PM

Font color: Text 1

Page 15: [50] Formatted Xiaohua Pan 10/30/19 2:14:00 PM

Font color: Text 1

Page 47: [51] Deleted Xiaohua Pan 10/30/19 2:11:00 PM